NI

NASA CR- 66382

CONCEPTUAL MECHANIZATION STUDIES FOR A HORIZON DEFINITION SPACECRAFT ATTITUDE CONTROL SUBSYSTEM

Horizon Definition Study

May 1967

Prepared under Contract No. NAS 1-6010 by

HONEYWELL INC.
Systems & Research Division
and Aerospace Division
Minneapolis, Minn.

for

NATIONAL AERONAUTICS AND SPACE ADMINISTRATION

NASA CR-66382

CONCEPTUAL MECHANIZATION STUDIES FOR A HORIZON DEFINITION SPACECRAFT ATTITUDE CONTROL SUBSYSTEM

By Norris W. Tidwell
Calvin G. Senechal
Eldon L. Tesch
Howard A. Knudtson, Jr.
David J. Hartman

HORIZON DEFINITION STUDY

May 1967

Prepared under Contract No. NAS 1-6010 by
Honeywell Inc.
Systems and Research Division
and Aerospace Division
Minneapolis, Minnesota
for

NATIONAL AERONAUTICS AND SPACE ADMINISTRATION

CONTENTS

FOREWORD

This report documents Phase A, Part II of An Analytical and Conceptual Design Study for an Earth Coverage Infrared Horizon Definition Study performed under National Aeronautics and Space Administration Contract NAS 1-6010 for Langley Research Center.

The Horizon Definition Study was performed in two parts. Part I, which was previously documented, provided for delineation of the experimental data required to define the infrared horizon on a global basis for all temporal and spatial periods. Once defined, the capabilities of a number of flight techniques to collect the experimental data were evaluated. The Part II portion of the study provides a measurement program plan which satisfies the data requirements established in the Part I study. Design requirements and the conceptual design for feasibility of the flight payload and associated subsystems to implement the required data collection task are established and documented within this study effort.

Honeywell Inc., Systems and Research Division, performed this study program under the technical direction of Mr. L. G. Larson. The program was conducted from 28 March 1966 to 10 October 1966 (Part I) and from 10 October 1966 to 29 May 1967 (Part II). This Part II portion of the study was the joint effort of the Aerospace Division and the Systems and Research Division of Honeywell Inc.

Gratitude is extended to NASA Langley Research Center for their technical guidance, under the program technical direction of Messrs. L. S. Keafer and J. A Dodger with direct assistance from Messrs. W. C. Dixon, Jr., E. C. Foudriat, and H. J. Curfman, Jr., as well as the many people within their organization.

Recognition is given to Messrs. Jensen and Caine of NASA Goddard Space Flight Center for supplying a computer program for the calculation of the earth's magnetic field.

May 1967 NASA CR-66382

CONCEPTUAL MECHANIZATION STUDIES FOR A HORIZON DEFINITION SPACECRAFT ATTITUDE CONTROL SUBSYSTEM

By Norris W. Tidwell, Calvin G. Senechal, Eldon L. Tesch, Howard A. Knudtson, Jr., David J. Hartman

ABSTRACT

A feasible attitude control subsystem concept utilizing magnetic torquing and ground commanding was developed for the Horizon Definition Study spacecraft. A V-head sensor operating in the 14- to 16-micron infrared region will be used for coarse attitude sensing. The spin rate of the spacecraft will be maintained at three rpm. Orbital regression will be compensated for by magnetic torquing coils.

ILLUSTRATIONS

TABLES

CONCEPTUAL MECHANIZATION STUDIES FOR A HORIZON DEFINITION SPACECRAFT ATTITUDE CONTROL SUBSYSTEM

By Norris W. Tidwell
Calvin G. Senechal
Eldon L. Tesch
Howard A. Knudtson, Jr.
David J. Hartman

SUMMARY

This report documents the final results of an analytical study and conceptual design of an attitude control subsystem for an earth orbiting, spin stabilized scientific spacecraft. The purpose of the spacecraft is to carry an experiment package which maps the earth's infrared horizon radiance profiles in the 15 micron, carbon dioxide absorption band for a one-year period. The data gained can serve as a useful input in many atmospheric sciences studies and will also provide the data base for developing improved infrared horizon sensing systems for spacecraft attitude measurement and control.

The analytical portion of the study was concerned principally with the development of the disturbing forces due to the orbital environment and the free-body motions of a rigid, spinning spacecraft. For the free-body case an analytical solution was used to examine the effects of parametric variations of the spacecraft characteristics. The composite effects of the free and torqued body motions were examined with an extensive computer program designated as HDMP. The two prinicpal disturbing torques on the spacecraft were determined to be due to an interaction with the earth's magnetic field. A despinning "drag" torque is caused by rotation of the conducting skin of the spacecraft in the earth's field. A precessional torque is created by an interaction of the spacecraft's magnetic moment with the earth's field.

After completing a system functional requirements analysis an attitude control subsystem concept was evolved. The most significant characteristics of this concept are as follows:

- The attitude control subsystem achieves reorientation and spin-up forces from interactions with the earth's magnetic field.
- A V-head horizon sensor operating in the CO_2 band supplies coarse attitude information.

- The subsystem is ground controlled and is activated once each five days for a period of 0.5 orbit to correct spacecraft attitude drift. The spacecraft free floats for all other times except for applied constant torques to compensate known drift factors due to residual magnetic moments and orbit regression.

- The prime STADAN stations for attitude information reception and command transmission are College, Alaska, and Rosman, North Carolina.

INTRODUCTION

The attitude control subsystems study documented herein is a portion of the Horizon Definition Study (HDS) conducted for NASA Langley Research Center, Contract NAS 1-6010, Part II. The purpose of the Horizon Definition Study is to develop a complete horizon radiance profile measurement program to provide data which can be used to determine the earth's atmospheric state, especially at high altitudes. These data can then be effectively used in many atmospheric sciences studies and in the design of instruments and measurements systems which use the earth's horizon as a reference

Part I of the HDS resulted in the following significant contributions to the definition of the earth's radiance in the infrared spectrum:

- The accumulation of a significant body of meteorological data covering a major portion of the Northern Hemisphere.
- Computation of a large body of synthesized horizon radiance profiles from actual temperature profiles obtained by rocket soundings.
- Generation of a very accurate analytical model and computer program for converting the temperature profiles to infrared horizon profiles (as a function of altitude).
- An initial definition of the quantity, quality, and sampling methodology required to define the earth's infrared horizon in the CO_2 absorption band for all temporal and spatial conditions.
- An evaluation of the cost and mission success probabilities of a series of flight techniques which could be used to gather the radiance data. A rolling-wheel spacecraft was selected in a nominal 500 km polar orbit.

The Part II study effort was directed toward the development of a conceptually feasible measurement system, which includes a spacecraft to accomplish the measurement program developed in Part I. In the Part II HDS, a number of scientific and engineering disciplines were exercised simultaneously to design conceptually the required system. Accomplishments of Part II of the study are listed below:

- The scientific experimenter refined the sampling methodology used by the measurement system. This portion of the study recommends the accumulation of approximately 380 000 radiance profiles taken with a sampling rate that varies with the spacecraft's latitudinal position.
- A conceptual design was defined for a radiometer capable of resolving the earth's radiance in the 15-micron spectrum to 0.01 watt/meter^2-steradian with an upper level of response of 7.0 watt/meter^2-steradian.

- A starmapper and attitude determination technique were defined capable of determining the pointing direction of the spacecraft radiometer to an accuracy of 0.25 km in tangent height at the earth's horizon.

  The combination of the radiometer and starmapper instruments is defined as the mission experiment package.

- A solar cell-battery electrical power subsystem conceptual design was defined which is completely compatible with the orbital and experiment constraints. This system is capable of delivering 70 watts of continuous electrical power for one year in the sun-synchronous, 3 o'clock nodal crossing, 500 km orbit.

- A data handling subsystem conceptual design was defined which is capable of processing in digital form all scientific and status data from the spacecraft. This subsystem is completely solid state and is designed to store the 515 455 bits of digital information obtained in one orbit of the earth. This subsystem also includes command verification and execute logic.

- A communications subsystem conceptual design was defined to interface between the data handling system of the spacecraft and the STADAN network. The 136 MHz band is used for primary data transmission and S band is used for the range and range-rate transponder.

- A spacecraft structural concept was evolved to contain, align, and protect the spaceborne subsystems within their prescribed environmental constraints. The spacecraft is compatible with the Thor-Delta launch vehicle.

- An open-loop, ground-commanded attitude control subsystem conceptual design was defined utilizing primarily magnetic torquing which interacts with the earth's field as the force for correcting attitude and spin rates.

- The Thor-Delta booster, which provides low cost and adequate capability, was selected from the 1972 NASA "stable".

- Western Test Range was selected as the launch site due to polar orbit requirements. This site has adequate facilities, except for minor modifications, and is compatible with the polar orbit requirements.

This report contains the results of a mathematical description and analysis of the vehicle motion and an attitude control concept feasibility study. Requirements for the conceptual design of the attitude control subsystem and a feasible subsystem to meet these requirements are established. The analytical process involves the mathematical modeling of the dynamics of a vehicle whose environment is a near polar, circular orbit of 500 km altitude.

The model consists of Euler's free-body dynamical equations and the torque equations based on the vehicle's environment. The torque equations describe the environment of the vehicle and are subsequently added to the free-body equations to provide a complete description of the vehicle motion. The free-body and torqued-body motion were used to determine design and operational constraints on the spacecraft, to establish the relative significance of the environmental torques, and as predictions of spacecraft motions in the attitude determination subsystems study.

The attitude control mechanization study consisted of tradeoffs to establish a feasible and compatible subsystem that would meet overall vehicle system constraints and requirements. Selection of the open-loop, magnetic - torquing attitude control concept was based on providing a simple control system which will prohibit the introduction of indeterministic torques during the experiment data collection cycle.

STUDY REQUIREMENTS AND OBJECTIVES

The following list itemizes the basic and detailed requirements of the Horizon Definition Study

BASIC REQUIREMENTS

Radiance Profile Measurements

- Spectral interval: 615 to 715 cm^{-1} (14.0 to 16.28μ)
- Profile accuracy
  - ► Tangent height range: +80 km to -30 km
  - ► Instantaneous value of radiance measured must be assignable to a tangent height value to within ±0.25 km.
  - ► Radiance characteristics and resolution:

    Maximum peak radiance = 7.0 W/m^2 - sr.

    Minimum peak radiance = 3.0 W/m^2 - sr.

    Maximum slope = 0.6 W/m^2 - sr - km.

    Minimum slope = 0.02 W/m^2 - sr - km.

    Maximum slope change = 0.15 W/m^2 - sr - km^2.

    Radiance magnitude resolution = 0.01 W/m^2 - sr.
  - ► Horizontal resolution: 25 km
- Data requirements - Data requirements for the Horizon Definition Study (HDS) experiment, as refined during the study, are as follows:

Minimum requirements. --

- ► One-year continuous coverage
- ► "Uniform" time sampling in each space cell over each time cell, i.e., no more than two samples/space cell/day
- ► 13 time cells (28 days/cell)
- ► 408 space cells

Latitude (60°S to 60°N)	320
Latitude (60°N to 90°N)	44
Latitude (60°S to 90°S)	44

- Samples per cell
  - Latitude (0° to 60°) 16
  - Latitude (60° to 90°) 38
- Total samples (one year) 110 032

Recommended requirements. --

- One-year continuous coverage
- Maximum of 10° latitude separation between successive samples
- 13 time cells (28 days/cell)
- 588 space cells
  - Latitude (30°S to 30°N) 128
  - Latitude (30°N to 60°N) 134
  - Latitude (60°N to 82.6°N) 96
  - Latitude (30°S to 60°S) 134
  - Latitude (60°S to 82.6°S) 96
- Average number of samples per cell
  - Latitude (30°S to 30°N) 45
  - Latitude (30°N to 60°N) 39
  - Latitude (60°N to 82.6°N) 67
  - Latitude (30°S to 60°S) 39
  - Latitude (60°S to 82.6°S) 67
- Total samples (one year) 378 508

Mission Profile

Nominal circular, polar orbit of approximately 500 km altitude.

Tracking and Data Acquisition

Limited to the existing Satellite Tracking And Data Acquisition Network (STADAN) with minimum modification.

Experiment Package

- Passive radiometric and attitude measurements with redundancy (more than one unit) in the experiment package for the radiometer and attitude determination device.
- Minimum scan rate >0. 5 scans/min average.
- Maximum scan angle with respect to orbit plane ≤5°.

Spacecraft

- Rolling-wheel configuration (spin axis normal to the orbit plane).
- Weight in less than 800 pound class mandatory.

State of the Art

Proven subsystems shall be employed wherever possible.

Mission Effectiveness/Reliability

Reliability shall be approached on the basis of "designing in" successful performance of the one-year, data-collection mission, i. e., the effort is to be biased strongly toward mission effectiveness. Consequently, the mission effectiveness/reliability effort should involve continuing tradeoffs in each subfunction area against the criteria of maximum effectiveness. A numerical estimate of the probable system MTBF shall be made on the final configuration.

Strong consideration should be given to the use of reserve spacecraft as a "backup" means rather than as a continuously ready standby. Specifically, the "backup" concept (as opposed to ready continuously) is of more significance on a Thor-Delta sized vehicle than on a Scout vehicle.

ATTITUDE CONTROL SUBSYSTEM REQUIREMENTS

From the basic mission requirements, a description of the functions of the attitude control subsystem were made and are given in Figure 1. Having established the functions to be performed by the attitude control subsystem, analysis of the spacecraft dynamics and consideration of constraints imposed on the ACS by other factors led to more detailed requirements for each ACS function and to the conceptual design of an attitude control system to meet these requirements. Table 1 describes these requirements and their origins.

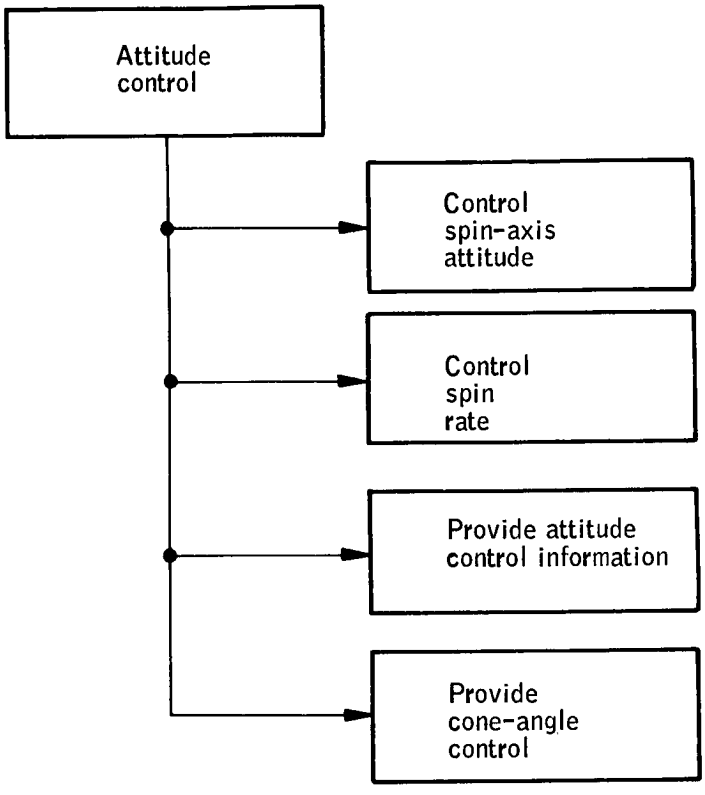

Figure 1. Attitude Control Functional Requirements Diagram

TABLE 1. - ATTITUDE CONTROL SUBSYSTEM REQUIREMENTS

Function	Requirements	Remarks
Control spin axis attitude	The attitude control subsystem (ACS) shall provide a magnetic bias torquer. It shall be used to reduce the residual magnetic moment along the spin axis and compensate for orbit regression.	The most significant torques acting on the vehicle are due to interactions with the earth's field. It appears quite logical to take advantage of the existence of these fields and use interactions with them to re-erect periodically the attitude of the spacecraft, correct for orbital regression, and reduce the spacecraft residual magnetic moment.
	The ACS shall provide a magnetic quarter-orbit torquer capable of correcting ± 5.0 degrees of spin-axis attitude in one half orbit.	Attitude correction should take place in as short a period as possible. Two quarter orbit periods are required to minimize cross coupling when trying to correct an attitude error.
	The ACS shall provide at least two levels of torquing in the quarter orbit torquer.	Two levels permit versatility in choice of torquing intervals. To maximize system effectiveness, spin axis attitude corrections are made at the same time that spin rate corrections are made.
	The ACS quarter orbit torquer shall not operate during the data cycle.	The attitude determination system can not operate with the induced vehicle rates that will exist with the torquers operating.
Control spin rate	The ACS shall provide a torquer capable of correcting ± 5 percent of the nominal spin rate within one half orbit.	Spin rate must be corrected when it exceeds 5 percent of nominal to avoid complexities in data storage and attitude determination computation. The best earth's field conditions for correction of spin rate occur over the magnetic poles.
Provide attitude position information	The ACS shall provide a sensor to measure spin axis attitude and spin rate. The spin axis attitude shall be measured to ±0.5 degree, and spin rate shall be measured to ±0.5 percent of the nominal spin rate.	An accuracy of ±0.5 degree is required by attitude determination for initial estimation of attitude. Sensor output is also used for ground base attitude computations to determine ACS sequences required.
Provide cone angle control	The ACS shall provide a damper to reduce body half cone angle to 0.5 degree.	The cone angle must be kept small in order to maintain the radiometer scan vector within ±5 degrees of the orbit plane for longer periods of time. Present calculations give 180 days to grow one degree due to the residual magnetic moment and eddy-current torques.
	The ACS damper shall not operate during the data cycle.	
	The ACS damper shall have the capability to remove eight degrees of cone in no more than two orbits.	The vehicle may have approximately eight degrees of half-cone angle generated due to booster tipoff rates. The operational plan is such that two orbits are available for cone-angle damping. Ninety percent of the cone angle should be removed during the first orbit.
	The ACS shall be designed to operate for a vehicle with inertia ratio I_s/I_t greater than or equal to 1.2 and a spin rate greater or equal to 3 rpm.	The inertia ratio was determined by the packaging constraints and the dynamics of a spinning body. It was shown in the analysis that a spinning body is stable about its maximum moment of inertia axis for a flexible spacecraft. Packaging constraints showed that an inertia ratio of approximately 1.4 could be obtained. Analytical results showed that the vehicle was stable for an inertia ratio of 1.2 at 3, 4, and 5 rpm. Since the HDS spacecraft is adequately stable for r = 1.2 and packaging constraints allow up to a 1.4 inertia ratio, it is then recommended that r be greater than or equal to 1.2. The 1.2 ratio gives a margin of safety to the maximum moment of inertia axis.
	The ACS shall be designed to operate for a vehicle whose asymmetry about the preferred spin axis is not greater than three percent.	The spacecraft will undergo more complex motion since an asymmetric body causes the cone angle to vary about a mean, and the extent of variation is directly related to the asymmetry of the body. The body is more unstable about a preferred axis as the asymmetry about that axis increases. For ACS control, three-percent asymmetry was found to be acceptable.

VEHICLE CONSTRAINTS

The spacecraft is a spinning hexagonal cylinger with six solar paddles extending perpendicular to the cylinder. The vehicle will be assumed to be rigid and have the mission characteristics itemized below. These itemized characteristics are nominal values.

- Mission characteristics
  - ► Duration: one year
  - ► Orbit: earth orbiting, 500 km circular, sun-synchronous orbit for 3 a.m. or 3 p.m. launch.
- Vehicle characteristics
  - ► Inertia: I_s = 65.5 slug-ft^2, I_t = 54.6 slug-ft^2 where I_s is the principal moment of inertia about preferred spin axis and I_t is the principal moment of inertia about transverse axis; $I_s/I_t \approx 1.2$.

    The spacecraft will contain a cryogenic cooler which will decrease I_s by 0.5 lb-ft^2 and I_t by 5 lb-ft^2 after one year of operation.
  - ► Geometry: right hexagonal cylinger 40 inches long by 46.8 inches from flat to flat (see Figures 2 and 3). Solar panels, extending from each of the six flat sides of the cylinger, are 44-inches long and 23-inches wide.
  - ► Aspect: the spin axis is oriented perpendicularly to the orbit plane, and the transverse axes are nominally in orbit plane.

    Spacecraft tip-off rate $\approx$ 3 degrees/second.
- Stabilization - system conditions
  - ► Normal stabilization limits: spin axis within ±5° of the orbit normal.
  - ► Rate band: ±5 percent of the nominal spin rate.

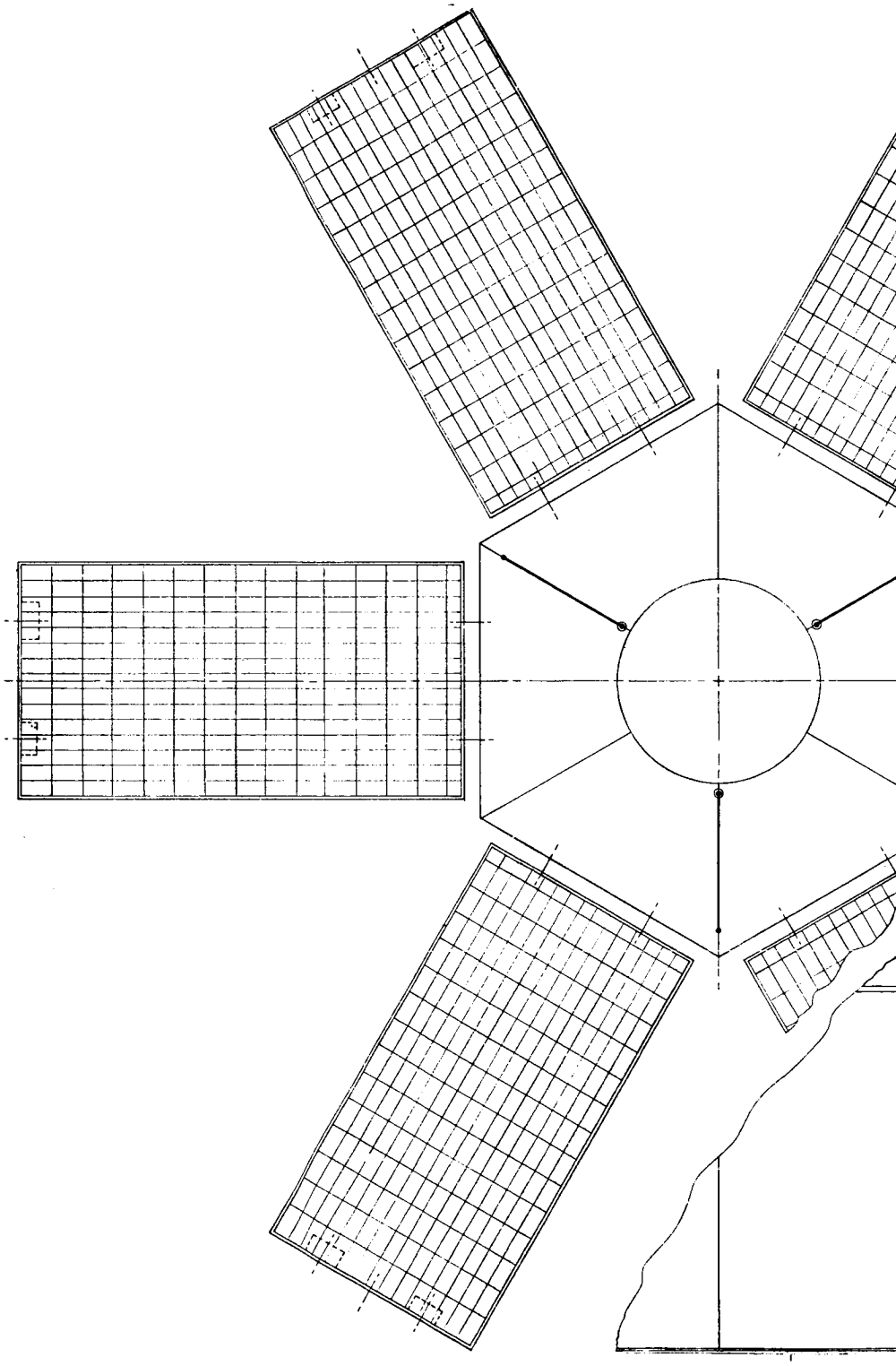

Figure 2. Con

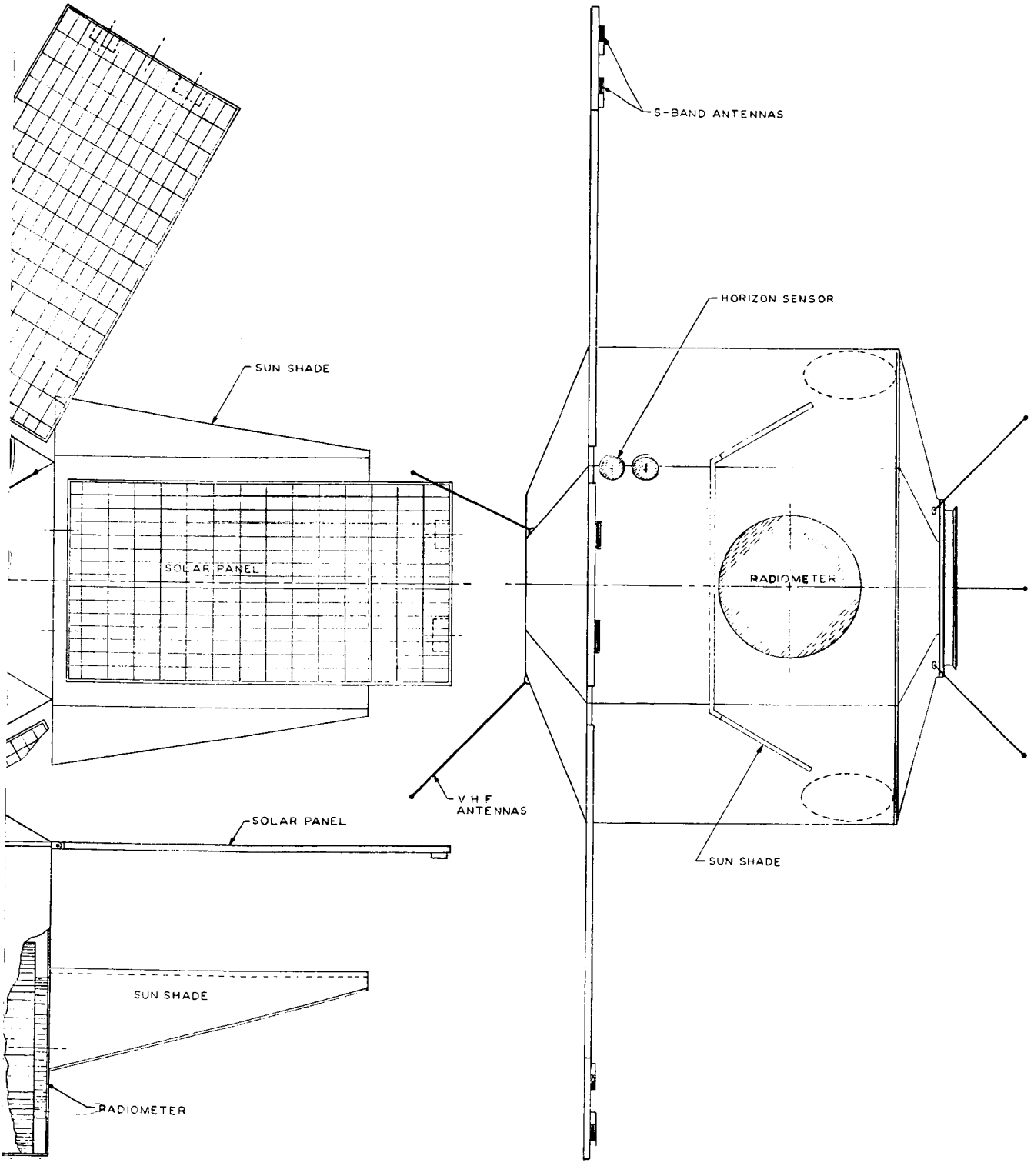

ceptual Spacecraft, External Layout

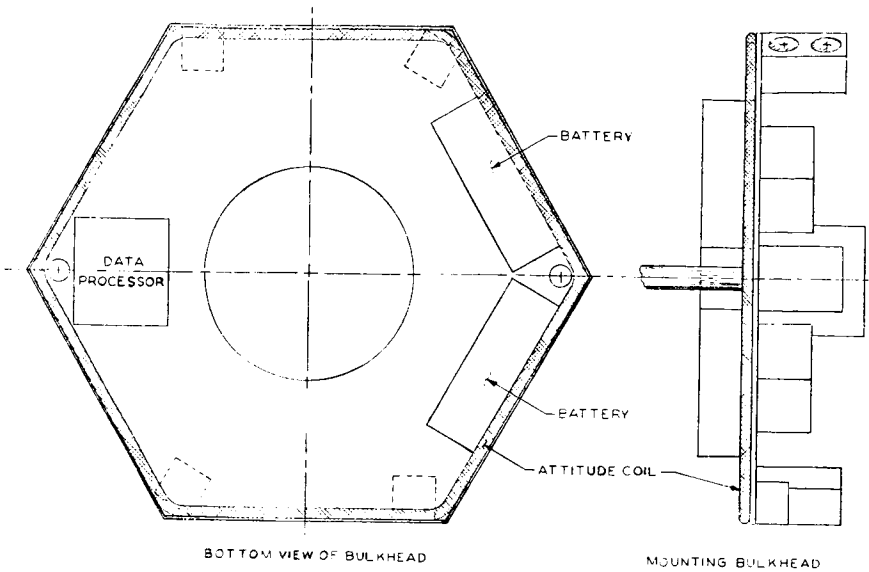

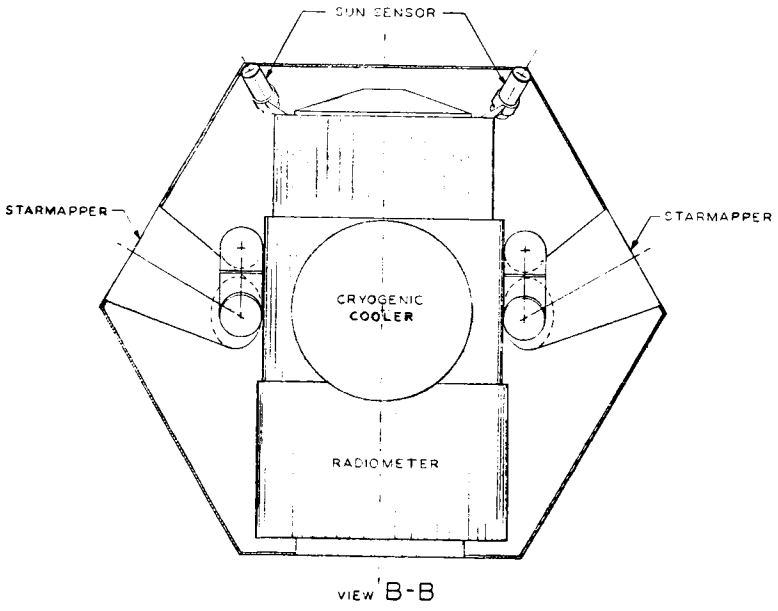

Figure 3. Conce

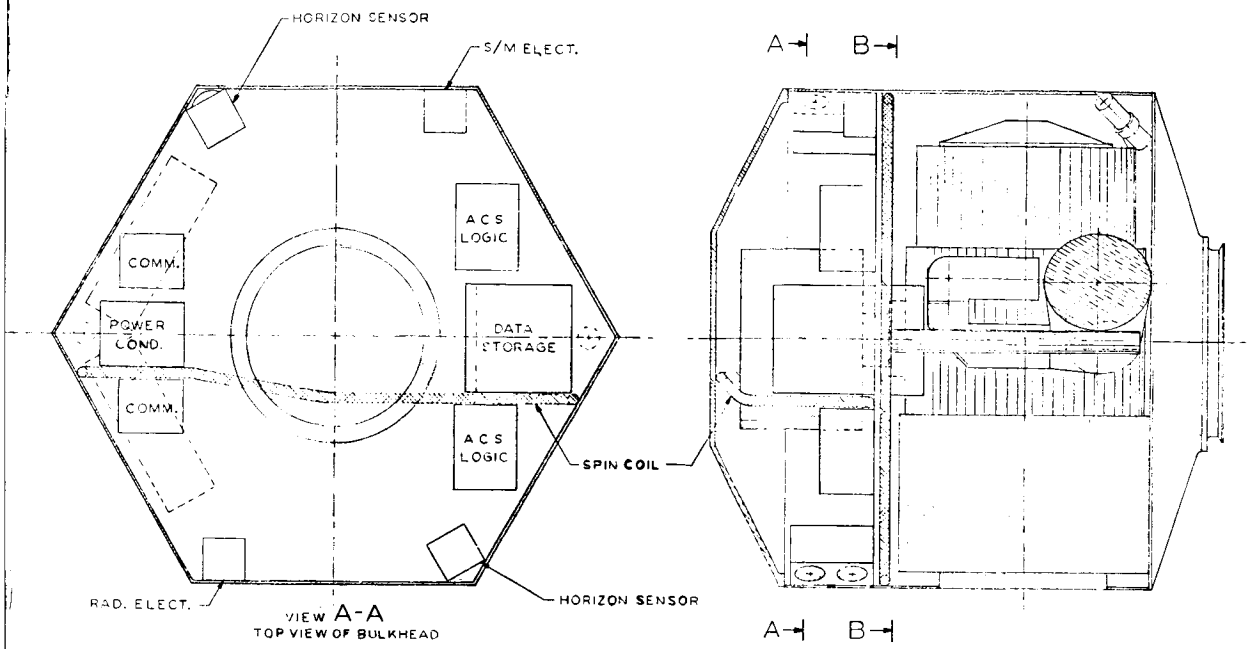

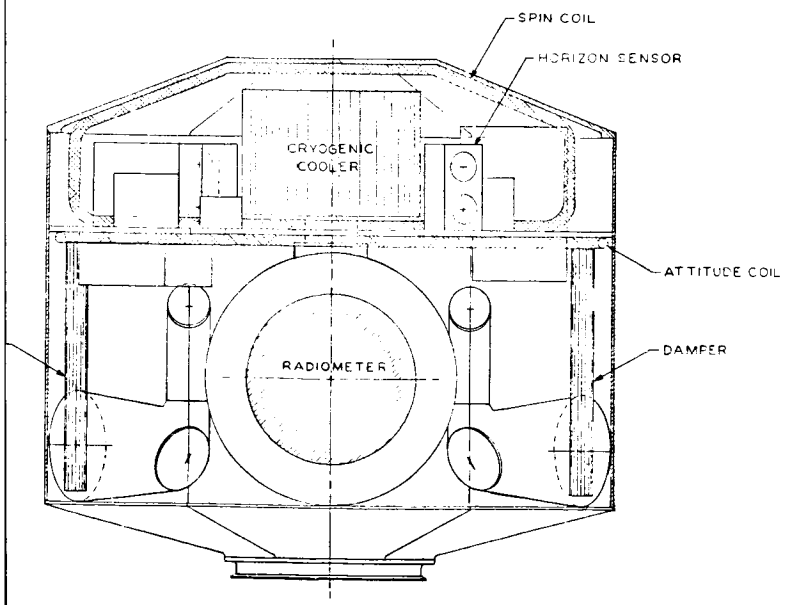

ptual Spacecraft, Internal Layout

SPACECRAFT DYNAMIC ANALYSIS STUDY

The purpose of the analysis of spacecraft motion is to provide an adequate description of the spacecraft's motion that will be incorporated into the attitude determination model and to establish analytical requirements of the attitude control system.

The analysis will consist of two parts: free-body motion and torqued-body motion. The free-body motion analysis is conducted using an analytical solution as opposed to the numerical solution used to analyze the torqued-body motion. The analytical solution (free body) provides a concise form of the body motion that can be easily visualized. The spacecraft dynamics analysis study plan is shown in Figure 4.

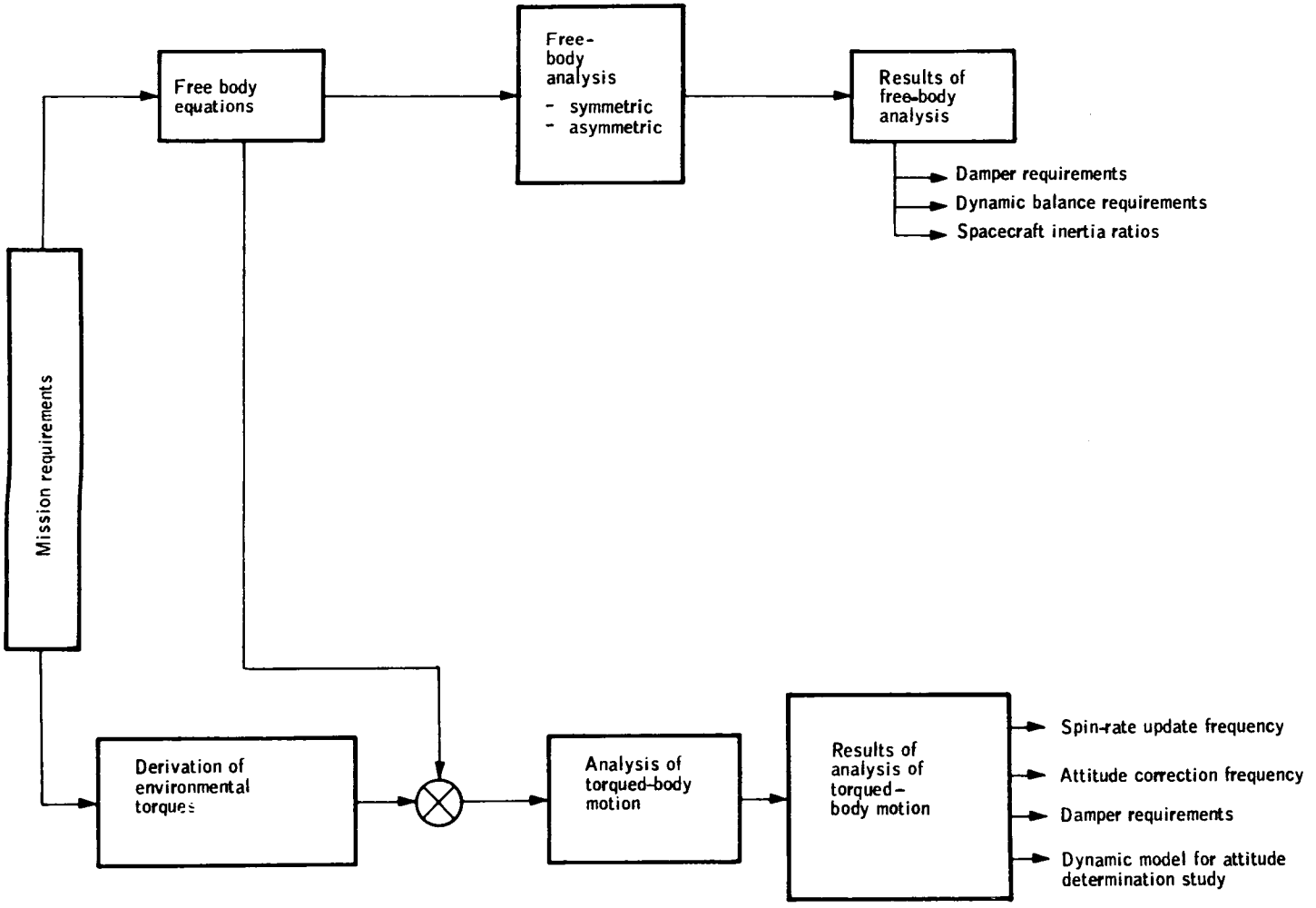

Figure 4. Spacecraft Dynamics Analysis Study Plan

FREE-BODY EQUATIONS

Definition of Symbols

ϕ -- precession angle measured from the inertial x_I axis to the x_1 (line of nodes)

$\dot{\phi}$ -- inertial precession rate

ψ -- proper rotation angle measured from x_2 to the x_3 body axis

θ -- cone angle measured from the inertial z_I axis to the body z_3 axis

N -- lowest harmonic frequency variation of θ

$\Delta\theta$ -- extent of nutation

η -- angle between the vehicle's principal body z_3 axis and the spin vector $\vec{\omega}$

$\vec{\omega}$ -- the spin vector, principally aligned along the body z_3 axis

$\omega_{x_3}, \omega_{y_3}, \omega_{z_3}$ - components of $\vec{\omega}$ along the body axis

$\omega_{x_0}, \omega_{z_0}$ -- initial values of the body rates for the x and z axes (ω_{y_0} is zero)

Rigid-Body Dynamic Equations

The equations of motion of a rigid body are well known and are expressed relative to the principal axes of the body.

$$\left.\begin{aligned} L_x &= I_x \dot{\omega}_x + (I_z - I_y)\,\omega_y\,\omega_z \\ L_y &= I_y \dot{\omega}_y + (I_x - I_z)\,\omega_z\,\omega_x \\ L_z &= I_z \dot{\omega}_z + (I_y - I_x)\,\omega_x\,\omega_y \end{aligned}\right\} \qquad (1)$$

where L_x, L_y, L_z are the component torques in the body frame, and ω_x, ω_y, ω_z are the rates about the body principal axes.

Since the analysis is twofold, one analysis to investigate free-motion characteristics and a second to investigate torqued-body motion characteristics, it became expedient to conduct the free-body analysis with different coordinate transformation than the torqued-body analysis. These transformations are defined in each analysis.

Several characteristics of free-body motion that are to be investigated are:

- Cone angle of body as a function of η, body asymmetry, and inertia ratio.
- Stability of a spinning body.
- Nutation of the body as a function of body asymmetry and η.
- Precession of the body as a function of body asymmetry and η.

Dynamic equations for the motion are given by equation (1) with L_x, L_y, and L_z equal to zero. A coordinate transformation is required to transform the body motion to an inertial angular momentum system for analysis.

The inertial frame will have its z axis aligned to the vehicle's angular momentum vector. Body coordinates x_3, y_3, z_3 are then transformed to inertial coordinates by means of Euler-angle rotations (ϕ, θ, ψ) (see Figure 5).

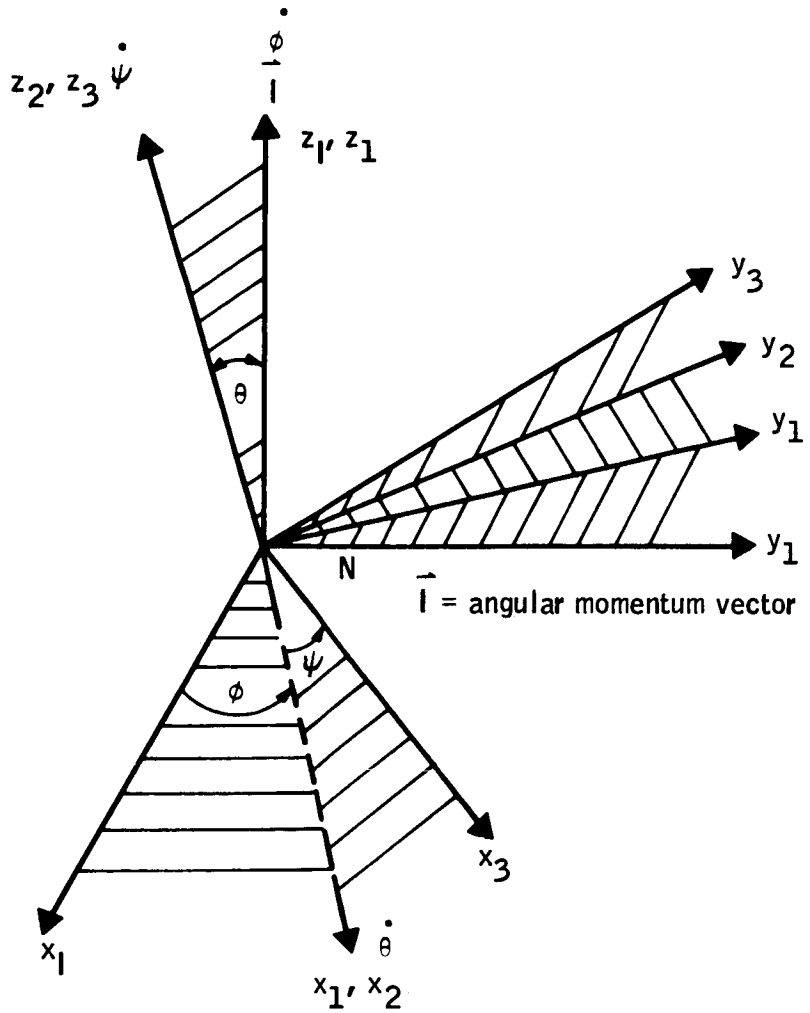

Figure 5. Body Coordinates Related to Inertial Coordinates

Coordinate System

The transformation from body to inertial can be accomplished by three consecutive rotations as follows:

$$\begin{bmatrix} x_I \\ y_I \\ z_I \end{bmatrix} = \begin{bmatrix} \cos\phi & -\sin\phi & 0 \\ \sin\phi & \cos\phi & 0 \\ 0 & 0 & 1 \end{bmatrix} \begin{bmatrix} x_1 \\ y_1 \\ z_1 \end{bmatrix} \tag{2}$$

$$\begin{bmatrix} x_1 \\ y_1 \\ z_1 \end{bmatrix} = \begin{bmatrix} 1 & 0 & 0 \\ 0 & \cos\theta & -\sin\theta \\ 0 & \sin\theta & \cos\theta \end{bmatrix} \begin{bmatrix} x_2 \\ y_2 \\ z_2 \end{bmatrix} \tag{2a}$$

and

$$\begin{bmatrix} x_2 \\ y_2 \\ z_2 \end{bmatrix} = \begin{bmatrix} \cos\psi & -\sin\psi & 0 \\ \sin\psi & \cos\psi & 0 \\ 0 & 0 & 1 \end{bmatrix} \begin{bmatrix} x_3 \\ y_3 \\ z_3 \end{bmatrix} \tag{2b}$$

Therefore, the complete transformation from body to inertial space is

$$\begin{bmatrix} x_I \\ y_I \\ z_I \end{bmatrix} = A \begin{bmatrix} x_3 \\ y_3 \\ z_3 \end{bmatrix} \tag{3}$$

where

$$A = \begin{bmatrix} (\cos\phi\cos\psi - \cos\theta\sin\phi\sin\psi) & (-\cos\phi\sin\psi - \cos\theta\sin\phi\cos\psi) & (\sin\theta\sin\phi) \\ (\sin\phi\cos\psi + \cos\theta\cos\phi\sin\psi) & (-\sin\phi\sin\psi + \cos\theta\cos\phi\cos\psi) & (-\sin\theta\cos\phi) \\ \sin\theta\sin\psi & -\sin\theta\cos\psi & \cos\theta \end{bmatrix}$$

The inverse transformation is accomplished by

$$\begin{bmatrix} x_3 \\ y_3 \\ z_3 \end{bmatrix} = A^{-1} \begin{bmatrix} x_I \\ y_I \\ z_I \end{bmatrix} \tag{3a}$$

The body rate $\vec{\omega}$ in terms of the Euler rates are

$$\vec{\omega} = \dot{\theta}\ \hat{i}_2 + \dot{\phi}\ \hat{k}_1 + \dot{\psi}\ \hat{k}_3 \tag{4}$$

$$= \omega_{x_3}\ \hat{i}_3 + \omega_{y_3}\ \hat{j}_3 + \omega_{z_3}\ \hat{k}_3$$

Then,

$$\begin{bmatrix} \omega_{x_3} \\ \omega_{y_3} \\ \omega_{z_3} \end{bmatrix} = \begin{bmatrix} \cos\psi & \sin\theta\sin\psi & 0 \\ -\sin\psi & \sin\theta\cos\psi & 0 \\ 0 & \cos\theta & 1 \end{bmatrix} \begin{bmatrix} \dot{\theta} \\ \dot{\phi} \\ \dot{\psi} \end{bmatrix} \tag{5}$$

and

$$\begin{bmatrix} \omega_{x_I} \\ \omega_{y_I} \\ \omega_{z_I} \end{bmatrix} = \begin{bmatrix} \cos\theta & 0 & \sin\theta\sin\phi \\ \sin\phi & 0 & -\sin\theta\cos\phi \\ 0 & 1 & \cos\theta \end{bmatrix} \begin{bmatrix} \dot{\theta} \\ \dot{\phi} \\ \dot{\psi} \end{bmatrix} \tag{6}$$

The equation of motion and the required coordinate transformation have been identified and derived such that the free-body motion can be analyzed.

FREE-BODY MOTION ANALYSIS

For a free-body, symmetric or asymmetric, an analytical solution is realizable. The equations of motion were solved by means of Jacobi's elliptic function (ref. 1), sn(Nt), cn(Nt), and dn(Nt). The solution is analytical and gives the attitude in Euler angles, illustrated in Figure 5, as a function of time.

Symbols

$\tilde{\psi}(t)$ -- the expression for the oscillation about the mean value of ψ.

K -- the complete elliptic integral of the first kind with modulus k.

I -- magnitude of the total angular momentum of the vehicle.

k -- modulus of the elliptic integral of the first kind.

K' -- the complete elliptic integral of the first kind with modulus k'.

k' -- modulus of the elliptic integral of the first kind.

ω_ψ -- mean value of the proper rotation of the vehicle.

ℓ -- a constant for a particular rigid body.

$\tilde{\phi}(t)$ -- the oscillatory term of the velocity of precession.

ω_p -- the mean value of the velocity of precession.

The details of the solution will not be entertained here but are stated in the final form. Reference 1 provides the necessary details of the solution.

Solution

The solution utilized the following initial conditions:

$$\psi_o = \frac{\pi}{2}; \phi_o = 0° \text{ at time } t = 0 \text{ sec.}$$

Also the solutions are good when $I_x > I_y > I_z$ or $I_x < I_y < I_z$. The latter case will be used for the vehicle under analysis.

The proper rotation is defined as ψ and is given by

$$\psi = \frac{\pi}{2} - \omega_\psi t + \tilde{\psi}(t) \tag{7}$$

where

$$\omega_\psi = \frac{\pi N}{2K}$$

$$\tilde{\psi} = \frac{\sqrt{k' \ell}}{k' + \ell} \left(A_1 \sin \frac{\pi N}{K} t - A_2 \sin \frac{2\pi N}{K} t + \cdots \right)$$

$$\ell = \frac{I_y (I_x - I_z)}{I_x (I_y - I_z)}$$

$$k^2 = \frac{I_x (I_x - I_y)}{I_z (I_y - I_z)} \frac{\omega_{x_o}^2}{\omega_{z_o}^2}$$

$$k' = \sqrt{1 - k^2}$$

$$N^2 = \frac{(I_y - I_z)(I_x - I_z)}{I_x I_y} \omega_{z_o}^2$$

$$A_1 = 2 \left(\frac{k' + \ell}{k' - \ell} \right) \left(\frac{k' + \ell - 2\sqrt{k' \ell}}{2\sqrt{k' \ell}} \right)$$

$$A_2 = \left(\frac{k' + \ell}{k' - \ell} \right) \left[1/2 \left(\frac{k' + \ell}{k' - \ell} \right) \left(\frac{k' + \ell - 2\sqrt{k' \ell}}{2\sqrt{k' \ell}} \right) \right] - \frac{k' + \ell}{2\sqrt{k' \ell}}$$

The precessional rotation is defined by ϕ and is given by

$$\phi = \omega_p t + \tilde{\phi}(t) \tag{8}$$

where

$$\omega_p = \frac{I}{2 I_x I_y} \left[(I_x + I_y) - (I_x - I_y) \left(\frac{\sqrt{k'} - \sqrt{\ell}}{\sqrt{k'} + \sqrt{\ell}} \right) \right]$$

$$I = \sqrt{I_x^2 \omega_{x_o}^2 + I_y^2 \omega_{y_o}^2 + I_z^2 \omega_{z_o}^2}$$

$$\tilde{\phi}(t) = -\frac{I(I_x - I_y)}{I_x I_y} \left(\frac{2k'\ell}{k'^2 - \ell^2}\right) \frac{K}{\pi N} \left(A_1 \sin \frac{\pi N}{K} t - A_2 \sin \frac{2\pi N}{K} t + \cdots \right)$$

The nutation is defined as θ and is given by

$$\cos \theta = \frac{I_z \omega_{z_o}}{I} \, dn \, (Nt) \tag{9}$$

where dn (Nt) is the Jacobi elliptic function. N is the lowest frequency component of the nutation, and the exact nutation is represented by a mean value and by harmonics of N. But for the purpose of the analysis, the extent of nutation $\Delta\theta$ and period of the lowest frequency is of interest.

Therefore, $\Delta\theta = \theta_{max.} - \theta_{min.}$

where

$$\text{Cos } \theta_{max.} = \frac{I_z \omega_{z_o}}{I} \sqrt{1 - k^2}$$

$$\text{Cos } \theta_{min.} = \frac{I_z \omega_{z_o}}{I}$$

Symmetric-Body Analysis Results

The analysis was conducted for a body symmetric about the z_3 axis (Figure 5). The inertias for the vehicle analyzed were determined from analysis conducted in ref. 2. The inertias used in this analysis are not the final values given in the report because of iterations in the concept study.

Parameters used in the analysis are

$$I_x = I_y = 54.6 \text{ slug-ft}^2$$

$$I_z = 65.5 \text{ slug-ft}^2$$

$$\omega_{z_o} = 0.312 \text{ radian/second} = \omega_o \cos \eta$$

$$\omega_{x_o} = \omega_o \sin \eta$$

The ω_{z_o} is maintained constant because it is a vehicle requirement.

The objective is to establish the stability of the spacecraft for various inertia ratios-preferred spin axis to the transverse axis. The preferred spin axis is the z_3 principal axis where internal alignment of the vehicle's experiment package is required to minimize the mismatch angles of the experiment and the body principal axis. The experiment axes are assumed to be aligned sufficiently such that the offset angles can be set to zero for analysis purposes.

Stability of a spinning body. -- It is well known that a rigid body which is torque free and spinning about an arbitrary axis will be stable about that axis. However, the spacecraft is not completely rigid and eventually will spin about the maximum moment of inertia axis.

The stability is investigated from an energy point of view. Thomson and Reiter (ref. 3) show that a body which dissipates energy is stable about the maximum moment of inertia. This can be seen in the equation

$$\dot{T} = I_z \omega_o^2 (r-1) \sin\theta \cos\theta \dot{\theta} \tag{10}$$

where

$\dot{T}$ = rate of change of energy

r = inertia ratio = $\frac{I_z}{I_x}$,

ω_o = absolute value of the spin vector, and

θ = cone angle (wobble).

If $\dot{T}$ is negative (energy loss), and for $r > 1$ $\dot{\theta}$ is negative, and for $r < 1$ $\dot{\theta}$ is positive. Therefore, the minimum moment of inertia axis is unstable. Rearranging the equation,

$$\dot{\theta} = \frac{\dot{T}}{I_z \omega_o^2 (r-1) \sin\theta \cos\theta} \tag{10a}$$

Now, if $\dot{T} = -E_o$ (constant), $\dot{\theta}$ decreases for constant energy dissipation as r increases. If $r = 1$, the body has no maximum moment of inertia. For the HDS spacecraft, the inertia must be greater about the preferred spin axis than the transverse axes to assure long-term stability. The inertia ratio should be sufficiently larger than one to provide a margin of safety for the maximum moment of inertia axis.

Moment of inertia calculations on the conceptual spacecraft (ref. 2) has indicated that an inertia ratio of at least 1.2 but not greater than 1.4 can be attained. An inertia ratio of at least 1.2 is recommended.

The cone angle θ is related to the angle η (see Figure 6) by

$$\left.\begin{aligned} \tan\theta &= \frac{I_x}{I_z}\tan\eta \\ \tan\theta &= \frac{1}{r}\tan\eta \end{aligned}\right\} \qquad (11)$$

Assuming η is held constant, it is observed that tan θ is an inverse function of the inertia ratio. The cone angle, or "wobble", approaches zero as r approaches infinity when $\eta < 90°$. This implies greater inertial stability of the maximum principal moment of inertia axis. Equation (11) shows that for $r = 1.2$ the cone angle is nearly equal to η. However, the rate at which the vehicle precesses about the angular momentum vector increases as a direct function of the inertia ratio. That is,

$$\Omega_p = r\,\omega_{z_o} \qquad (12)$$

No constraint is imposed on the upper limit of the inertia ratio for attitude control. But, attitude prediction may require an upper limit for r because of the sampling rate of the attitude measurement device. The attitude determination analysis (ref. 4) shows that at least four star samples per revolution of the vehicle are required to determine attitude. Then, an inertia ratio of four allows one sample per cycle of the precession frequency. Intuitively, 10 samples per cycle of the frequency is desired to determine adequately the motion of a frequency. However, fewer samples can be taken if loss of accuracy can be tolerated. The inertia ratio of 1.2 is well below four, and results for the attitude determination study show that a sampling rate of four is adequate for the accuracy required.

Because the vehicle must maintain its experiment scan vector within ±5° of the orbit plane, a limit on the cone angle must be determined. Figure 7 illustrates the relation of the cone angle as a function of η. The cone angle is smaller than η by a constant factor for $r = 1.2$.

The launch vehicle at separation imparts a 3°/second transverse rate to the spacecraft which creates a half-cone angle of eight degrees. A damper must be employed to reduce the cone angle to a specified level less than five degrees. The level to which the damper must reduce the cone angle will be determined from the asymmetric, torqued-body, and mechanization analyses. The free, symmetric body motion provides an insight to the asymmetric body analysis which follows.

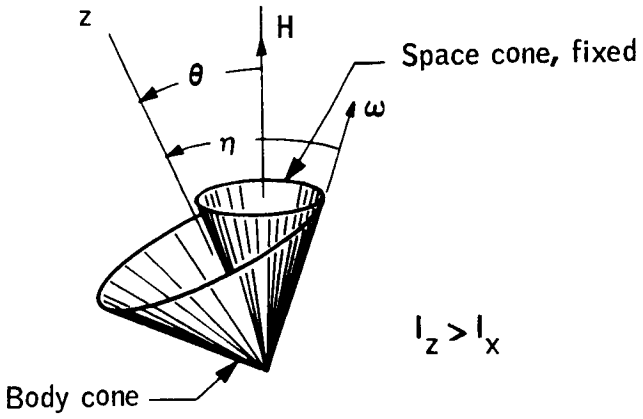

Figure 6. Retrograde Precession of Spin Axis

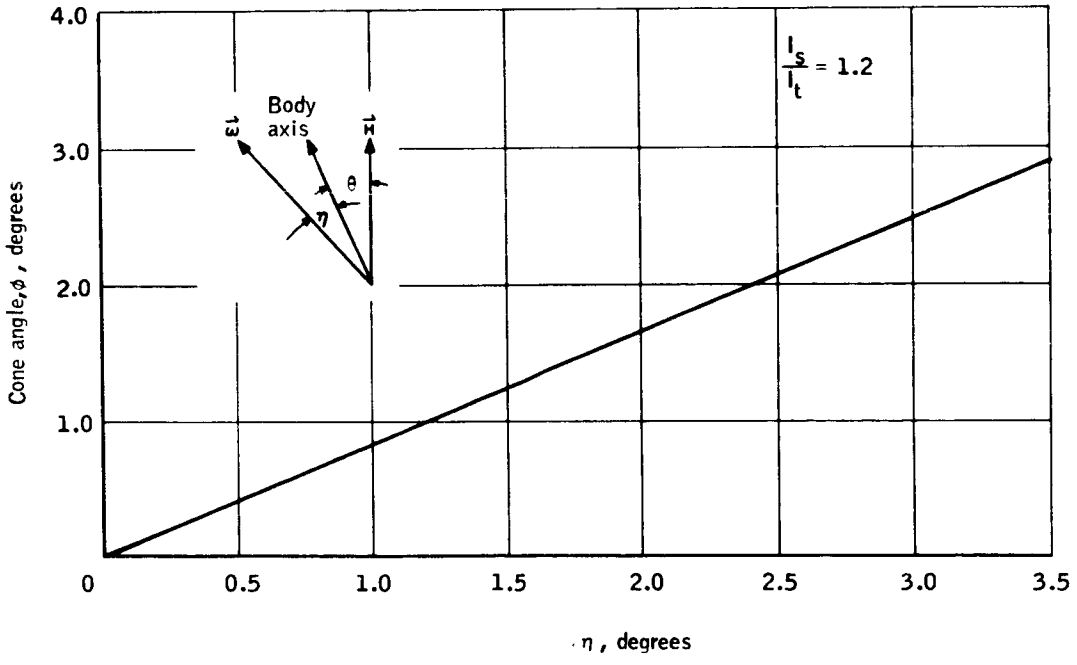

Figure 7. η versus θ

Asymmetric-Body Analysis

In practice an exact symmetrical body cannot be achieved. There is always some small percentage of asymmetry ϵ existing due to limitations on dynamic balancing techniques. The analysis intent is to show the effects of various levels of asymmetry and to draw conclusions as to the effect on attitude control requirements and the attitude prediction task.

The analytical solution given previously is utilized to obtain the characteristics of the asymmetric free-body motion. The parameters involved in the analysis are given below.

I_z = 65.5 slug-ft^2

I_x = $I_o - \epsilon_1$, where I_o = 54.6 slug-ft^2

I_y = $I_o + \epsilon_1$, where I_o = 54.6 slug-ft^2

ω_{z_o} = 3.0 rpm = 0.312 radians/sec

η = 0.0°, 0.5°, 1.0°, and 2.0° body cone angle

ϵ = 0.0%, 0.5%, 1.0%, 2.0%, and 3% of I_o

ϵ_1 = 100 I_o ϵ

Extent of nutation. -- The extent of nutation is the difference between maximum and minimum cone angle θ. It was calculated as a function of ϵ for various angles η. The results are shown in Figures 8, 9, and 10. Figure 8 shows for ϵ = 0.5-percent asymmetry that the extent of nutation is 45.0 seconds of arc and that it increases rapidly to 289 seconds of arc for ϵ = 3.0-percent asymmetry. Figures 9 and 10 show that the cone angle θ and the extent of nutation increases directly with η.

The attitude control function is not significantly affected by the extent of nutation for asymmetry up to three percent, because the extent of nutation is small in comparison to the requirement of maintaining preferred spin axis within ±5 degrees of the orbit normal. The attitude control is adequately represented by symmetrical-body formulation insofar as extent of nutation of a three percent or less asymmetric body is concerned.

However, the attitude determination model must include the asymmetry. The extent of nutation is such at 0.5-percent asymmetry and η = 0.5 degrees that the asymmetry of the vehicle must be represented in the attitude determination model. The model must predict the attitude of the vehicle within 10 seconds of arc.

In conclusion, the vehicle should be as dynamically balanced as well as existing equipment and facilities will permit to minimize the effects of asymmetry on attitude determination.

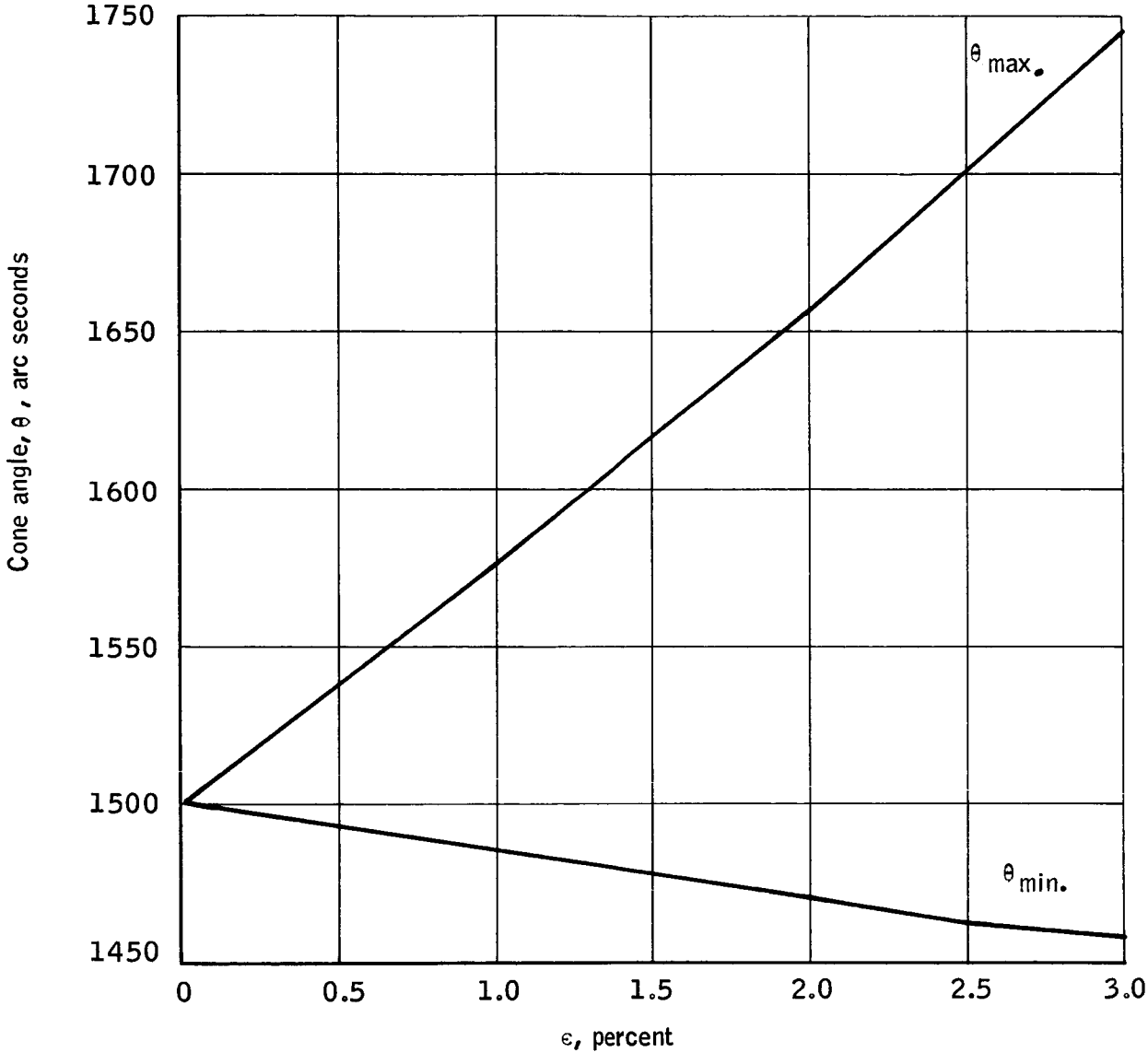

Figure 8. Extent of Nutation When $\eta = 0.5$

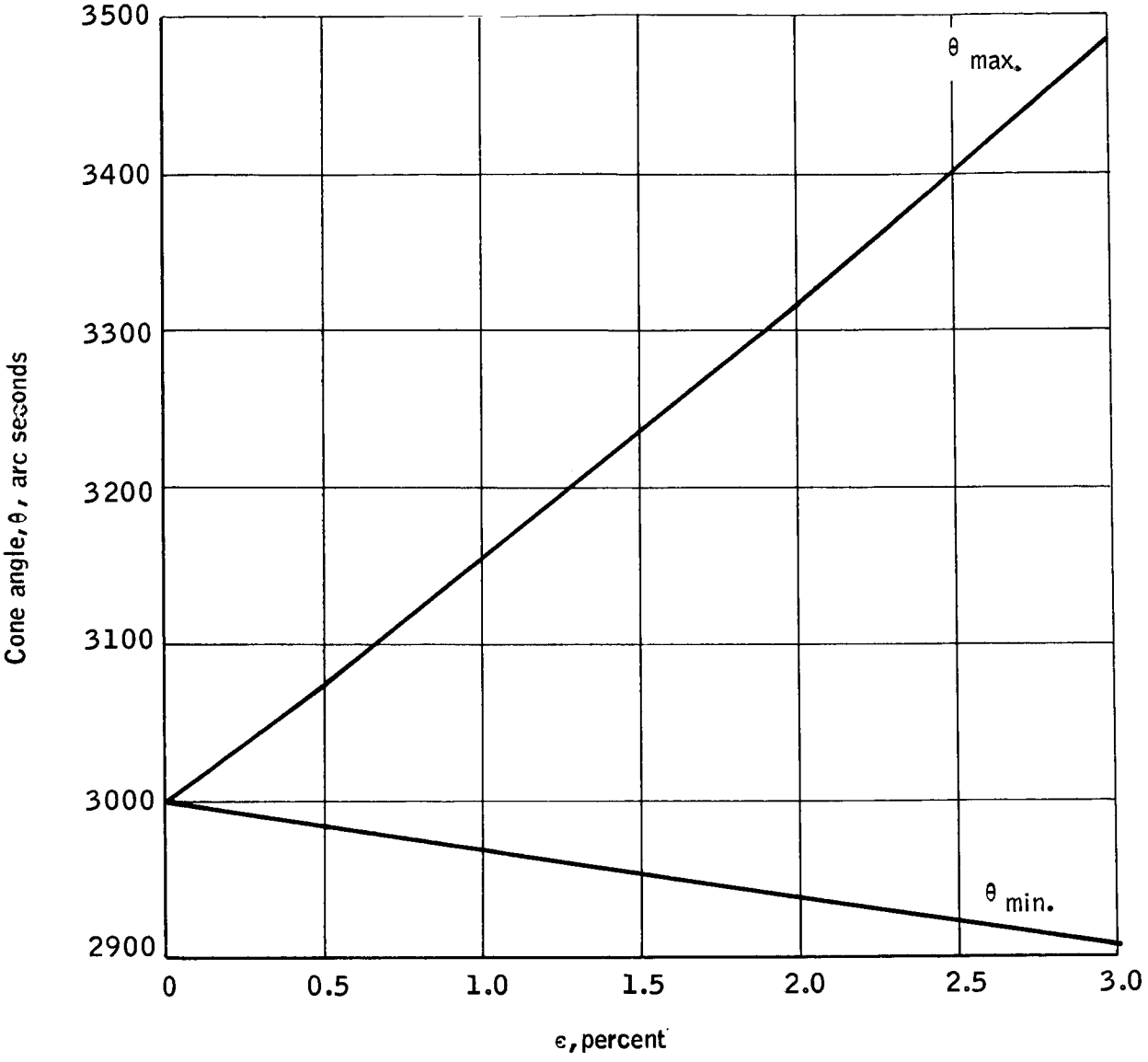

Figure 9. Extent of Nutation When $\eta = 1.0$

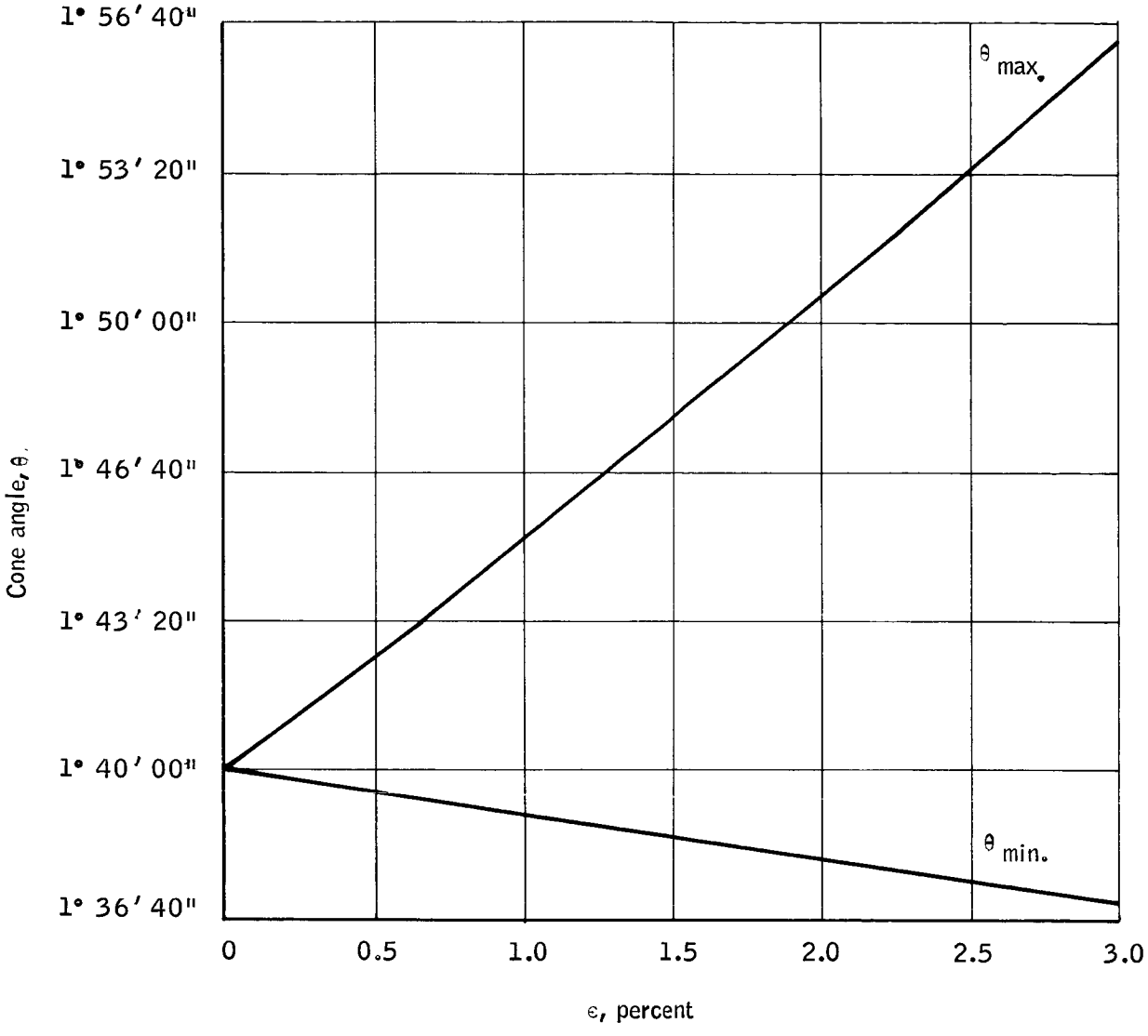

Figure 10. Extent of Nutation When $\eta = 2.0$

Nutation and precession periods. --

Nutation period: The nutation period is the time for the extent of nutation to complete one cycle from a minimum to a maximum. Figure 11 illustrates the results. The period is not a function of the angle η but rises rapidly as a function of body asymmetry. The period has increased 1.1 sec from ϵ = 0.0 percent to a body of 3.0-percent asymmetry. The spin period is approximately one fifth that of the nutation period.

The attitude control model is not required to account for small variations in the nutation period of at least up to 3.0 percent asymmetry.

Attitude determination again must include asymmetry because the prediction must be good to 10 seconds of arc.

Precession period: The precession period is the mean time required for the principal z_3 axis to traverse one revolution about the angular momentum vector. Figure 12 illustrates that the mean precession period is a function of ϵ and η. Notice the difference in the periods for the three values of η. The period shortens more rapidly as η becomes larger.

Attitude determination must have a knowledge of the changes in η. Attitude control subsystems should provide a damper to maintain a small η to minimize the variation of the precession period. If the damper is maintained operative during the data cycle, the model of the damper will have to be included in the attitude determination. On the other hand, a damper which is inoperative during the data cycle is desired because attitude determination accuracy is improved when fewer parameters are involved.

The torqued-body analysis will determine the feasibility of a part-time operative damper.

Precession rate: Figures 13 and 14 illustrate the effect of various degrees of body asymmetry on the precession rate. A plot of the precession rate $\dot{\phi}$ as a function of time is illustrated. The rate varies with the body asymmetry but not with the angle η. The mean spin period of the body z_3 axis is near 20.0 seconds. Then, during one revolution of the vehicle, the precession rate will vary by approximately 0.0106 rad/sec for ϵ = 1 percent when η = 0.5 degree or η = 1.0 degree.

Body rate: Another illustration is made in Figures 15 and 16 showing variation of the body z_3 axis rate as a function of time. The extent of the rate variation is a function of the body asymmetry alone. The asymmetry causes a shift in the mean rate with a sinusoidal variation about the mean. For purposes of accurate prediction of attitude, the objective again would be to minimize the body asymmetry.

It is realized that the vehicle will not be completely free of the asymmetry, but it can be dynamically balanced within state-of-the-art limits.

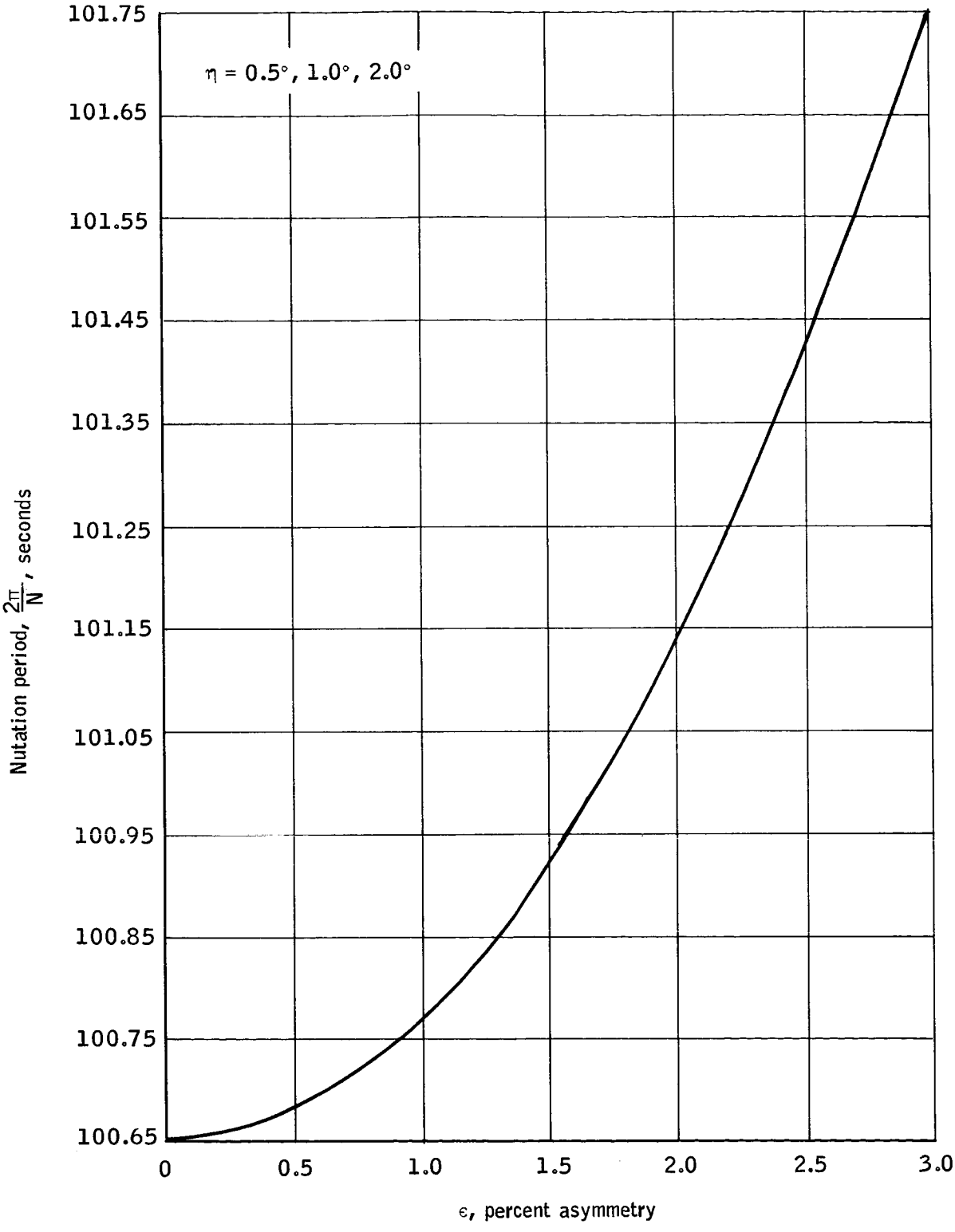

Figure 11. Period For One Cycle of Nutation

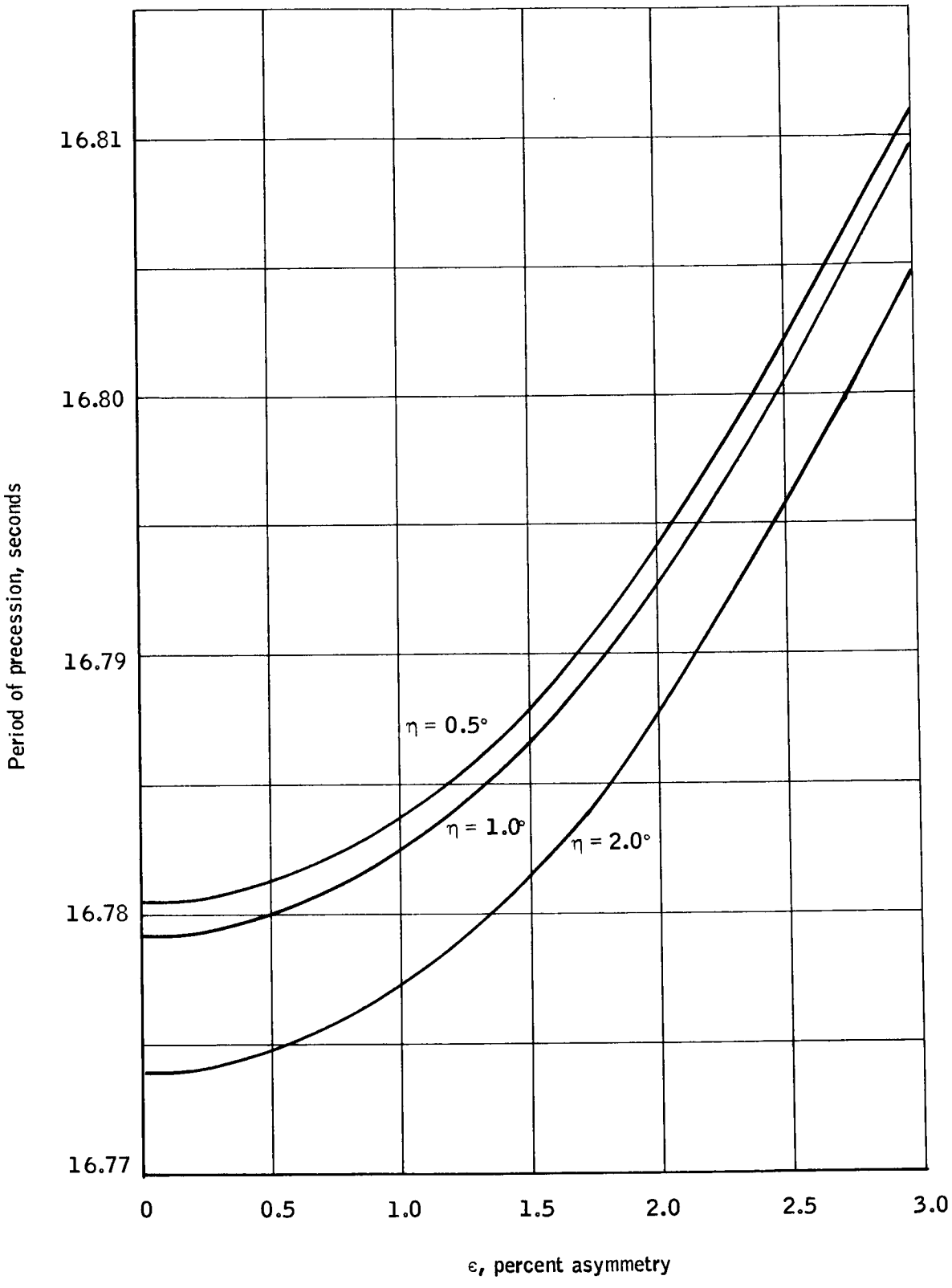

Figure 12. Period For One Cycle of Precession

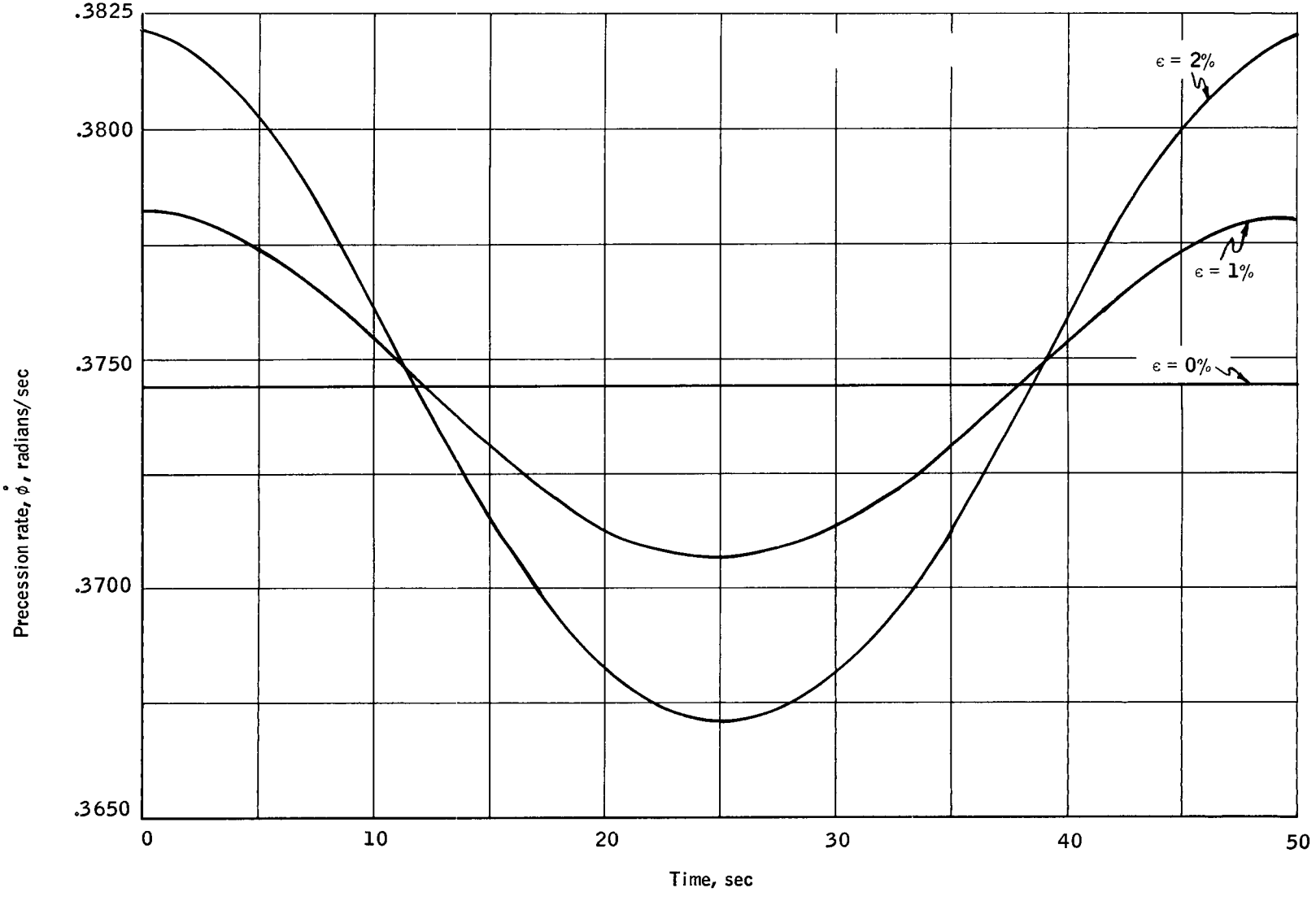

Figure 13. Precession Rate When $\eta = 0.5$

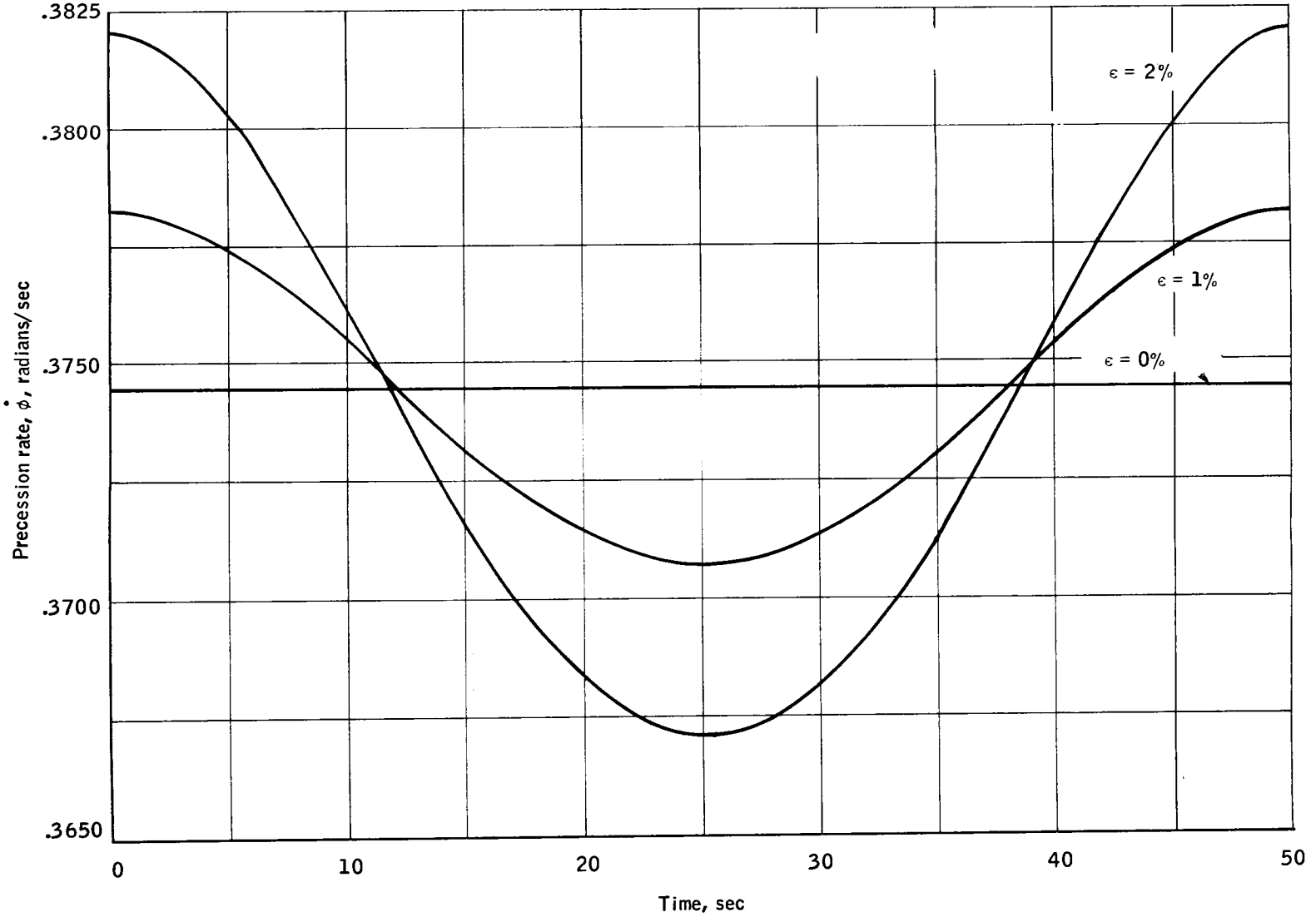

Figure 14. Precession Rate When η = 1.0

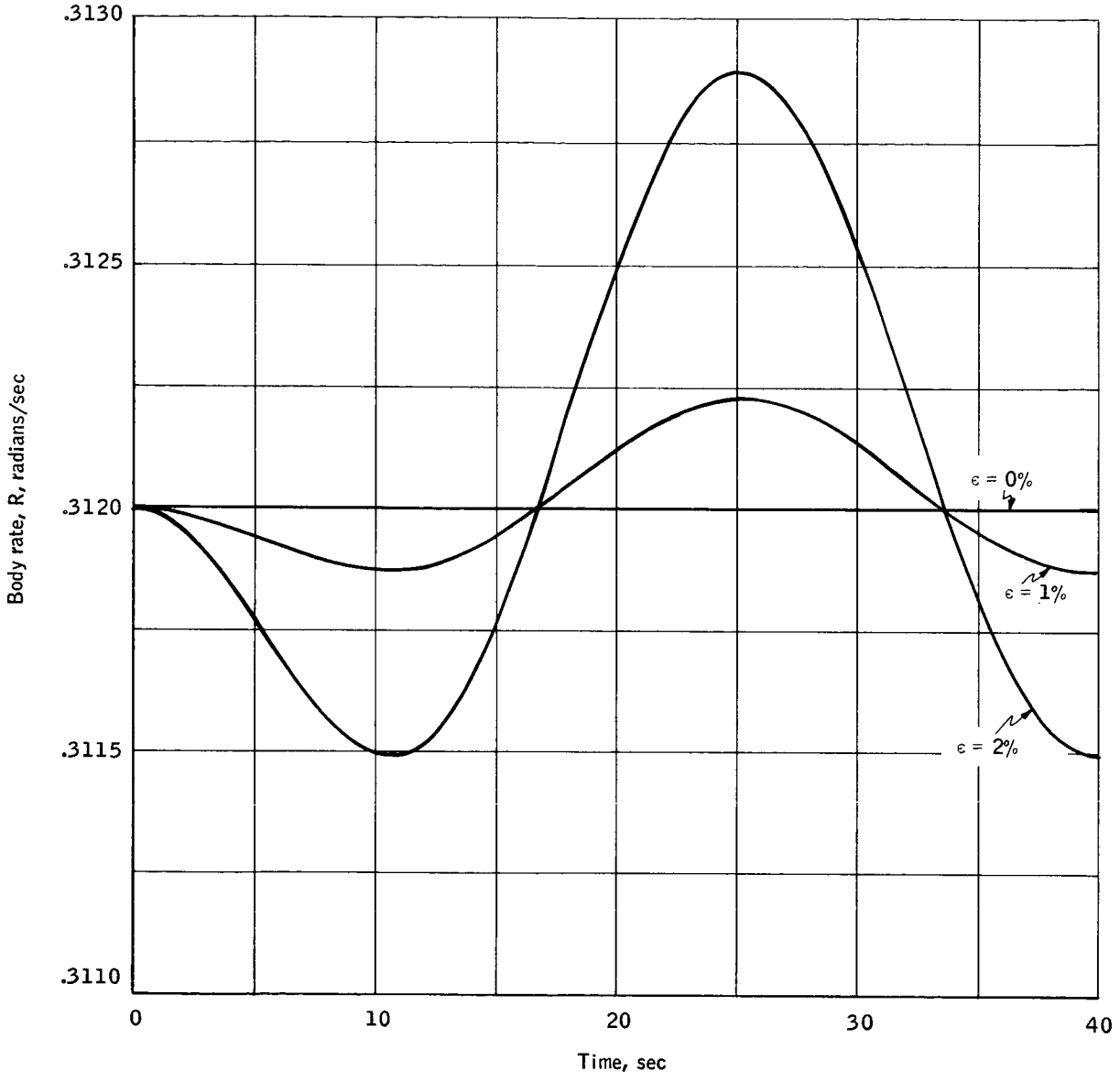

Figure 15. Z Body Rate When η = 0.5

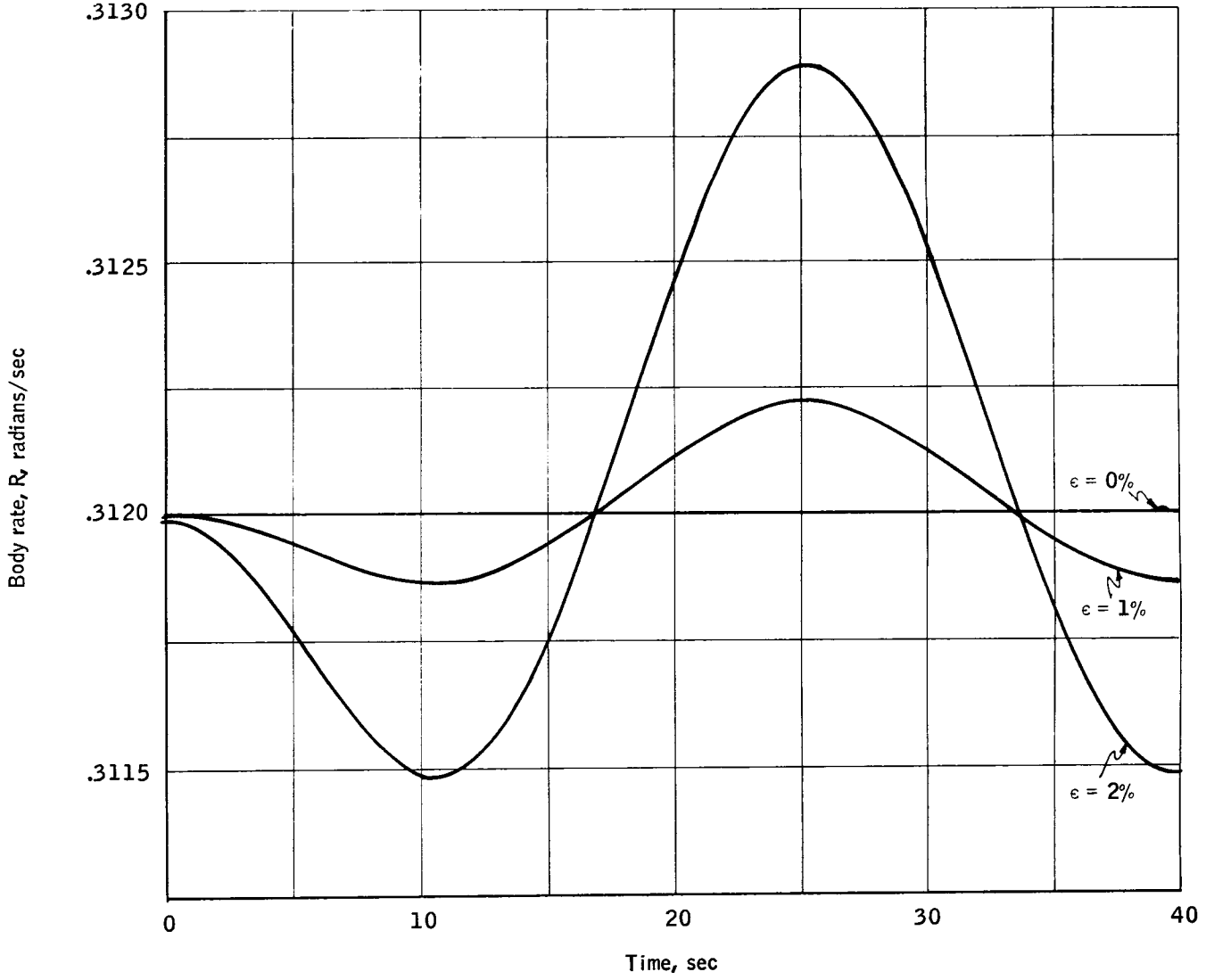

Figure 16. Z Body Rate When $\eta = 1.0$

Asymmetry due to spacecraft inertia variation. -- Cryogenic coolant sublimation will cause changes in the inertia. A worst-case sublimation effect would be for the asymmetry to change by the maximum amount of transverse axis inertia change. Assuming this, asymmetry would become approximately 0.3 percent. The affect of 0.3 asymmetry is not sufficient to warrant the inclusion of asymmetry in the attitude control model, but it must be included in the attitude prediction model. The 0.3-percent asymmetry is assumed to occur over a one-year time span and is also assumed to change linearly. The attitude prediction model can easily handle the long time constant variations.

The analysis has been conducted on the assumption that the experiment axes are perfectly aligned to the principal axes. Alignment techniques are sufficiently accurate that small misalignment, e.g., 0.5 degree, causes insignificant effects as far as attitude control is concerned. The attitude determination model must include the misalignment of the experiment axes. The alignment angles are discussed in ref. 4.

Summary of Free-body Motion Analysis

The analysis was conducted for a symmetric, spinning cylinder whose inertia ratio I_s/I_t is greater than one. The objective was to determine the characteristic motion of this specific body. Secondly, the analysis extended to the asymmetric spinning body (transverse inertia very nearly equal).

The results of the symmetric body analysis indicate that:

- Motion is stable about the maximum moment of inertia, assuming small perturbation to the vehicle.

- Computation of the inertia of the vehicle indicates that an inertia ratio of 1.2 can be obtained. The analysis shows that the vehicle is stable for $r = 1.2$ due to a flexible body.

- Tip-off rates and other perturbations require that a cone-angle damper be supplied to damp the initial spin vector to coincide nearly with the preferred spin axis. The damper will be required to remove approximately eight degrees of half-cone angle that was generated by the maximum booster tip-off rates. The operational plan provides for two orbits of damping prior to performing mission. The preferred spin axis is the principal moment of inertia y axis. Small misalignment of the experiment axes are assumed.

The results of the asymmetric body motion shows

- That the extent of nutation $\Delta\theta$ is a direct function of η the angle of the spin vector to the body principal axis (Figures 8, 9, and 10).

- That the variation in precession rate and body rate, is independent of η but is very dependent on the asymmetry of the vehicle (Figures 13, 14, 15, and 16).

- That for a body spin period of 20 seconds, the period of the extent of nutation (Figure 11) is the same as the period of nutation and is greater than 100 seconds and is a function of the asymmetry and η. The period of nutation is the time required for the spin vector to complete one cycle in the body.

- That body asymmetry up to three percent can be tolerated without significant effect on the attitude control of the HDS spacecraft. However, for attitude prediction accuracies the asymmetry should be minimized because asymmetry produces variations in the frequencies of motion of the vehicle and results in degradation of the attitude determination. It is well within state of the art for dynamic balancing techniques to balance to one percent. It is then recommended that the spacecraft be balanced as well as the state of the art allows to minimize complex motion. The design intent is to have a vehicle spinning about a preferred vehicle body axis. Since an exact coincidence is not possible, the objective is to design the vehicle to spin as near to the preferred spin axis as possible.

- The attitude control math model can be adequately represented by a symmetric body, providing the asymmetry is less than three percent.

- The attitude prediction model must include asymmetry effects regardless of the level of asymmetry.

MODEL OF ENVIRONMENTAL TORQUES FOR THE HDS SPACECRAFT

The model for the environmental torques is discussed in detail in Appendix A. The ensuing discussion will summarize the torques derived.

The task of modeling the torques involved the identification of the torques, derivation of the torques in principal body coordinates, calculations of coefficients which are dependent on the vehicle's configuration, and estimation of coefficients which are calculated from the vehicle's characteristics.

The torques experienced by the vehicle in a near-earth polar orbit are

- Solar pressure
- Aerodynamic pressure
- Gravity gradient
- Meteoroid disturbance
- Rotating internal equipment
- Vehicle outgassing disturbance
- Magnetic interaction
  - Eddy current
  - Residual magnetic moment

Solar Pressure

The results of the derivation (Appendix A) showed that the particle radiation pressure is more than an order of magnitude less than the electromagnetic radiation pressure. Particle radiation pressure was, therefore, neglected.

A constant pressure of 1×10^{-7} lb/ft^2 was used for a surface normal to the sun line with no variation due to solar activity. For the present the reflectivity and absorptivity properties of the vehicle were not established due to continuing concept iteration. The vehicle is assumed to be completely absorbing.

The torque in body coordinates is represented by

$$\tau_B = C^{-1} \tau_E \qquad (13)$$

where τ_E is the torque expressed in experiment coordinates and τ_B is in body principal coordinates, and C is the transformation from body to experiment axes. The torque in experiment axes is

$$\tau_E = \begin{bmatrix} S_o\, j_E\, k_E & (\ell_y A_y - \ell_x A_x) \\ 0 & \\ -S_o\, i_E\, j_E & (\ell_y A_y - \ell_x A_x) \end{bmatrix} \tag{14}$$

where S_o is the magnitude of the pressure.

$$\begin{bmatrix} i_E \\ j_E \\ k_E \end{bmatrix} = CE \begin{bmatrix} i_I \\ j_I \\ k_I \end{bmatrix} \tag{15}$$

and E is the transformation from inertial coordinates to body principal coordinates.

The transformations C and E are expressed by

$$C(\epsilon_1, \epsilon_2, \epsilon_3) = \begin{bmatrix} (\cos\epsilon_3\cos\epsilon_1 - \sin\epsilon_1\sin\epsilon_2\sin\epsilon_3) & (\sin\epsilon_1\cos\epsilon_3 + \cos\epsilon_1\sin\epsilon_2\sin\epsilon_3) & (-\sin\epsilon_3\cos\epsilon_2) \\ (-\sin\epsilon_1\cos\epsilon_2) & (\cos\epsilon_1\cos\epsilon_2) & \sin\epsilon_2 \\ (\sin\epsilon_3\cos\epsilon_1 + \sin\epsilon_1\sin\epsilon_2\cos\epsilon_3) & (\sin\epsilon_3\sin\epsilon_1 - \cos\epsilon_1\sin\epsilon_2\cos\epsilon_3) & (\cos\epsilon_2\cos\epsilon_3) \end{bmatrix} \tag{16}$$

$$E(\psi, \phi, \theta) = \begin{bmatrix} (\cos\theta\cos\psi - \sin\psi\sin\phi\sin\theta) & (\sin\psi\cos\theta + \cos\psi\sin\phi\sin\theta) & (-\sin\theta\cos\phi) \\ (-\sin\psi\cos\phi) & (\cos\psi\cos\phi) & \sin\phi \\ (\sin\theta\cos\psi + \sin\psi\sin\phi\cos\theta) & (\sin\theta\sin\psi - \cos\psi\sin\phi\cos\theta) & (\cos\phi\cos\theta) \end{bmatrix} \tag{17}$$

The surface areas and moments were computed, and the coefficient

$S_o = 1 \times 10^{-7}$ lbs/ft^2 was used to determine

$$\tau_{E_x} = 0.8 \times 10^{-5} \; j_E \, k_E$$

$$\tau_{E_y} = 0$$

$$\tau_{E_z} = -0.8 \times 10^{-5} \; j_E \, k_E$$

The solar torque was determined for solar aspect angles of 30 to 65°.

Aerodynamic Torque

The aerodynamic pressure generates a torque on the vehicle when a yaw angle of attack is present.

Appendix A shows that the tangential pressure component does generate a torque when the vehicle geometric axis is at an angle to the orbit normal. Also, the coefficients are not the same for yaw angles of opposite signs. Torque equations were derived for two cases: $F_{y_E} \leq 0$ and $F_{y_E} > 0$. This corresponds to the positive and negative angle of attack attitude, respectively.

If $F_{y_E} \leq 0$,

$$\tau_E = \begin{bmatrix} 2.8064 \times 10^{-5} \; j_E \, k_E \text{ ft-lbs} \\ 0 \\ -8.4224 \times 10^{-5} \; i_E \, j_E \text{ ft-lbs} \end{bmatrix} \tag{14a}$$

If $F_{y_E} > 0$,

$$\tau_E = \begin{bmatrix} 1.0061 \times 10^{-5} \; j_E \, k_E \\ -8.102 \times 10^{-6} \; j_E \, k_E \\ 8.102 \times 10^{-6} \; j_E \, j_E \; - 1.9389 \times 10^{-5} \; i_E \, j_E \end{bmatrix} \tag{14b}$$

Gravity Gradient

A gravity-gradient torque on the vehicle is due to the variation of the earth's gravity field with altitude. The HDS vehicle, with an inertia ratio of greater than one and an attitude error in roll or yaw, will experience a gravity-gradient torque. The torque is given by

$$T_{x_N} = \frac{3G}{R^3}(I_y - I_x) \sin\phi \cos\psi \cos\phi \qquad (18)$$

where ϕ and ψ are roll and yaw principal body angles relative to inertial space, respectively, R is the distance from the center of the earth to the vehicle, and G is the universal gravitational constant.

Meteoroid Disturbance Torque

The equivalent pressure force of the meteoroid impacts is 5.89×10^{-10} lb/ft^2 which is several orders of magnitude below solar radiation pressure (1×10^{-7} lb/ft^2).

To evaluate the effects of meteoroid impacts on the vehicle, it is assumed that the vehicle will respond to each individual impact, and that there is no cancelling of momentum due to omni-directional impact. Each impact, therefore, will induce an impulsive step input into the vehicle body rates. A magnitude 9 meteoroid travelling at 72 km/sec will induce an impulse of 8.5×10^{-2} lb-sec to the vehicle. The probability of encountering smaller meteoroids increases, but the individual impact effect decreases. For this analysis, 8.5×10^{-2} lb-sec will be considered maximum. The step impact into each vehicle body rate is given as

$$\left.\begin{aligned} \Delta\omega_y &= \frac{0.085\ell_1}{I_y} \\ \Delta\omega_x &= \frac{0.085\ell_2}{I_x} \\ \Delta\omega_z &= \frac{0.085\ell_3}{I_z} \end{aligned}\right] \qquad (19)$$

where

ℓ_1, ℓ_2, ℓ_3 are the impact moment arms (currently 2.25 feet), and

I_x, I_y, I_z are the vehicle moments of inertia.

Rotating Internal Equipment

Rotating equipment within the HDS spacecraft will induce opposing rotational motion. Start-up acceleration will impart impulse torque to the vehicle. The HDS spacecraft experiment package contains the only moving parts which must be analyzed. The radiometer contains three shutters which are intended to operate once per revolution of the vehicle. The shutters are part of the radiometer calibration and impart step-input torques to the vehicle. The shutters return to their initial position at the end of the calibration period (approximately 300 milleseconds). Computation for the resultant impulse gave 0.0018 to 0.063 in.-lbs-sec. However, the orientation of this motion relative to the spacecraft body axes is not entirely defined. Appendix A shows that the impulse could be significant in one orbit period, depending on the alignment of the torque. This may require that radiometer calibration actuation torques be compensated.

Vehicle Outgassing Disturbance

Outgassing from the vehicle produces an unpredictable disturbance torque on the vehicle. Sources of outgassing torques are

- Trapped air in crevices and joints.
- Reaction-jet valve leakage.
- Cooling system outgassing.

Trapped air pockets in crevices and joints will produce an exponentially decaying torque. While the magnitude of this torque cannot be easily determined, its decay is rapid, and it may be considered negligible.

The HDS spacecraft does not use reaction jets. Therefore, no torque can be considered.

The cooling system employed by the experiment package is the only source of outgassing. Appendix A shows that this torque amounts to incorporating only 0.044 ft-lbs-seconds of momentum over one year. Therefore, this disturbing force may be neglected.

Magnetic Interaction

Residual magnetic moment. -- A disturbance torque will exist due to the interaction of the magnetic moment of the spacecraft and the earth's magnetic field. The torque is given by

$$\vec{T} = \vec{M} \times \vec{B} \tag{20}$$

In body axes this is

$$\left.\begin{aligned} T_{x_m} &= M_y B_z - B_y M_z \\ T_{y_m} &= M_z B_x - B_z M_x \\ T_{z_m} &= M_x B_y - B_x M_y \end{aligned}\right] \tag{21}$$

where

M_x, M_y, M_z are the body axis residual magnetic moments, ft-lb/gauss, and

B_x, B_y, B_z are body axis components of the earth's magnetic field, gauss.

The residual magnetic moment is normally given in units of amp-turns-meters^2, which can be converted into ft-lb/gauss directly.

Eddy-current torques. -- Eddy-Current disturbance torques are due to the spacecraft rotating in a magnetic field. The torque retards vehicle spin and produces a precession of the spin axis. The general expression is given by

$$\vec{T} = K (\vec{\omega} \times \vec{B}) \times \vec{B} \tag{22}$$

Expanding in body principal axes gives

$$\left.\begin{aligned} T_{x_E} &= -K\left[(B_y^2 + B_z^2)\,\omega_x - (B_x B_y \omega_y + B_x B_z \omega_z)\right] \\ T_{y_E} &= -K\left[(B_x^2 + B_z^2)\,\omega_y - (B_x B_y \omega_x + B_y B_z \omega_z)\right] \\ T_{z_E} &= -K\left[(B_x^2 + B_y^2)\,\omega_z - (B_x B_z \omega_x + B_y B_z \omega_y)\right] \end{aligned}\right\} \quad (23)$$

Summary of Environmental Torque Model

The environmental torques have been derived and discussed in the preceding paragraphs. The significance of the torques as they pertain to the HDS spacecraft are investigated and the results are presented in the ensuing section.

The effects on the motion of the spacecraft of the solar pressure, gravity gradient, aerodynamic pressure, and magnetic torques were investigated by adding to the free-body equations. However, several other torques were examined in a cursory fashion and found to have insignificant effect on the motion of the spacecraft. These torques - internal rotating equipment, cryogenic outgassing, and meteoroid impact - should be reviewed as the spacecraft design becomes firm. Further analysis should also be made to determine how the meteoroid impact should be incorporated in the equation of motion.

ANALYSIS OF TORQUED BODY-MOTION

An analysis of the influence of disturbance torques on vehicle motion was performed to determine requirements for the attitude control system, bounds on candidate vehicle spin rates, and a base for the attitude determination model. Since the attitude control system may not correct attitude continuously, but rather update attitude at periodic intervals, the magnitude of spin axis decay and spin axis precession defines the interval between control update periods.

Computer Program

The analysis of torqued-body motion was conducted using a digital computer program. A block diagram of the program is shown in Figure 17. The rigid body equations which were programmed were derived from the well-known relationship that the torque exerted on a rigid body is equal to the rate of change of the body's momentum. This is expressed as

$$\vec{T} = \frac{d\vec{H}}{dt} + \vec{\omega} \times \vec{H} \qquad (24)$$

where

$\vec{T}$ = torque exerted on the body

$\vec{H}$ = momentum of the body

$\vec{\omega}$ = angular velocity of the body

These equations are

$$\left.\begin{aligned} T_x &= I_x \dot{p} - I_{xy}(\dot{q} - rp) - I_{yz}(q^2 - r^2) - I_{xz}(\dot{r} + pq) - (I_y - I_z)\,qr \\ T_y &= I_y \dot{q} - I_{xy}(\dot{p} - qr) - I_{yz}(\dot{r} - pq) - I_{xz}(r^2 - p^2) - (I_z - I_x)\,rp \\ T_z &= I_z \dot{r} - I_{xy}(p^2 - q^2) - I_{yz}(\dot{q} + rp) - I_{xz}(\dot{p} - qr) - (I_x - I_y)\,pq \end{aligned}\right\} \qquad (25)$$

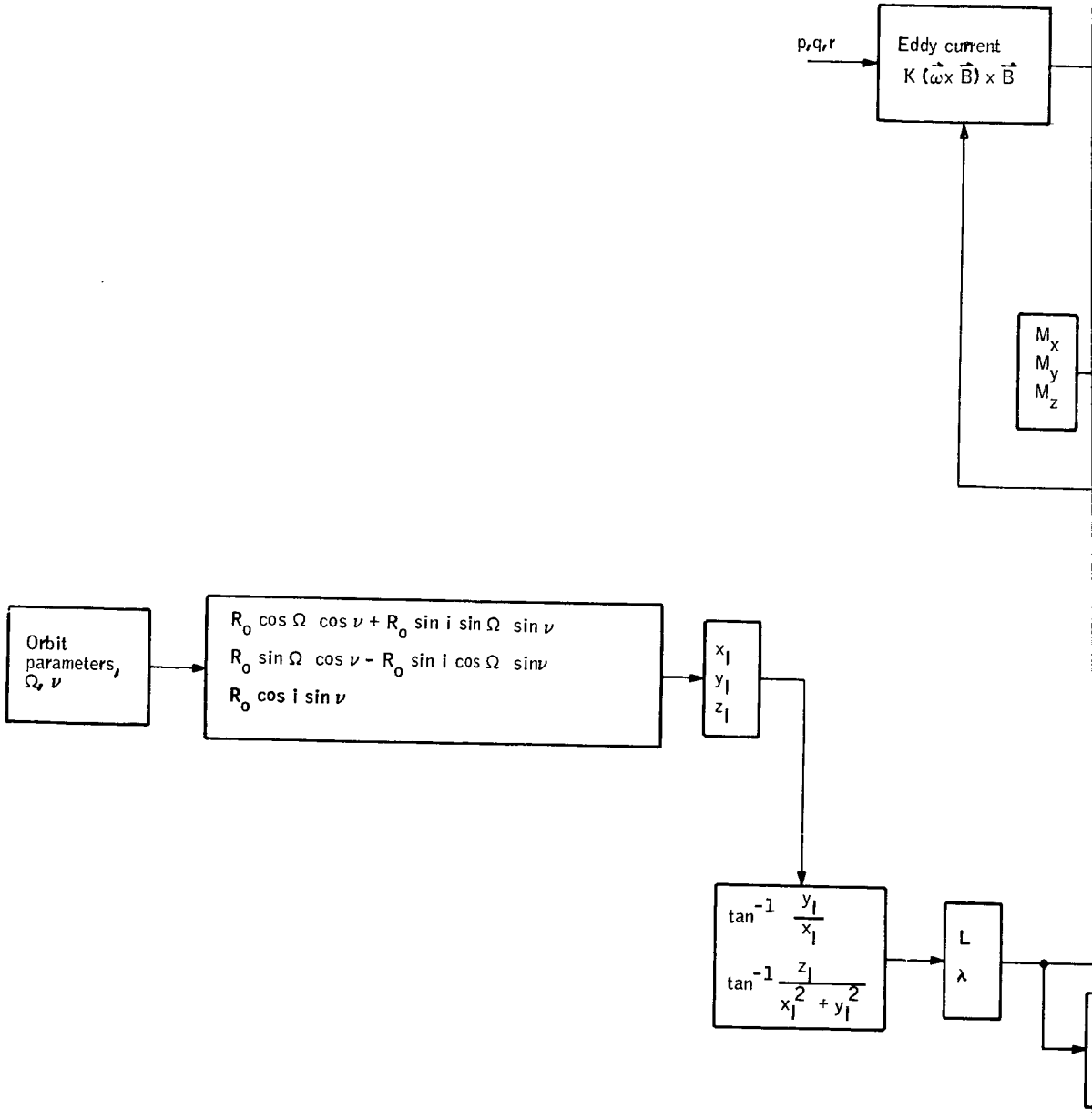

Figure 17. Torqued Bod

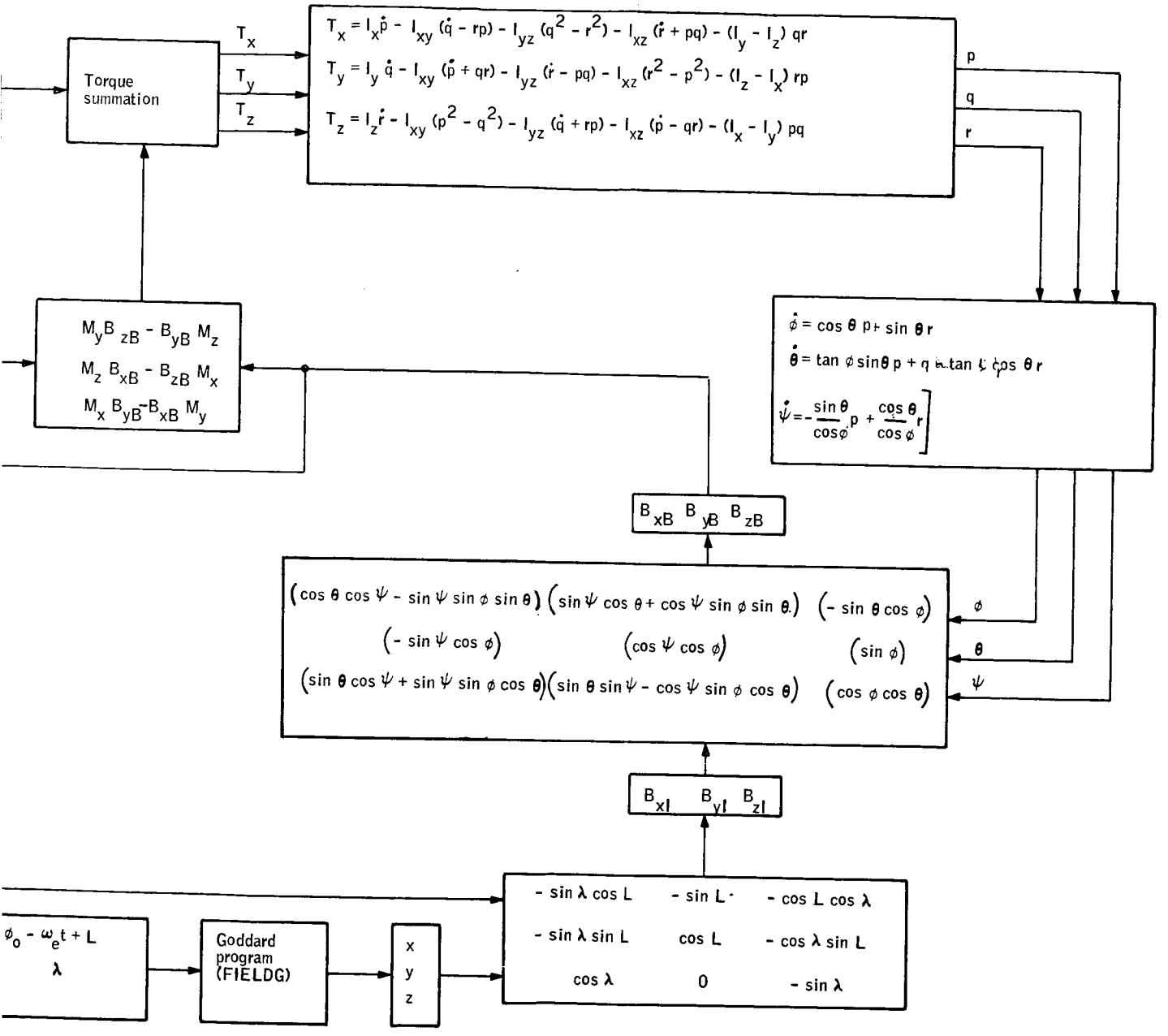

ly Motion Analysis Computer Program

where

T_x, T_y, T_z = body torques in x, y, z axes

p, q, r = roll, pitch, yaw body rates

I_x, I_y, I_z = moment of inertia

I_{xz}, I_{yz}, I_{xy} = product of inertia

The above equations are inverted to give the expressions for $\dot{p}$, $\dot{q}$, and $\dot{r}$.

The Euler angle rate derivation resulted from a rotation sequence of ψ, ϕ, θ. This rotation avoids the singularity which occurs as θ goes through large angles.

The Euler rate equations for the ψ, ϕ, θ sequence are

$$\left.\begin{aligned} \dot{\phi} &= p \cos\theta + r \sin\theta \\ \dot{\theta} &= p \tan\phi \sin\theta + q - r \tan\phi \cos\theta \\ \dot{\psi} &= -p \frac{\sin\theta}{\cos\phi} + r \frac{\cos\theta}{\cos\phi} \end{aligned}\right] \qquad (26)$$

where ϕ, θ, ψ = roll, pitch, yaw Euler angles as shown in Figure 18.

The body components of the various disturbance torques were equated to T_x, T_y, and T_z. Solution of the equations of motion on the computer yielded p, q, r, ϕ, θ, and ψ.

To determine the effects of the earth's magnetic field interacting with the vehicle magnetic moment and generating of eddy currents, the NASA Goddard program FIELDG was obtained. The earth's latitude and longitude are necessary as inputs to the Goddard earth's field program. A nominal orbit is assumed to find this with $\Omega = 45°$, $i = 7.38°$, an altitude of 500 km, and a period of 94.62 minutes. The inertial axes x_I, y_I, z_I have their origin at earth's center with z_I toward the North Pole and x_I toward the First Point of Aries. The rotations through Ω and i to the orbit plane determined by x_o, z_o are shown in Figures 19 and 20.

The above two rotations give the following equations for the inertial coordinates of the vehicle in terms of the orbit parameters:

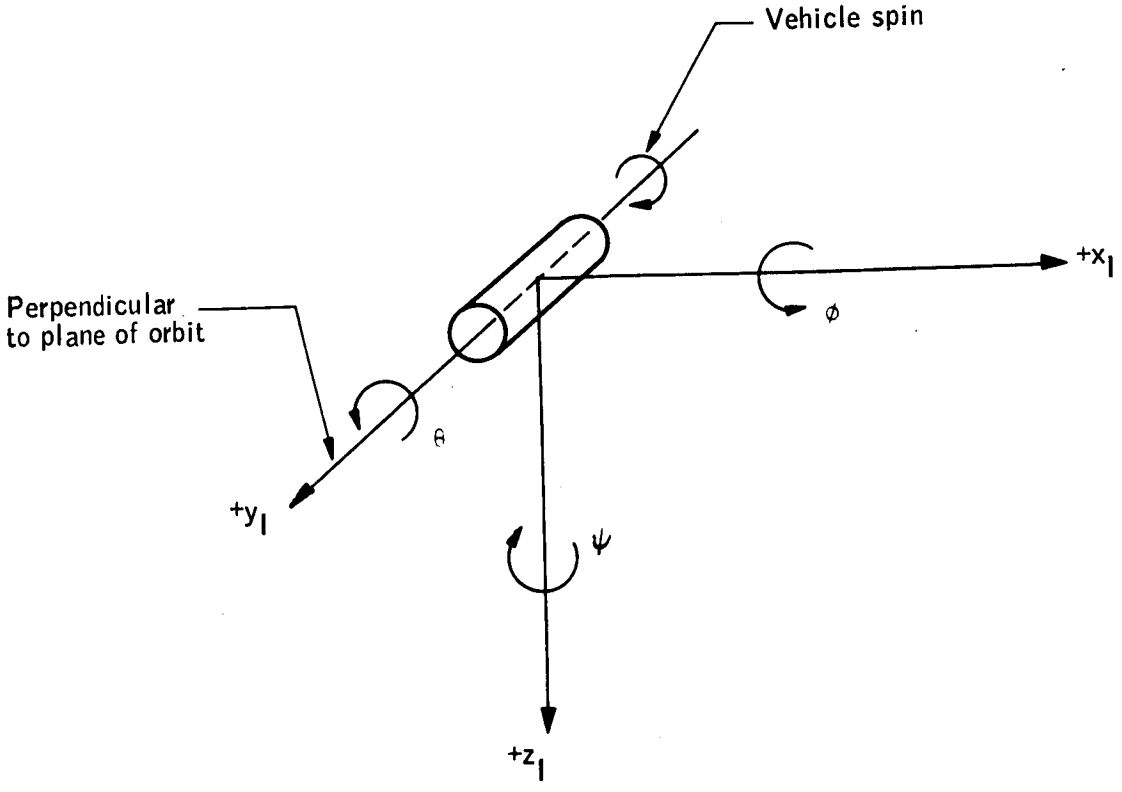

Figure 18. Reference Coordinate System for Body Axis Relative to Inertial Frame

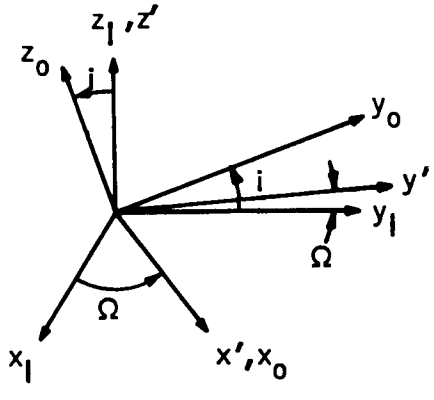

Figure 19. Reference Coordinate System for the Spacecraft Orbit Relative to Inertial Frame

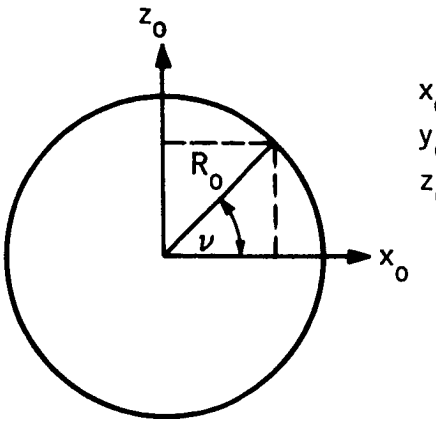

$x_0 = R_0 \cos \nu$
$y_0 = 0$
$z_0 = R_0 \sin \nu$

$\nu_0 = \omega_0 t + \nu_0$ radians

For 94.62 min period, $\omega_0 = 0.00110674$ rad/sec

Figure 20. Spacecraft Position in the Orbit Plane

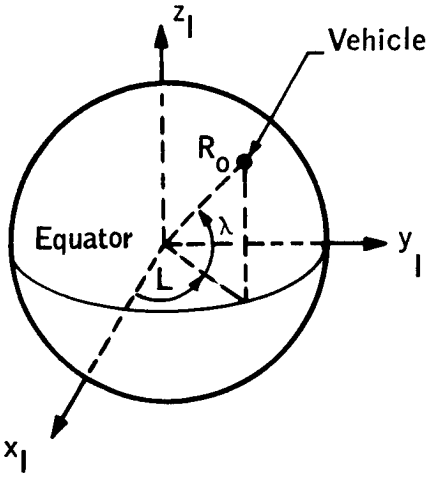

Figure 21. Spacecraft Position Relative to Inertial Space in Terms of Latitude and Longitude

$$\left.\begin{aligned} x_I &= R_o \cos \Omega \cos \nu + R_o \sin i \sin \Omega \sin \nu \\ y_I &= R_o \sin \Omega \cos \nu - R_o \sin i \cos \Omega \sin \nu \\ z_I &= R_o \cos i \sin \nu \end{aligned}\right] \qquad (27)$$

The inertial angles L and λ (respectively RL and RLAM in program) are then determined by

$$L = \tan^{-1} \frac{y_I}{x_I} \qquad (28)$$

$$\lambda = \tan^{-1} \frac{z_I}{x^2_I + y^2_I} \qquad (29)$$

as seen in Figure 21.

Then

earth latitude (DLAT) = λ

and

earth longitude = $\phi_o - \omega_e t + L$ (30)

where

ϕ_o = longitude of First Point of Aries at $t = 0$, and

ω_e = earth's rotation rate .

Additional input for the field routine FIELDG are the altitude in km, the epoch TM, the degree of series expansion + 1 = NMX, and L (previously set $\neq 0$ to read in coefficient data cards). Outputs from the routine give the earth's field in gammas (10^{-5} gauss) in north (x), east (y), and downward (z) components as well as the total field F.

These field components are converted to inertial field components by the equations

$$\left.\begin{aligned} B_{x_I} &= -y \sin L - (x \sin \lambda + z \cos \lambda) \cos L \\ B_{y_I} &= y \cos L - (x \sin \lambda + z \cos \lambda) \sin L \\ B_{z_I} &= x \cos \lambda - z \sin \lambda \end{aligned}\right] \qquad (31)$$

These are converted to body coordinates by the equations

$$\left.\begin{aligned}
B_{x_B} &= (\cos\theta\cos\psi - \sin\psi\sin\phi\sin\theta)\,B_{x_I} \\
&\quad + (\sin\psi\cos\theta + \cos\psi\sin\phi\sin\theta)\,B_{y_I} - \sin\theta\cos\phi\,B_{z_I} \\
B_{y_B} &= -\sin\psi\cos\phi\,B_{x_I} + \cos\psi\cos\phi\,B_{y_I} + \sin\phi\,B_{z_I} \\
B_{z_B} &= (\sin\theta\cos\psi + \sin\psi\sin\phi\cos\theta)\,B_{x_I} \\
&\quad + (\sin\theta\sin\psi - \cos\psi\sin\phi\cos\theta)\,B_{z_I} + \cos\phi\cos\theta\,B_{z_I}
\end{aligned}\right\} \quad (32)$$

Then assuming a spacecraft magnetic moment of $M_x = M_y = M_z = -0.516 \times 10^{-4}$ ft-lb/gauss, the equations for body coordinate torques T_x, T_y, and T_z are

$$\left.\begin{aligned}
T_x &= M_y B_{z_B} - B_{y_B} M_z \\
T_y &= M_z B_{x_B} - B_{z_B} M_x \\
T_z &= M_x B_{y_B} - B_{x_B} M_y
\end{aligned}\right\} \quad (33)$$

Also terms are added to the above three equations to account for the eddy-current effects.

Results of Torqued-Body Analysis

Analysis of the disturbance torques indicates that solar pressure, gravity gradient, vehicle outgassing, and aerodynamic torques are small compared to magnetic interaction and eddy-current torques. Meteoroid impact torques are impulsive and unpredictable, and must be handled in the attitude determination model as impulsive changes to body rates. In addition, the rotating elements in the radiometer calibration system could impose large coning motions if symmetric balancing was not employed.

In this analysis, the major continuous torques considered are the magnetic-interaction torque and the eddy-current torque. A nominal residual magnetic moment of 1.0 amp-turns-m^2 and an eddy-current conductivity coefficient of 2.86×10^{-5} ft-lb-sec/$gauss^2$ were used. The 1.0 amp-turn-m^2 residual magnetic moment was of the order of magnitude experienced by the earlier Tiros satellites. The residual on the HDS spacecraft is expected to be less because of the symmetrically illuminated solar panel configuration. The eddy-current coefficient is based on the average spin-down rates of previous operating satellites. The 1.0 amp-turn-m^2 moment was assumed to be 45° tothe three body axes. The 1.0 amp-turn-m^2 is resolved into the body axes and converted to ft-lbs/gauss. The disturbed motion of the vehicle was determined parametrically for 3, 4, and 5 rpm. The spin-rate decay resulting in a time-varying pitch attitude change is shown in Figure 22. As the spin rate increases, the pitch attitude change due to eddy-current torques increases. The combined influence of magnetic interaction and eddy currents, however, causes the spin-axis precession to decrease as spin rate is increased. This is shown in Figure 23 for a period of one orbit. By projecting through multiple orbits, as shown in Figure 24, the spin-axis precession will accumulate to five degrees in 55 or 72 orbits for spin rates of 3 or 4 rpm, respectively. This assumes that no attempt is made to balance continuously the observed residual magnetic moment or orbit regression by applying a balancing current to the attitude update magnetic coils. Spin-rate decay will amount to a five-percent decrease in about 125 orbits due primarily to eddy-current torque effects. This then provides a basis for establishing requirements on the attitude control systemand update interval. In addition, the form and magnitude of the motion provides a basis for the attitude determination model.

Summary of Analysis of Torqued-Body Motion

The results of the analysis were

- A mathematical description of the significant disturbance torques for use in the attitude determination model was completed. The major torques are the magnetic interaction torque and the eddy-current torque.
- A spin rate of three rpm was selected because of the minimum composite effect of residual and eddy-current torque on the pointing vector prediction. Further, the lower spin rate increases the energy received by the radiometer on each interception of the horizon.
- Spin rate need be updated only once every 125 orbits to keep spin rate within five percent of nominal.
- Attitude correction due to spin axis precession needs updating once per 55 orbits if the residual moment is not compensated. With compensation for residual moment and orbit regression, the update period can possibly be extended to 300 orbits.
- Magnetic torques cause no significant increase in cone angle over a period of four orbits.

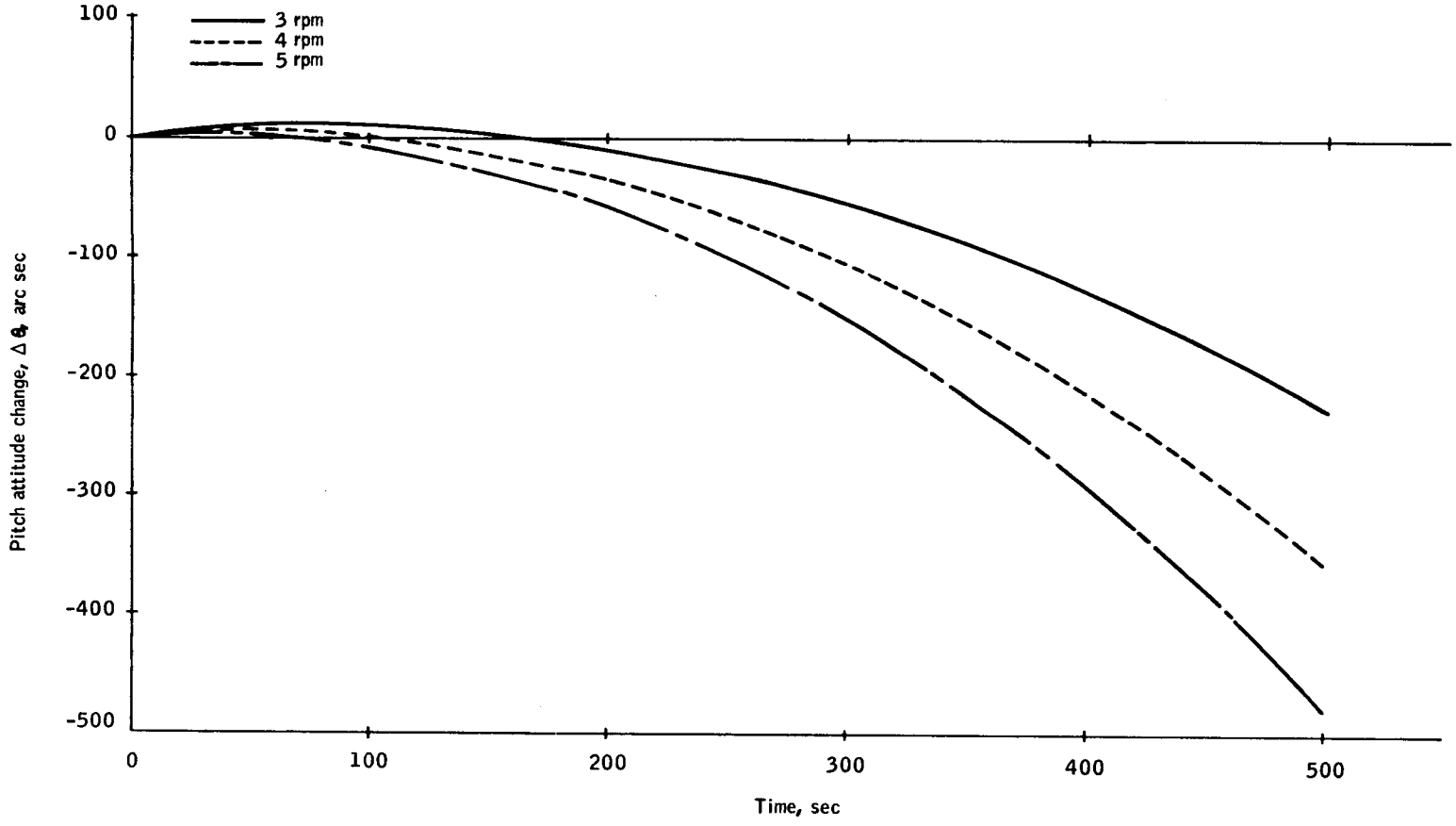

Figure 22. Magnetic Moment and Eddy-Current Torque Effects on Body Pitch Attitude as a Function of Time

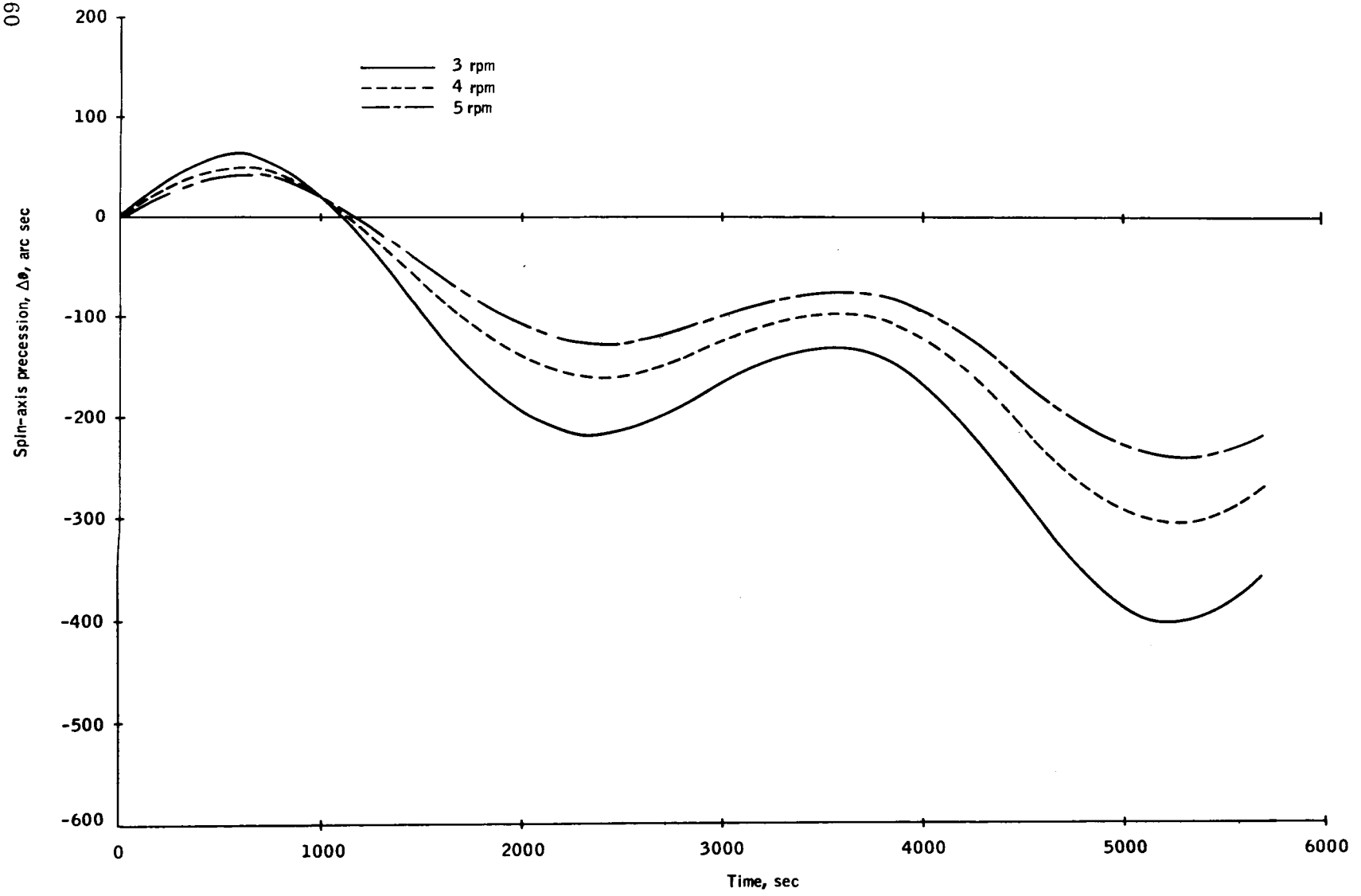

Figure 23. Magnetic Moment and Eddy-Current Torque Effects on Spin-Axis Attitude as a Function of Time, One Orbit

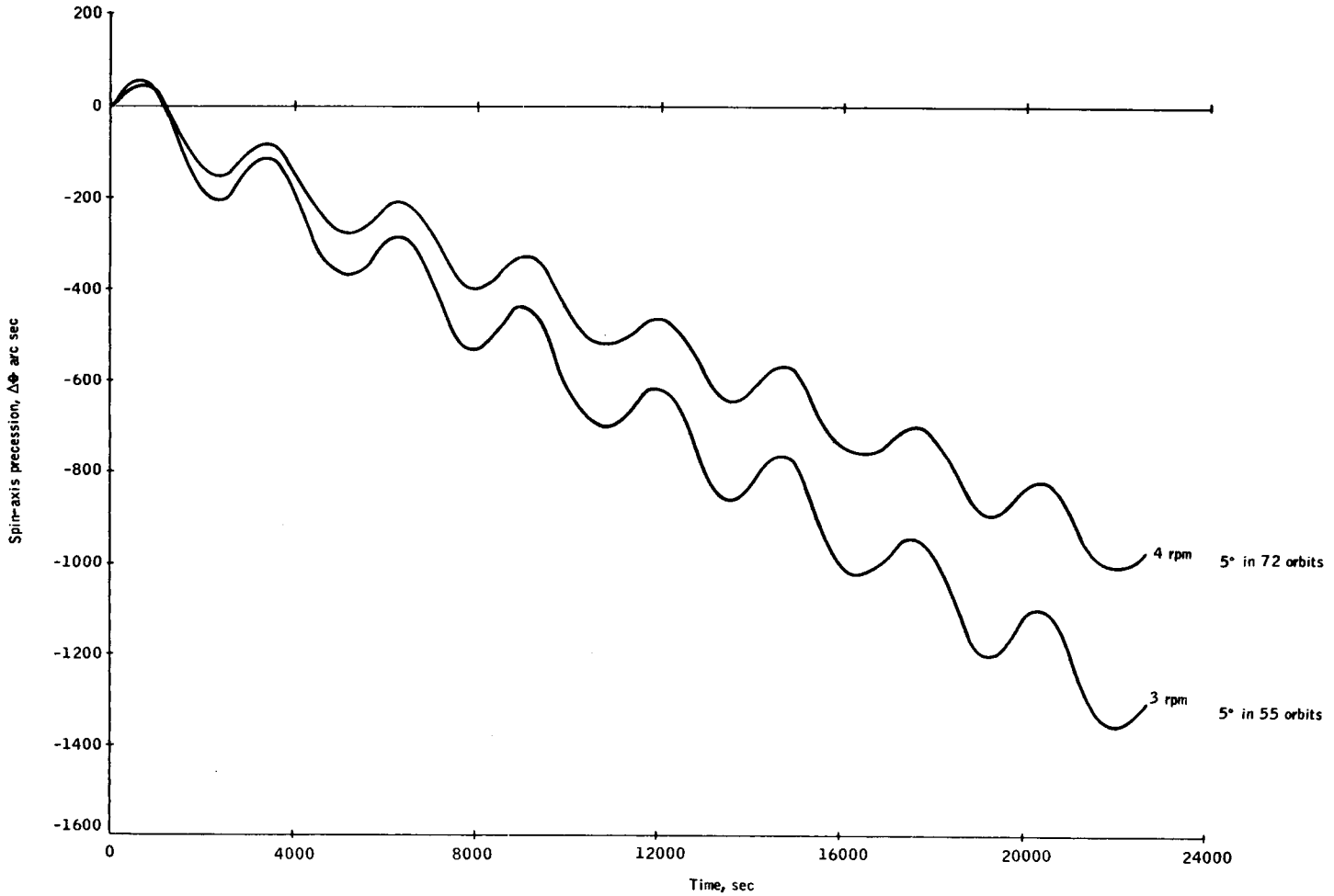

Figure 24. Magnetic Moment and Eddy-Current Torque Effects on Spin Axis Attitude as a Function of Time, Several Orbits

ATTITUDE CONTROL SUBSYSTEM CONCEPT STUDY

CONCEPT SUMMARY OF ATTITUDE CONTROL SUBSYSTEM

The attitude control subsystem for HDS is a simple, part-time, ground-commanded, magnetically torqued control system which reacts with the earth's magnetic field.

The HDS satellite derives its basic attitude stability from the gyroscopic properties of the spinning body. Because of this and the experiment requirements, an active control system is not required continuously, and the subsystem will only be used when necessary to correct attitude. The desired attitude for HDS is with the spin axis normal to the orbit plane. Disturbance torques such as gravity gradient, solar pressure and magnetic moment will cause the spin axis to drift from this desired orientation. Because of attitude determination observations and radiometer pointing, it is desired to keep the spin axis within ±5 degrees. Also no torques are to be applied during attitude determination observations; therefore, the attitude control subsystem will be normally de-energized. The spin control portion of the ACS will be operated in the same manner. Attitude and spin rate will be monitored by ground personnel who will decide when the attitude and spin rate are to be corrected.

The attitude control subsystem consists of four units

- V-head horizon sensor (14- to 16-micron CO_2 band)
- Logic control unit
- Three torquer coils
- Passive damper

A block diagram of the subsystem is shown in Figure 25.

The V-head sensor provides information to determine the angle between the spin axis and the normal to the orbit plane, the coning angle, and to commutate the spin control coil. The sensor will measure the angle between the spin axis and the local horizontal plane. This angle is determined by comparing the earth intercept periods of the two heads. The difference in the two periods is an indication of the roll angle. As shown in the block diagram, the difference in periods is found by counting up on an up-down counter when one head intercepts the earth and counting down when the other head intercepts the earth. The remaining count is proportional to the local roll angle. This measured roll angle is observed for a period of time to determine the relationship of the spin axis to the orbit plane normal.

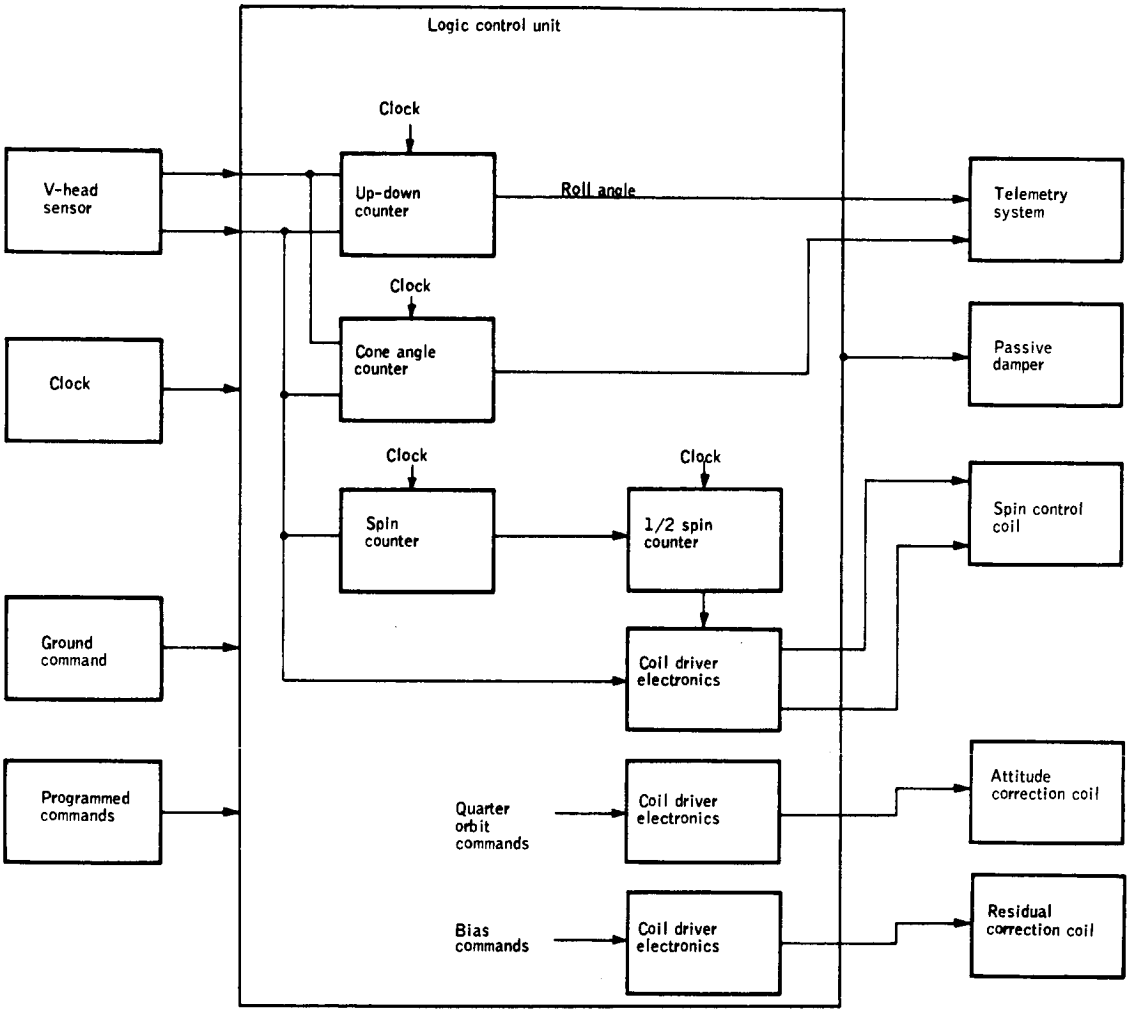

Figure 25. Attitude Control Subsystem Block Diagram

The V-head sensor can also provide cone angle information. This is found by noting the difference in on-times of the two heads. One head starts the count and the other head stops the count. This will be measured on every revolution of the spacecraft for a period of time. The roll angle will be essentially constant over this period; therefore, variations in this reading will be due to the cone angle. A curve fitting can then determine the magnitude of the angle.

The V-head sensor also provides the information necessary to commutate the current in the spin-control coil. The output of one head initiates a counter at the first "on-time" and stops it on the second "on-time." A right shift is performed on the counter, and the contents are transferred to the 1/2 spin counter which is counted down by the clock. The output of the head accomplishes one current change, and the output of the 1/2 spin counter accomplishes the second current change one-half spin cycle later. The spin-control coil is oriented in the vehicle so that the current change occurs at the proper time relative to the magnetic field.

The logic control unit contains the counters indicated above plus the logic necessary to perform the required operations. It also contains the coil driver electronics. These consist of a bridge-type circuit for reversing the current through the coil and adjusting the current level.

The control coils are air-core coils wound on frames which are oriented in the spacecraft to generate a magnetic field as required for control torques. The attitude and residual correction coil can be wound on the same frame and oriented so that the plane of the coil is perpendicular to the spin axis of the spacecraft. The residual coil also provides the required moment for orbit regression compensation. The spin-control coil is oriented so that its plane is parallel to the spin axis and is 68 degrees from the optical axis of the V-head sensor. This provides the proper orientation so that the current will be switched when the plane of the coil coincides with local vertical.

The passive damper is used to reduce the coning angle which may be introduced by the separation of the spacecraft from the booster. As indicated, the damper is designed to remove this energy passively. Extrapolation of data from presently designed and tested dampers indicate that damping the spacecraft to 0.5 degrees is quite feasible.

A summary of the weight, size, and power consumption is shown in Table 2.

A summary of estimated failure rates and reliabilities for the ACS is given in Table 3.

TABLE 2. - ATTITUDE CONTROL PHYSICAL DESCRIPTION

Component	Weight, pounds	Volume, cu in.	Power, watts
V-head sensor, redundant	10.0 (5 each)	256 (128 each)	1.0
Logic and control unit, redundant	16.0 (8 each)	460 (230 each)	4.0
Attitude correction coil	8.0	130	3.0
Residual correction coil	2.0	30	0.5
Spin control coil	3.0	60	1.5
Passive damper	4.0	192	
Totals	43.0	1128	10.0

TABLE 3. - ATTITUDE CONTROL SUBSYSTEM RELIABILITY

ACS component	Failure rate	Operating hours	Single reliability	Redundant reliability
V-head sensor	7.02×10^{-6}	8760	.94	.9981
Logic and control unit	8.16	8760	.93	.9974
Residual coil	0.1	8760	.9991	---
Spin and attitude coil	0.2	60	.9999	---
Passive damper	1.6	6	.99999	---

The total system reliability without use of redundancy is 0.873.

With redundancy the reliability is 0.9945.

Operational Plan

This operational plan delineates the procedure for the attitude control functions during initial orientation of the spin axis and for attitude error and spin rate corrections.

Initial orientation. -- The operational plan is based on having the booster orient the spacecraft spin axis normal to the orbit plane. The orientation is expected to be within two degrees of the normal. Before separating the spacecraft from the booster, the solar panels are extended and the spacecraft is spun to three rpm ± five percent by the spin table on the Delta stage.

With a tip-off rate of three degrees per second and a spin rate of three rpm, the spacecraft will be precessing with a half-cone angle of eight degrees. The sequence of operation is shown in Figure 26. All commands for attitude control will be transmitted from the College station.

Upon separation of the spacecraft from the booster the passive damper is activated. One full orbit has been allowed for damping of the coning motion. Attitude and spin rate measurements are made for approximately 2/3 of an orbit, so that, the data can be read out at the second pass over the College station. The deviation of the spin axis from normal should not exceed five degrees, so one correction period should be adequate to correct the attitude as well as the spin rate. The desired corrections are computed on the ground and transmitted to the spacecraft on the third pass over the College station.

After torquing has been completed, an attitude measurement by the V-head sensor of approximately 20 minutes can be transmitted to College on the fourth pass. The passive damper will be deactivated at this time. Spacecraft attitude will then be monitored for a period of 10 to 12 orbits to determine the magnetic moment of the spacecraft. The command to cancel the residual moment can then be made in the 16th orbit or the 12th pass over College. If the drift during the 10 to 12 orbits has been large, it may be desirable to correct the attitude before starting to take data.

Orbital operations. -- The output of the V-head sensor will be monitored every two minutes during an orbit. In addition, every reading (three per minute) of the V-head sensor will be monitored for a 10-minute period prior to passing over the College station. The readings taken during the 10-minute period will provide knowledge of the coning angle. Spin rate will also be monitored.

When it is determined that an attitude and/or a spin rate correction is required, the command will be transmitted from the College station. The command will select the proper time delay required for the orbital conditions and the correction required.

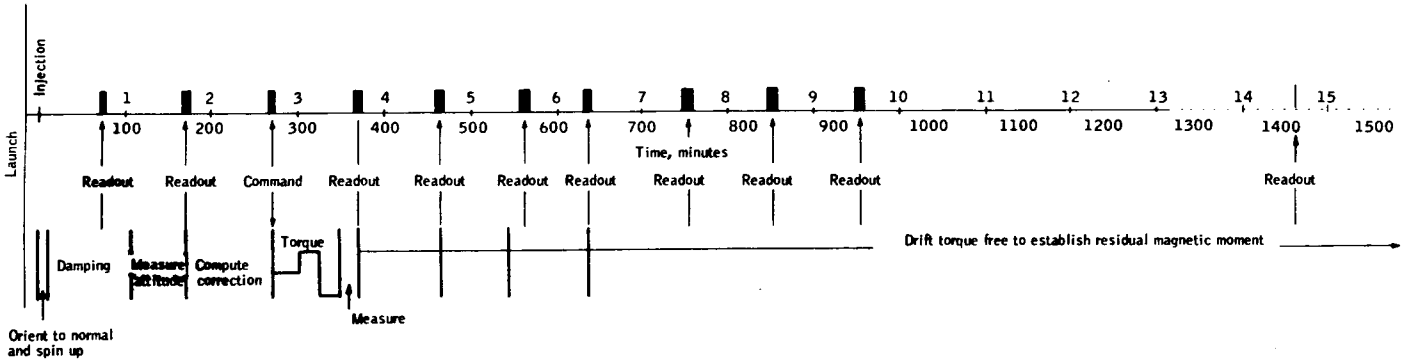

Figure 26. Operational Plan For Attitude Control

Attitude Computation with V-head Sensor

Computation method. -- A V-head horizon sensor configuration has been recommended for the HDS. A sketch of the sensor is shown in Figure 27. The details of the attitude error computation are discussed in this section. See Appendix B for details of the V-head horizon sensor concept.

The V-head sensor consists of two sensing elements operating in the 14- to 16-micron, CO_2 absorption band, each having a small field of view. The optical axis of each sensor is positioned, so that, it intercepts the earth's horizon on each revolution of the spacecraft. The optical axes are at equal angles on either side of the spin plane. When there is no roll error, the interception time of the horizon is the same on both sensors. When a roll error is present the interception time differs in the two sensing elements. Thus the difference in time is an indication of the roll error. The geometry concerned with determining roll error is shown in Figure 28.

From the spacecraft, the line of sight to the horizon forms the surface of a cone (earth cone - half angle of 68 degrees for 270 n. mi. altitude). The optical axis of the sensor also forms the surface of a cone (sensor cone) at right angles to the earth cone for no roll error. The half cone angle is designated in Figure 28. The computation consists of determining the time that the sensor cone and the earth cone intersect. The time can be determined from knowledge of the angle θ_s and time for one revolution. The angle θ_s can be determined from

$$\cos \theta_s = \frac{\cos 68^\circ - \cos \phi_s \sin \phi_e}{\sin \phi_s \cos \phi_e} \tag{34}$$

where

ϕ_s = angle of optical axis to spin axis

ϕ_e = roll attitude error angle

θ_s = 1/2 the intercept angle

This is found by expressing the optical axis of one of the sensing elements by the vector $\vec{R}_o$.

$$\vec{R}_o = \sin \phi_s \sin \theta_s = \hat{x}_I + (\cos \phi_s \cos \phi_e - \sin \phi_s \cos \theta_s \sin \phi_e)\, \hat{y}_I + (\cos \phi_s \sin \phi_e + \sin \phi_s \cos \theta_s \cos \phi_e)\, \hat{z}_I \tag{35}$$

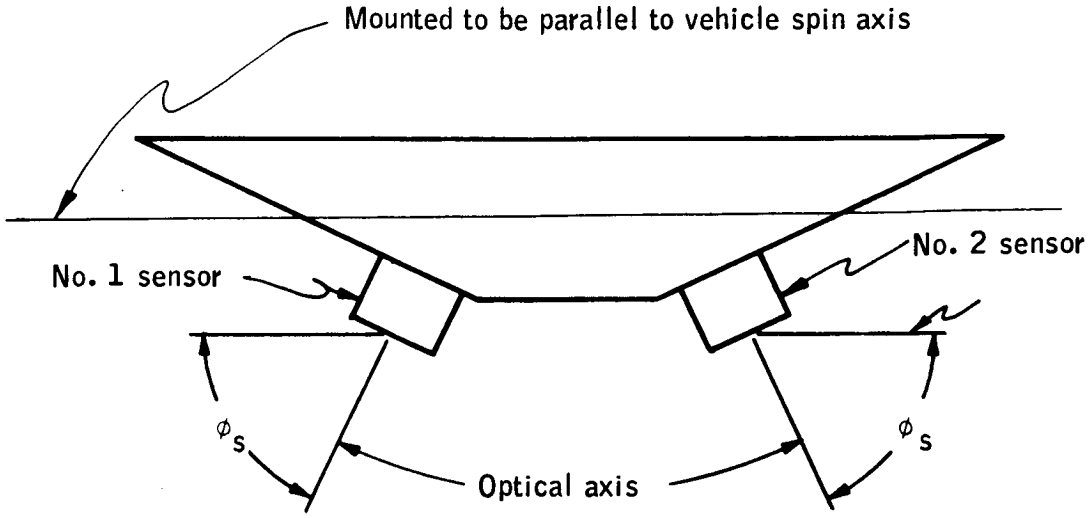

Figure 27. V-Head Horizon Sensor Configuration

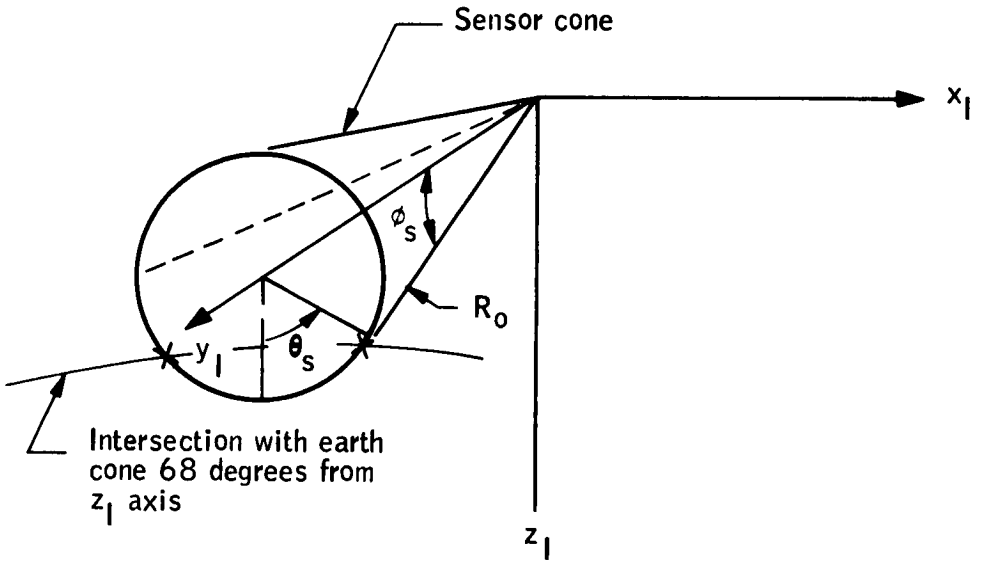

Figure 28. Horizon Sensing Geometry

Whenever the optical axis of the sensing element is less than 68 degrees with respect to the local vertical, the sensor is looking at the earth. The cosine of angle between $\vec{R}_o$ and $\hat{z}_I$ is the dot product $\vec{R}_o \cdot \hat{z}_I$. Equating this angle to 68 degrees, the following expression results:

$$\cos 68° = \cos \phi_s \sin \phi_e + \sin \phi_s \cos \theta_s \cos \phi_e \tag{34a}$$

Solution of the equation for $\cos \theta_s$ for one element results in

$$\cos \theta_{s_1} = \frac{\cos 68° - \cos \phi_s \sin \phi_e}{\sin \phi_s \cos \phi_e} \tag{34b}$$

The solution for the other sensing element can be expressed as

$$\cos \theta_{s_2} = \frac{\cos 68° + \cos \phi_s \sin \phi_e}{\sin \phi_s \cos \phi_e} \tag{34c}$$

The time for each sensing element is

$$\frac{\theta_s}{180°} \times \frac{\text{seconds}}{\text{revolution}} = t$$

A plot of the interception times as a function of the roll angle is shown in Figure 29. The plot is carried to eight degrees at which point the number two element no longer sees any earth. The number one sensor element will continue to see more earth until an angle of 52 degrees where the sensor will see all earth.

The roll angle as measured will be modified on a short-term basis by the coning motion of the spacecraft. To provide a more accurate indication of the short-term motion, the difference in on-time of the two heads may be obtained. The coning frequency is 1.2 times the spin frequency. If there is a variation in the difference of on-time, then it is due to the coning motion.

Mechanization and data storage required. -- As indicated above, the roll error will be determined by noting the difference in the intercept times. This results in a simple mechanization of an up-down counter to which are gated the clock pulses for an up count while number one sensor intercepts the earth and for a down count while number two sensor intercepts the earth. The clock pulses must be phased so that an up and a down count are not received at the same time. When both sensors have left the earth, the contents of the counter can be transferred to data storage. The up-down counter is then reset upon receipt of signal from either of the sensors.

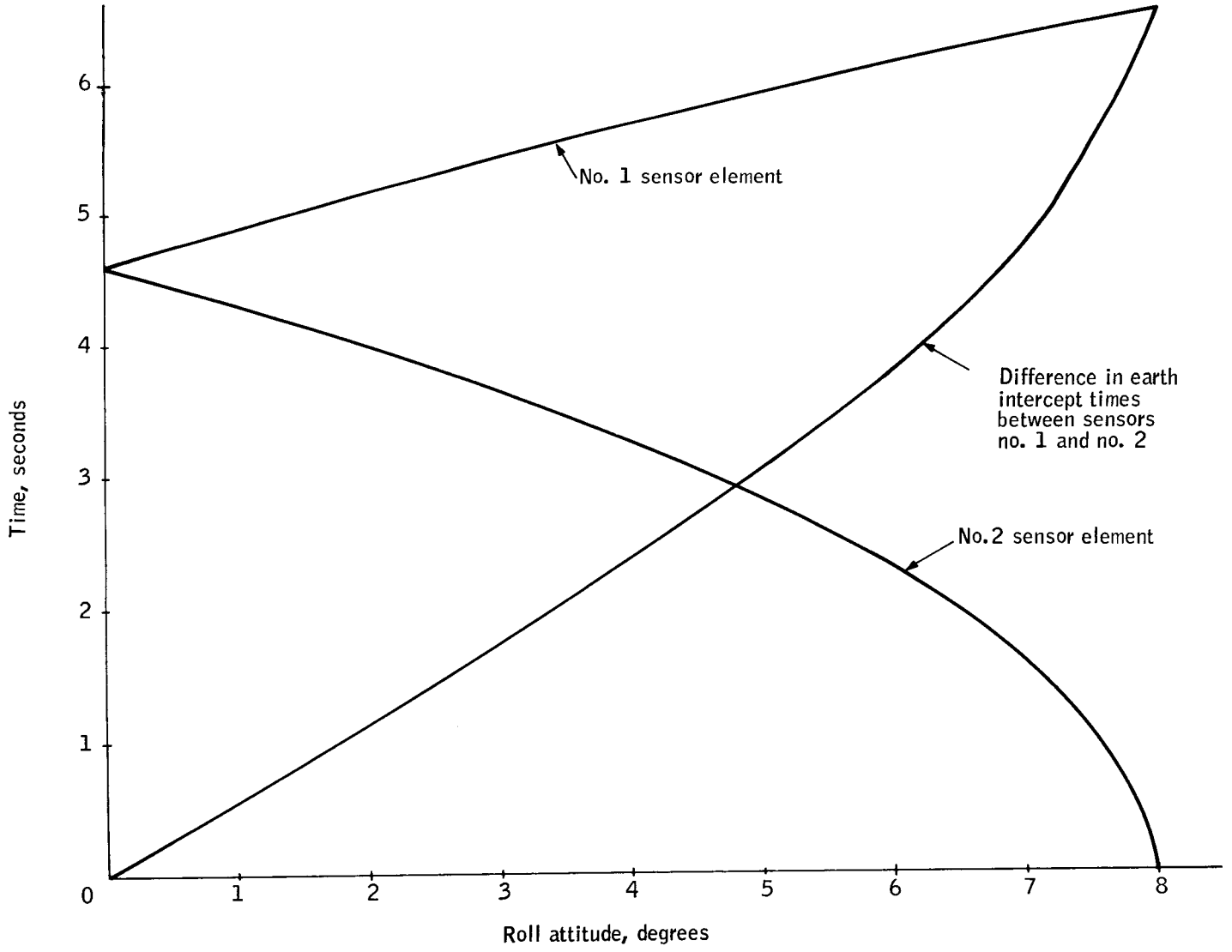

Figure 29. Earth Intercept Time as a Function of Roll Angle

To get the desired resolution it is noted that one degree equals 0.57 seconds. A resolution of at least 0.1 degree is required; therefore, time increments of 0.057 should be supplied. This is 20 pulses per second. A full count occurs when one sensor sees all earth, so 400 pulses must be stored. With one bit to indicate sign, a total of ten bits are required.

Because knowledge of the cone angle is important to attitude determination, a method is proposed for its measurement. The coning motion is a high frequency (1.2 times spin frequency) motion compared to the roll angle motion (orbital frequency). The cone angle can change from zero to the maximum during one intercept period of the earth.

The coning motion can be determined by measuring the difference in on-times between the two sensors. With a coning motion, the difference in on-times will vary from one measurement to the next. Thus, a number of successive readings with a curve fitting can determine the cone-angle.

The difference in on-time can be determined by starting a counter with the pulse from the other head. The difference in on-time for 0.5 degree is 0.146 seconds. A pulse rate of 40 pulses per second to the counter can provide a resolution of less than 0.1 degree for cone-angle measurement.

Accuracy. -- By using the 14 to 16 μ, CO_2 band, the accuracy in defining the attitude of the spacecraft is expected to be:

Instrument accuracy (Appendix B)	.073°
Horizon locator (50 percent normalized radiance - ref. 5) (Appendix B)	.136°
Alignment error	.15°
Counter resolution	.05°
Curving fitting	.15°
Other	.1°
Total rss	.29°

Attitude Error Correction

The magnetic torquers of the attitude control system will be activated by ground command whenever it is desired to correct the attitude error. For radiometric measurements and attitude determination computations it is desirable to maintain attitude within ±5 degrees of normal to the orbit plane.

The orbit position at which the maximum error occurred must be determined to establish a magnetic torquing period which will correct the error. The V-head horizon sensor measures roll angle in a local vertical system. In order to correct this roll angle, a component of the earth's field must be in the roll axis (x_L axis of Figure 30). Thus if the maximum error is measured at the number one position of Figure 30, the direction of the earth's field must be as indicated by B to correct the ϕ error. Since the field components are continually varying, it is necessary to select a torquing period which has the desired earth field component for the longest length of time. This minimizes the undesired cross coupling which takes place.

To develop an insight into the torquing procedure to be used, consider a simple dipole for the magnetic field and assume that it is lying in the plane of the orbit. An inclined orbit results in lesser magnitude of the components in the x and z axes and nonzero value in the y axis. The y-axis components are not effective in generating torques which precess the spin axis. Consider a coordinate system which is fixed inertially but follows the vehicle about the earth as shown in Figure 31. The components of the field in the x_I and z_I axis can be expressed as

$$B_{x_I} = K_1 \sin 2\omega_o t$$

$$B_{z_I} = K_1 (-\cos 2\omega_o t + 0.333)$$

For an altitude of 500 km $K_1 \cong 0.375$ gauss. These components are plotted as a function of orbit position on Figure 32 starting at the magnetic equator.

If an attitude error exists such that a B_x field component is required to correct it, the best torquing periods relative to the magnetic equator are from

0° to 90°
90° to 180°
180° to 270°
270° to 360°

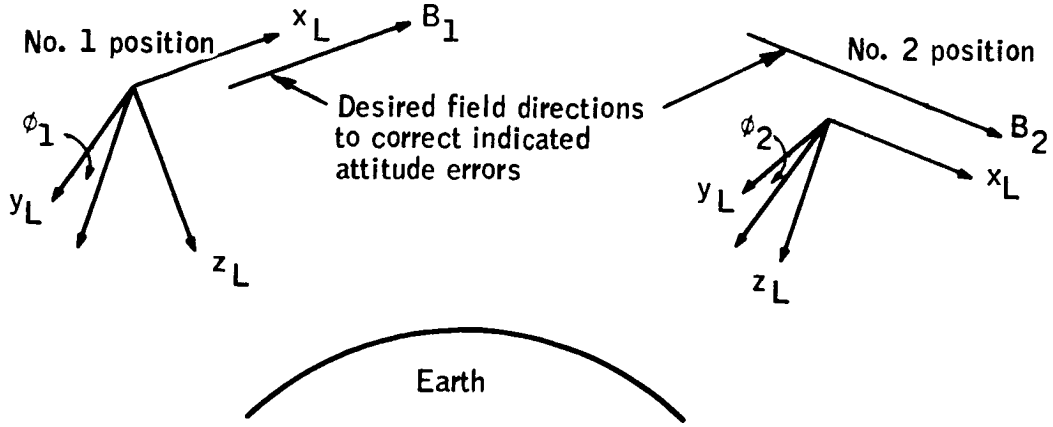

Figure 30. Field Direction to Correct Attitude Error

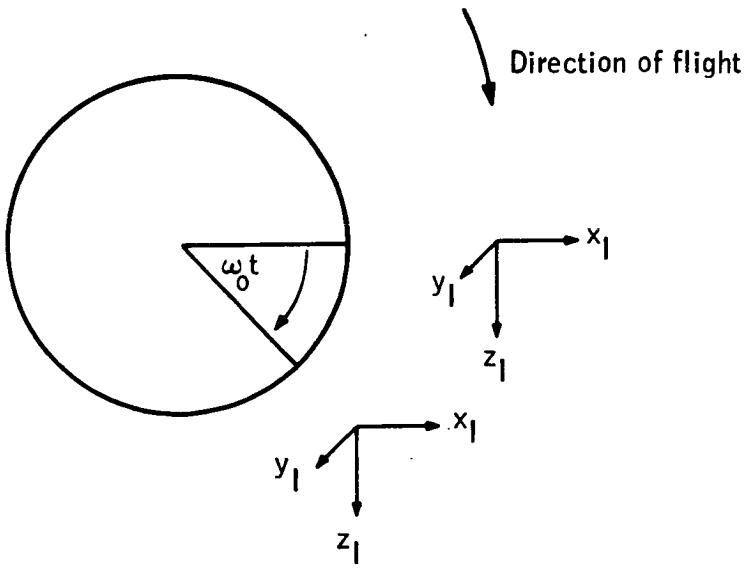

Figure 31. Inertial Coordinate System

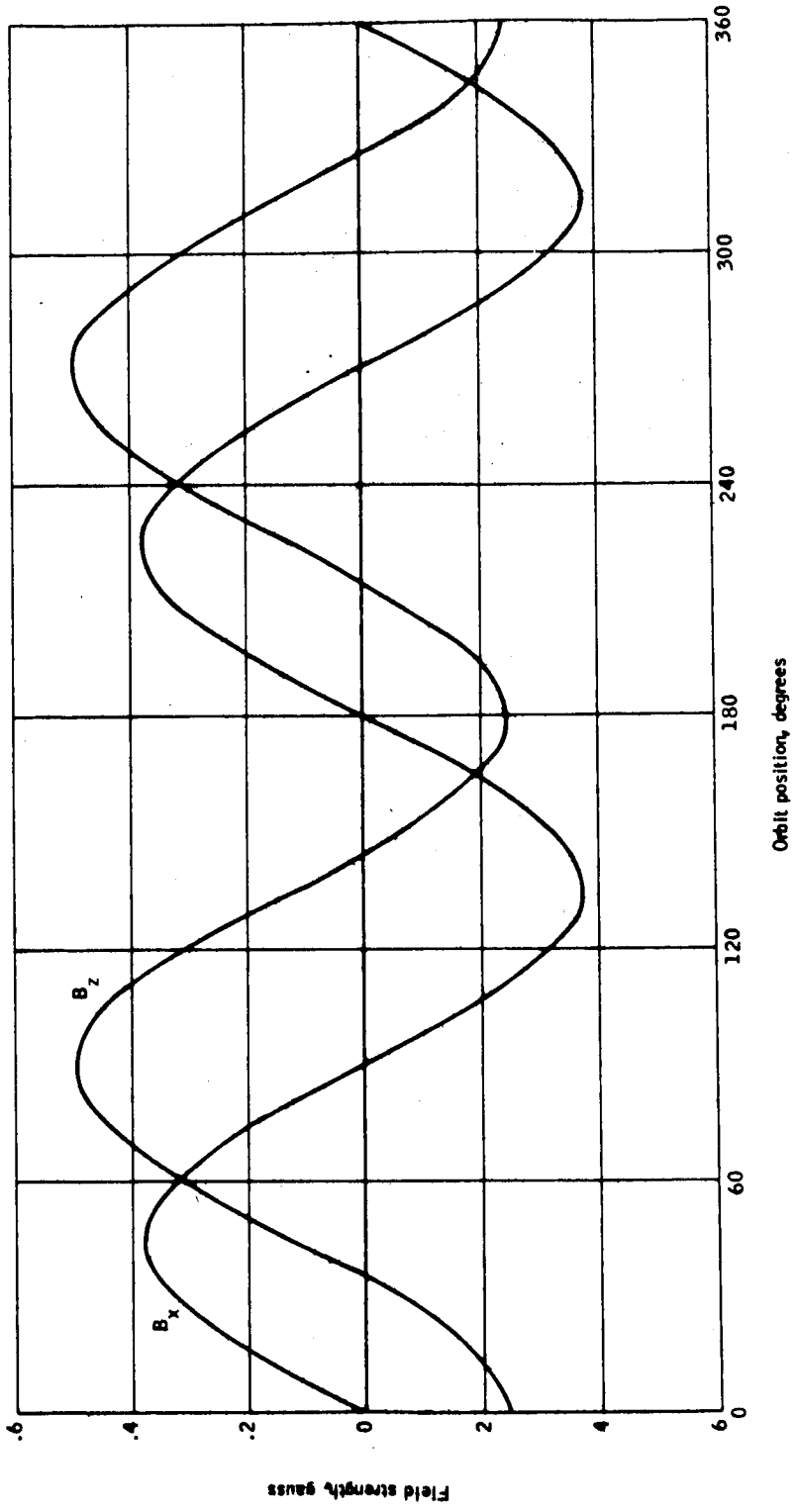

Figure 32. Earth's Magnetic Field Components versus Orbit Position

If an attitude error exists, such that a B_z field component is required to correct the error, the best torquing periods are from

36° to 144°

144° to 216°

216° to 324°

324° to 36°

Torquing over these periods would require a different torquing sequence than established for B_x corrections. Further, to make corrections where some component of both B_x and B_z are required, the torquing period would have to be variable between the above two conditions. Also, if the 0° to 90° torquing period were chosen, it is noted that the torques due to the B_z field will cause an angular error about the z axis. This cross coupling can be minimized by torquing over 180 degrees. This means reversing the current through the coil for the 90° to 180° period. Therefore, it is proposed to use the same two quarter-orbit torquing sequence for all attitude corrections. The time at which the torquing sequence is put into effect will be varied. This is the method used by Tiros.

The time delay to be introduced is the time between transmission of the command and crossing the magnetic equator plus the time between starting the torquing sequence and the crossing of the magnetic equator. The first time interval is a function of the station used and the spacecraft orbit. The second time interval is a function of attitude error. The total time delay range is from 17 (a north pass over the station) to 43 minutes (a south pass over the station).

The time delays which are selected by ground commands and the quarter-orbit torquing sequence are stored on-board the spacecraft. The desired range of time delay can be achieved by using combinations of fixed time delays and the time at which a command is made during the "in-sight" period. Considering an "in-sight" time of five minutes, only five fixed delays need to be stored on board.

Errors in choice of the time delay will result in cross coupling and a slight reduction of the desired correction. The errors which will result can be determined by considering the average value of the B_{z_I} and B_{x_I} components over the torquing periods. The average value of the constant part of B_{z_I} will always be zero over two quarter-orbit periods, so it is only necessary to consider the effects due to the sinusoids. If the time delay is in error by one minute the cross axis error could be 0.66 degrees while torquing five degrees. The error in the torqued axis will probably be of the same magnitude due to field variations, vehicle angular momentum, etc.

Two torquing levels will be provided; a high level which will change the attitude by five degrees in the two quarter orbit periods and low level which will change the attitude by 2.5 degrees.

Spin Control

While in orbit the vehicle spin rate will decrease due to eddy currents associated with rotation in the earth's magnetic field. The spin rate must be maintained if attitude determination and radiometric measurements are to be accomplished with minimum complexity.

It is proposed to maintain the spin rate within ±5 percent of the desired three rpm. The spin rate correction is to be made at the same time as the attitude error correction.

The spin rates of Tiros and Direct Measurement Explorer were controlled magnetically. To accomplish this a coil is mounted in the spacecraft with its plane coincident with the spin axis. The current through the coil must be commutated at the spin frequency to accelerate or decelerate the vehicle. For HDS, commutation can be accomplished using the V-head sensor and two counters. This requires that the plane of the coil be mounted 68 degrees from the line of sight of the V-head sensor. Whenever the V-head sensor goes from space to earth, the first current change occurs. The second current reversal occurs when the clock has counted down a counter which has previously been set for 1/2 spin cycle. The one counter counts the time between space-to-earth transitions. This is divided by two and stored in the second counter, which is then counted down to get the second point of commutations.

The commutation is then accomplished whenever the plane of the coil coincides with local vertical. The component of flux in local vertical is effective in producing a torque to accelerate the vehicle.

Field strength is a maximum in local vertical over the poles, so this is selected as the most desirable period in the orbit for spin rate correction. Since this is to be commanded from the College station, a number of time delays must be provided to assure the proper torquing period. The torquing period will be fixed relative to the magnetic equator with different time delays between command and initiation necessary due to changing orbit conditions.

In local vertical coordinates, the z component (the local vertical component) reaches a maximum of 0.5 gauss. Torquing for an equal period (1/4 orbit total) on either side of the maximum results in an average flux density of approximately 0.425 gauss. Because of orbit inclination and magnetic pole inclination this is further reduced by the cosine 20°. Therefore an average field strength of 0.4 gauss is used in establishing the coil size.

The spin increment to be made up on each correction is a maximum of five percent or 0.01575 rad/sec. The torque applied to the vehicle is a function of the sine of the angle between the earth's field and that produced by the coil.

This results in an average value of 0.636, so the peak torque is found by

$$\Delta\omega_S = \frac{0.636T}{I} \quad t \tag{36}$$

where

$\Delta\omega_S$ = Increment of spin velocity, radians/sec

T = torque, ft-lbs

I = inertia of spin axis, slug-ft^2

t = time, seconds

$$T = \frac{(.01575)\ (67.2)}{(.636)\ (1419)} = .00117 \text{ ft-lb}$$

The moment to be generated by the coil is

$$\frac{0.00117}{0.4} = 29.3 \times 10^{-4}\ \frac{\text{ft-lb}}{\text{gauss}}$$

The plane of the coil must be mounted to be coincident with the spin axis and 68 degrees from the line of sight of the V-head sensor.

The coil which will produce the required moment is estimated to weigh three pounds and to require 0.5 watt of power. The dimensions of the coil are 24 x 44.5 inches. The cross section of the coil is less than 0.5 inch in diameter. Further design effort may result in a more optimum power and/or weight.

Spin correction, as discussed above, consists of one torquing period for 1/4 orbit. Three commands to select the various time delays for the torquing period are required. A polarity command is also required to decelerate the spin rate, for instance after initial spin-up.

Ground Commands for Attitude Control

The following ground commands are required by the attitude control subsystem:

- Attitude error correction

	Number of commands
Select time delays	5
Select positive polarity	1
Select negative polarity	1
Select high torque level	1
Select low torque level	1

- Spin control

Select time delays	3
Select positive polarity	1
Select negative polarity	1

- Residual compensation

Select positive polarity	1
Select negative polarity	1
Select torque level	8

- Passive damper

On command	1
Off command	1

- Redundancy commands

Energize primary V-head sensor	1
Energize redundant V-head sensor	1
Energize primary logic	1
Energize redundant logic	1

It is assumed that the redundant units are placed on standby and will not be energized until needed.

It may be necessary to increase the number of torque levels for residual compensation if attitude determination requirements so dictate. To reduce the number of commands, the attitude control logic can incorporate a counter which sets the required current level based on the number of pulses commanded. Likewise, the on-off commands can be one command which toggles a flip-flop in the attitude control logic to provide the on-off function. The damper commands may not be necessary if it can be determined that the damping torques do not affect attitude determination.

Internal timing and command requirements. -- To provide for attitude error correction and spin control, ground commands initiate a programmed sequence. The sequence for attitude correction appears as

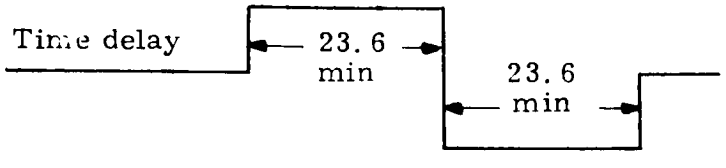

The sequence for spin control appears as

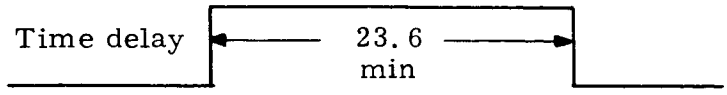

The time delays for attitude correction are 19, 24, 29, 34, and 39 minutes, and the time delays for spin correction are 30, 35, and 40 minutes.

The above sequences can be provided by the attitude control logic.

Test points. -- The following test points are suggested:

1. V-head sensor no. 1 output - on-off
2. V-head sensor no. 2 output - on-off
3. Attitude correction coil - measure plus or minus current level
4. Residual control coil - measure plus or minus current level
5. Spin control coil - measure plus or minus current level
6. Output of V-head sensor logic - This is the roll angle. This should be monitored continuously for a ten minute period to establish the coning angle. Thereafter, once per two minutes is sufficient. This output will appear as a 10-bit word.
7. Damper on - on-off
8. Power on ACS - on-off
9. Redundant V-head sensor on - on-off
10. Redundant logic on - on-off

Reliability Analysis

A reliability block diagram showing the redundancy employed is shown in Figure 33. The reliability for one year is calculated to be 0.9945.

Failure Modes and Effects Analysis

A simplified block diagram of the attitude control subsystem is shown in Figure 34.

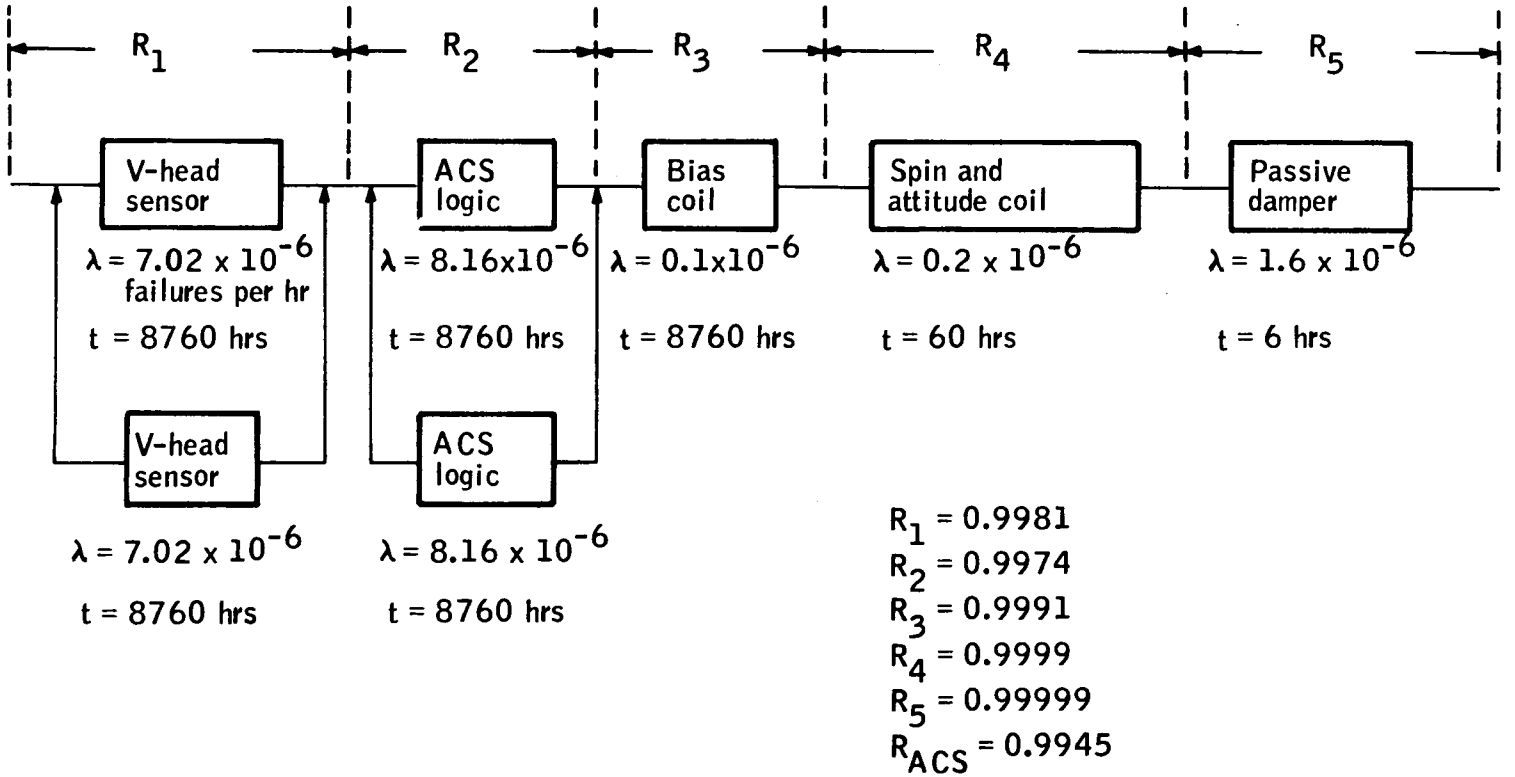

Figure 33. Reliability Block Diagram for the Attitude Control Subsystem

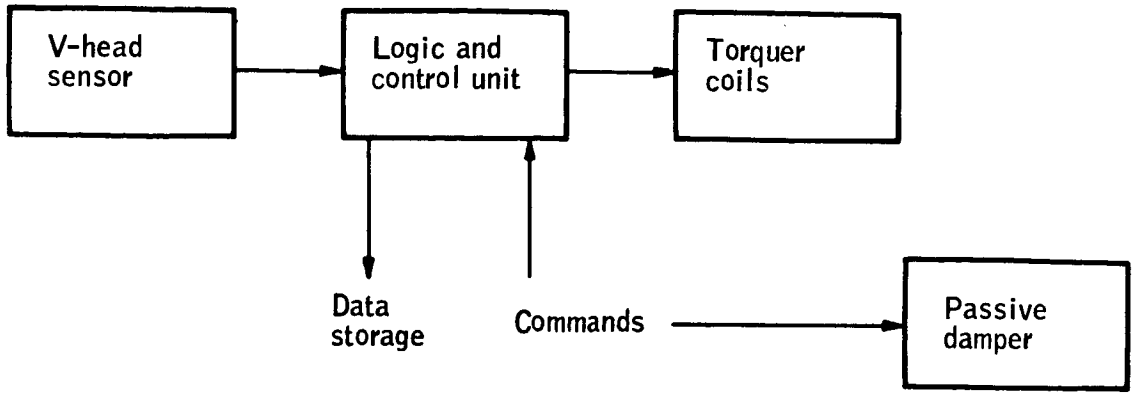

Figure 34. Attitude Control Subsystem Block Diagram

The V-head sensor supplies signals which are processed by the logic and control unit to give roll attitude error, cone angle, and spin rate commutation. Thus a failure of the V-head sensor can affect all three areas. Roll attitude error and cone angle can also be determined from the attitude determination computation; however, a longer time is required to reduce the data. Further, the attitude information from the V-head is used to supply initial conditions for the attitude determination computation. If only one head of the V-head is involved in the failure, the attitude error can be obtained if the altitude of the spacecraft is known. More ground computation will be required to determine the attitude error. Control of the spin rate can be accomplished with one head.

As indicated in the reliability analysis, the V-head sensor has success probability of 0. 94. The probability can be increased to 0.998 for one year, by providing another sensor in standby redundancy. Redundancy therefore has been provided for the V-head sensor.

The logic in the logic and control unit consists of the necessary counters and gates to measure roll attitude and cone angle and provide for commutation of the spin coil. Failure of the logic in any of these areas invalidates these functions.

The coil driving electronics are also contained in the logic and control unit. A failure in this control unit could result in an inability to open or close the torquer coil circuit. An open circuit would result in no attitude correction, and a closed circuit would result in continuous attitude changes of large magnitudes.

Either of these occurences would be obvious from a once per orbit look at attitude,and a corrective command to transfer to the redundant control unit would be made. The data from the next orbit or two after the failure was diagnosed would be lost because of the necessity to recorrect the attitude.

The probability of a coil failure is very low. Failure of the coil will result in a loss of torquing capability rather than a creation of a magnetic moment. No redundancy has been supplied.

The failure probability of the passive damper is also very low. A failure of the damper would prohibit reduction of the cone angle.

ATTITUDE CONTROL SUBSYSTEM TRADEOFF STUDIES

Torquers

An attitude control system is usually configured for control during the long-term mission and, secondarily, for initial orientation or other gross maneuvers. For the present concept of orientation of the HDS spacecraft, the booster will perform a 90-degree maneuver to place the spin axis in the desired orientation. Spin up of the spacecraft to three rpm ± five percent will be accomplished by a spin table on the Delta stage of the booster after burn-out and injection. Therefore, the torquing system need only to be configured for the long-term control.

The attitude control system will periodically correct the attitude when the scan vector of the radiometer exceeds ±5 degrees centered on the orbit plane and when the sun angle to the solar panel approaches 64 degrees. Control may only be required once every five days. Basic attitude stability is achieved by spinning the vehicle, so the source of control torque must be suitable for controlling a spinning vehicle.

Sources of control torque which are usually considered for space vehicles include:

- Momentum interchange
- Mass expulsion
- Use of ambient (gravity, magnetic, etc.)

Inertia wheels and control moment gyros work on the basic principle of momentum interchange between the wheels and vehicle to keep the total momentum constant. They can be used to damp wobble or coning motion due to initial rates in the transverse axes as well as to provide control for attitude correction. Rate sensors would be required to use them for damping of the coning motion. To remove vehicle momentum in a transverse axis requires that the wheel store that momentum. With momentum stored in the wheel, a continual interchange in momentum is required between the two transverse axes at the spin frequency which results in a continuous power consumption.

If wheels were used, their spin axis would have to coincide with the transverse axis, and the vehicle would be subject to gyroscopic cross coupling torques while momentum was stored in the wheels. The HDS attitude determination task requires knowledge of all torques acting on the vehicle, so this would mean a further complication of the determination computation. If the wheels were allowed to run down to eliminate the gyroscopic torques, the momentum storage would be lost and attitude error would exist. It appears that continuous control or torquing is necessary to hold attitude. This would require more complex sensors because a V-head horizon sensor does not provide continuous attitude error information in two axes.

If a control moment gyro were used, its spin axis would coincide with the vehicle spin axis. Controlling attitude and coning motions consists of torquing the gyro spin axis away from the vehicle spin axis. This would result in variation of the vehicle spin rate. The gyro wheel would have to be kept running during attitude determination periods. Starting and stopping the gyro wheel before and after correction periods would cause large perturbations in the vehicle spin rate.

Both the inertia wheels and control moment gyro will become saturated during control cycles because of secular disturbance torques. Another torque system is required to unload them and restore their effectiveness. This system could be a reaction jet or a magnetic torquing system.

The use of wheels or control moment gyros is not considered suitable for the HDS vehicle because of the complexities required for control. Also, with the constant interchange of momentum, wear on the moving parts may limit useful life. An additional control torquing system is required to unload the wheels. Assuming that there are no requirements for orientation maneuvers, this requires the same impulse for unloading the wheels as for controlling the vehicle directly with the unloading torque system.

Reaction jets provide a means of quickly correcting attitude errors; however, a control system must be provided which pulses the jets at the proper time during the spin cycle. The V-head horizon sensor can provide this information, but correction must be limited to periods when the V-head can measure an error. If the jet thrust is large, the pulsing will generate a cone angle which must be damped. The reaction jet system has moving parts, and a slight leak will apply an unknown torque to the vehicle which could make attitude determination impossible. Further, with depletion of the gas supply, mass shifts will occur which cause changes in the vehicle inertias. This also affects attitude determination. It is estimated that a cold gas reaction jet system to supply the impulse for the HDS vehicle would weigh 25 pounds. This weight estimate provides for a 100 percent contingency for a one-year mission.

A magnetic torquing system has no moving parts, and a simple on-board mechanization may be realized if ground commands can be used. The torques produced are small; therefore, the coning motion produced will be small. The torquing periods will have to be selected relative to the proper earth's magnetic field direction. Correction of an attitude error of five degrees will require one-half orbit. The torquing period consists of one-quarter orbit with one polarity and the next quarter orbit with the opposite polarity. This is the concept used on Tiros.

The magnetic torquing system can also be used to compensate the residual dipole of the spacecraft and thus reduce the attitude drift. It can also provide a compensation for the orbital regression which results in a yaw error of approximately one degree per day.

The magnetic torquing system is recommended for the HDS vehicle because

- It is a simple mechanization and has no moving parts.
- It does not introduce unwanted torques during attitude determination.
- It provides a compensation which extends the attitude determination periods.

The same torque sources as discussed above can be used to provide the necessary control of the spin rate. The same basic rationale as discussed above for the momentum interchange devices also applies to the spin-control system. It is expected that correction of the spin rate will be required less than once per five days.

A reaction-jet system could quickly increase or decrease the spin rate by firing a jet for a period of time. The total impulse with 100 percent contingency for a year is 150 ft lb-sec, and a cold gas system to supply this impulse would probably weigh less than six pounds. A strong disadvantage to this technique is if one of the jets developed a small leak, the spin rate would be constantly changing, making attitude determination impossible.

The spin rate can also be updated magnetically. This requires a coil whose plane is oriented to contain the spin axis. Current through the coil must be reversed every one-half revolution to yield an average torque. By orienting this coil properly with the optical axis of the V-head sensor, this switching can be accomplished. The coil will weigh less than three pounds. As a result of the above discussion it is recommended that a magnetic torquing system also be used for spin control.

It is proposed to use air-core torquing coils rather than iron-core coils. The iron-core coil in an off condition will have a residual field whereas the air core will not. Also, an iron-core coil, if used for spin control, would tend to decrease spin rate due to hysteresis losses as the spacecraft is spinning in the earth's field.

Sensors

Although the vehicle is spin stabilized, it will be forced from the desired attitude by the disturbance torques, and periodic correction will be required. An attitude sensor is required to measure the attitude error of the spin axis. Among the attitude sensors normally considered for spacecraft are

- Star trackers.
- Gyros.
- Sun sensors.
- Horizon sensors.

The HDS satellite will be in a sun-synchronous, circular orbit about the earth. Over a period of one year the spacecraft will turn through 360 degrees relative to the stars. Therefore, many different stars would have to be used as reference by a star tracker. A large field of view or gimbals would be required to measure attitude errors to five degrees, and, since the vehicle is spinning at three rpm, the tracker would have to be designed to track at this rate. Complicated signal processing would be required to compute the attitude error. The angle measured is the angle between the spin axis and the line of sight to the star. Additional information is needed to determine the angular error relative to a coordinate system.

Gyros, because of drift, will only provide an accurate measurement for a short period of time. The gyro drift would have to be corrected or updated by the use of another sensor. This sensor can just as well be used as the primary sensor for measuring attitude error. Because the vehicle is spinning, computation of attitude error from gyros is complex.

The sun is an ideal reference for use in measuring attitude with an optical instrument. A sun sensor mounted on the spin axis would measure the same angle as the star tracker, but with reference to the sun. For complete definition of the attitude error an additional reference is required, such as local vertical as measured by a simple horizon sensor (one half of a V-head sensor). Since the orbit is sun synchronous, the line of sight to the sun does not change through 360 degrees as would a star reference; however, there is sun-angle variation due to seasonal variation and precessional variation. This is shown on Figure 35. The variation takes place about a nominal 45 degrees and varies from 31 to 65 degrees. This variation must be taken into account on the computation of the attitude error.

The sun sensor could be a simple device: a simple mechanization can be obtained by using two slits perpendicular to the spin axis. The time between sun passage over the slits is an indication of the angle between the spin axis and the sun line. This requires an accurate knowledge of the spin rate, which could be measured by noting the time between sun illumination of a given slit.

Because of the occult periods which occur every orbit, the sun sensor could not provide continuous information.

Tiros used a digital, solar aspect indicator which provided a digital readout of the angle between the sun vector and the spin vector. This sensor was useful during initial days of the orbit when a large attitude maneuver was required. The resolution of this sensor was one degree.

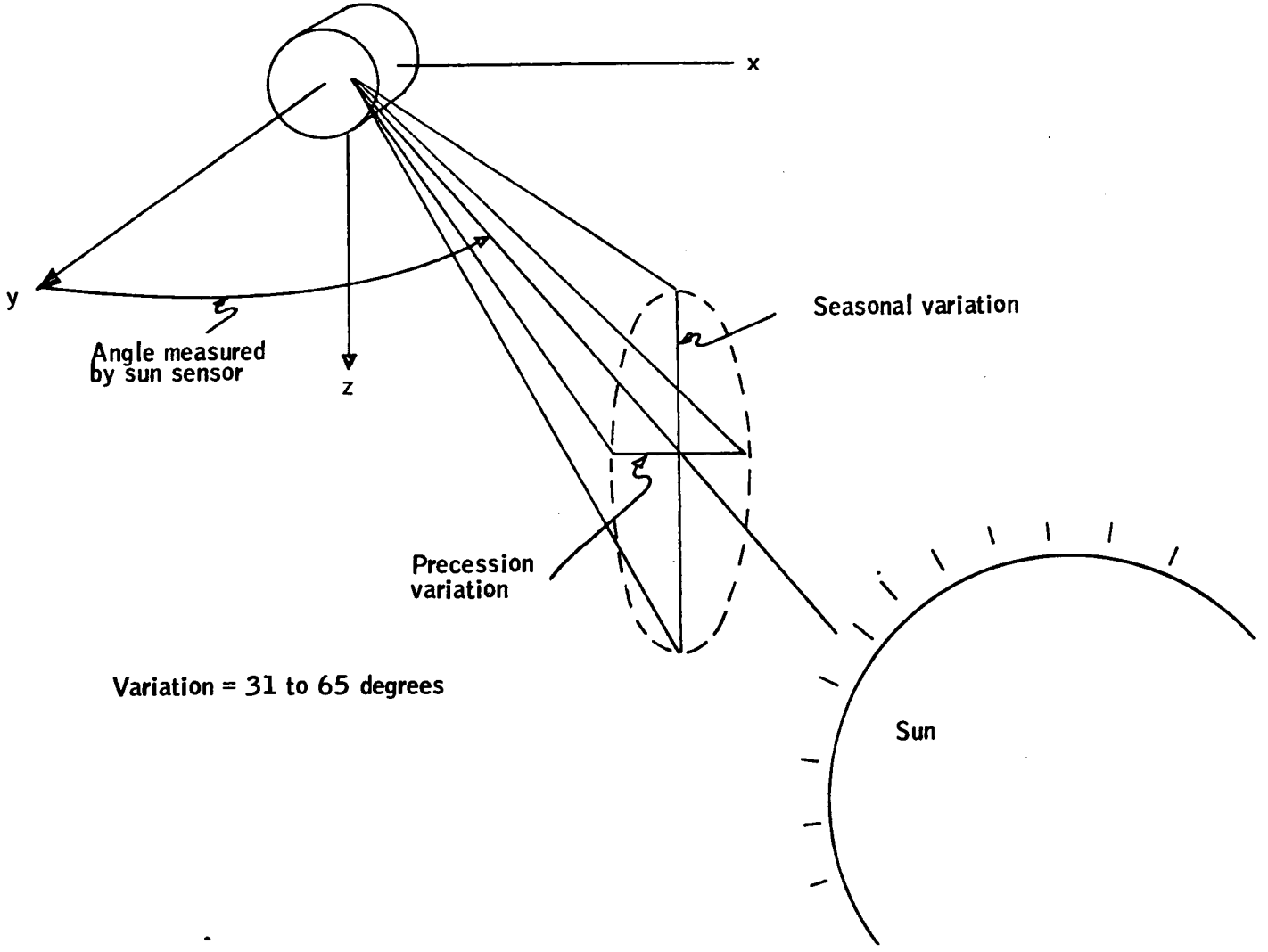

Figure 35. Sun-Angle Variation Relative to the Vehicle

For any earth-oriented satellite the horizon sensor provides the most direct method of establishing the satellite's attitude. Two basic types of horizon sensors are the scanning type and the radiometeric balance type. The scanning type has a moving line of sight which intercepts the earth. The time that the scanner sees the earth provides basic information for determining attitude. The radiometric type has dual detectors which look at opposite horizons. When balance is obtained between the two detectors, local vertical is indicated.

Since the HDS satellite is spinning, a simple horizon sensor without moving parts can be used. It consists of two sensors looking out at equal angles from the spin plane of the vehicle. When each head or sensor intercepts the earth for equal periods of time, the spin plane coincides with local vertical, or the spin axis is in the local horizontal plane. If the vehicle spin axis is tipped with respect to the horizontal plane, the periods that the two sensors see are different and the roll angle can be determined. The V-head sensor provides attitude error information in one axis only as is illustrated in Figure 36. For satellites such as the HDS, where corrections are not required on a continuous basis, this is not a problem. For a spinning vehicle the spin axis is inertial (except for small drift due to disturbance torques); therefore, the angle that the spin axis makes with local vertical is constantly changing as a function of orbit position. It is necessary only to monitor the output of the V-head sensor for a period of time to determine spin axis attitude by curve fitting. On Tiros, ten minutes of observation allowed the ground personnel to determine attitude of the spin axis.

The attitude measurement accuracy required for HDS has been specified as 0.5 degree. This accuracy can readily be achieved by sensors which are designed to operate in the 14- to 16-micron, CO_2 band. An error analysis presented later in this report shows an rss error of 0.29 degree (ref. 5). Tracking in this band will require somewhat larger optics than units tracking a wider band.

The V-head sensor can provide attitude information whether in sunlight or darkness,and the measurements are relatively independent of spin rate. The horizon sensor can also provide local vertical indication in the spin plane by dividing pulse length in half. This can easily be accomplished by a shift command on a counter.

The V-head infrared horizon sensor is recommended for attitude measurement over the sun sensor because

- It provides attitude information during occult periods.
- It measures attitude directly related to the earth reference over the entire mission period. The sun reference is changing because of seasonal and precessional variations.
- It is not as sensitive to spin rate as the sun sensor.
- Computation is less complex.

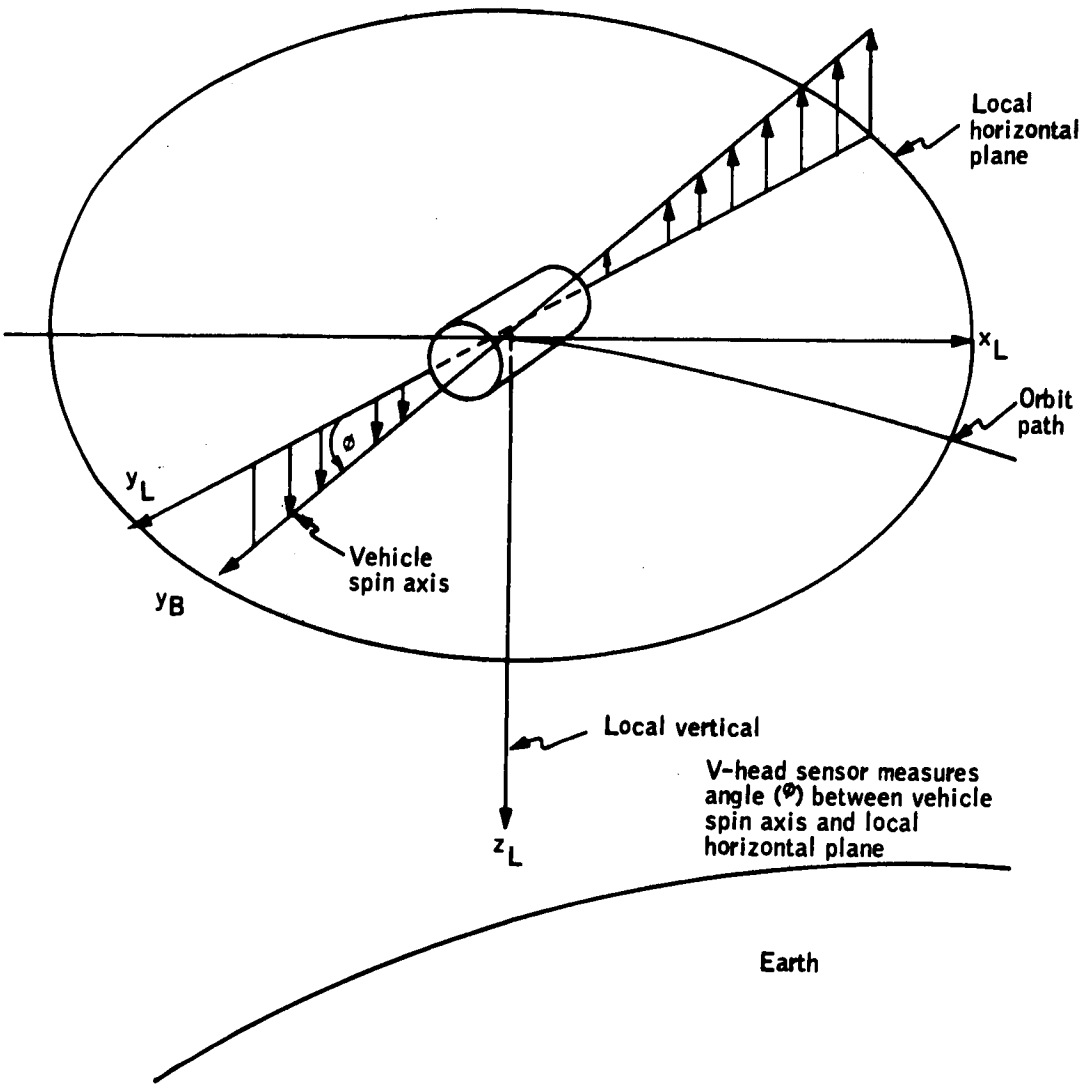

Figure 36. V-Head Horizon Sensor Measurements

Cone-Angle Damper

The first function of the attitude control system after the spacecraft is separated from the booster is to reduce the cone angle. With the present spin rate of three rpm and a spin axis inertia of 65.5 slug-ft^2 and transverse axis inertia of 54.6 slug-ft^2, a three degree per second tip-off rate results in a half-cone angle of eight degrees. This must be reduced before attitude control measurements can be made for adjusting attitude normal to the orbit plane. For operation of the experiments the half-cone angle must be reduced to approximately 0.5 degree. This results in a rate about the transverse axis of 0.0033 rad/sec (0.189 degree/sec). Accomplishment of this damping function by some passive means is preferred. Further, once the cone angle is reduced, the damping mechanism must be deactivated so that additional torques will not be introduced on the spacecraft. The alternative to deactivating the damper is to include the equations of its motion in the attitude determination computations. This is a very desirable alternate but the demonstration of its feasibility is beyond the scope of the present study effort.

Configurations. -- A brief of literature on passive dampers shows that a multitude of damper configurations exist.

The mercury ring damper has been used successfully on a number of spacecraft beginning with Pioneer I in 1958. This configuration consists of one or more circular channels attached about the axis of the spacecraft. Each channel is filled with enough mercury to form a complete ring when the spacecraft is spinning without coning motion. Coning motion perturbs this condition causing the mercury to be displaced. The displacement results in a dissipation of energy due to friction of the mercury with the tube.

A pendulum damper was used on Explorer 17. An analysis of a pendulum damper can be found in reference 6. This reference describes a damper consisting of four small pendulums attached to the main body and free to move in a plane perpendicular to the spin axis. The pivot point of the pendulum is attached to the satellite above the center of mass and at some distance from the spin axis. The viscous friction in the pivot points causes the precession energy to be dissipated. Damping can be accomplished with one or two pendulums.

A single pendulum damper is described in reference 7. It consists of a spherical pendulum located parallel to the spin axis. The pendulum is supported in some viscoelastic material. It is possible to tune the damper to the body precession frequency, thus making the damper more effective.

Damping on the Tiros satellites has been accomplished by a tuned energy absorbing mass. It consists of a sliding weight on a slightly curved track. The precession motion of the satellite caused the weights to move back and forth on the track with a resultant dissipation in energy. It is understood that future Tiros or ESSA satellites will use a fluid damper.

The Direct Measurement Explorer A (DME-A) used a ball in tube damper (ref. 8). Eddy currents generated in the copper balls provide viscous friction. The curved tubes are mounted in a plane perpendicular to the spin axis and above the center of mass. Permanent magnets attached to the tube create high local fields, and direction of magnetization is reversed from section to section such that the net dipole of each tube remains small. The attitude of the DME-A satellite is magnetically controlled.

Telstar uses a ball in gas filled tubes (ref. 9). The tubes have some curvature to drive the balls to the middle of the tube when no coning exists. The tubes are mounted on opposite sides of the vehicle and lie in the plane containing the spin axis. Precession forces the balls to move, creating viscous friction between the balls and the gas and static friction between the balls and the tubes. The precession energy is dissipated into heat through the resistance to the motion of the balls.

The ball in tube is really a pendulum. This is shown by the linearized equations developed in reference 9. Neglecting rolling friction, the equation of motion has the following form:

$$\ddot{\alpha} + 2n\dot{\alpha} + P^2\alpha = q \cos \Omega t \qquad (37)$$

The term Ω is the body precession rate.

This is similar to a pendulum which is subjected to an impressed harmonic force. As energy is being dissipated the value of α become less.

Damper for HDS. -- The successful use of passive dampers in many satellites indicates that coning can be reduced. Results have shown that damping can be accomplished quickly. Design of the damper involves choice of a damping medium, weight of pendulum mass, and tuning to the precession frequency. Packaging constraints of the HDS vehicle must also be considered.

One basic constraint required of the passive damper for HDS is that it must be inoperative during attitude determination and data taking periods. This restricts the design somewhat, in that a locking mechanism must be included to hold the damper inactive. This constraint eliminates the fluid in a tube configuration. The ball in a gas-filled tube also appears to be eliminated, unless the ball could be held by a magnetic field. A magnetically damped ball in a tube could be used. The ball could be held in position by a soft-faced plunger activated by a solenoid. A pendulum internal to the satellite structure could easily be caged or held.

To get some idea of the design parameters required of a damper for HDS, the equation for characteristic time as derived for a tuned damper in reference 9 was evaluated. The equation is

$$\tau_p = \frac{2c I_s (\lambda - 1)}{m^2 b^2 \lambda^2 \omega_s^2 (2 - \lambda)^2} \qquad (38)$$

where

τ_p = time constant, sec

c = damping coefficient, $lb\text{-}\frac{sec}{ft}$ = 0.00439

I_s = spin axis inertia, $slug\text{-}ft^2$ = 65.5

λ = ratio of spin inertia to transverse inertia = 1.2

m = mass of both balls, slugs = 0.0328

b = distance tubes are located from spin axis, ft = 1

ω_s = spin velocity, rad/sec = 0.315

This equation assumes there is no rolling friction and is satisfactory for cone angles greater than one degree. A ball diameter of 1.21 inches was assumed. The time constant resulting from the numbers used was 1170 seconds. One orbit (5670 seconds) has been allowed for damping in the operational plan.

In order to damp to a 0.5 degree cone angle, the damper must have a rolling friction of less than 3.4×10^{-6} lb. The Telstar configuration showed a rolling friction of 0.0002 lb (ref. 9). The Telstar satellite was rotating at a much higher velocity so the normal acceleration on the balls was much greater than for HDS. Considering rolling friction to be proportional to the force between the ball and the tube, the friction for HDS would be 0.8×10^{-6} lb. The DME-A configuration has a rolling friction of 0.11×10^{-6} lb (ref. 8). These values are less than the required value (3.4×10^{-6} lb) to damp to 0.5 degree cone angle. It appears feasible to damp to 0.5 degree.

On-Board Control Versus Ground Command Control

Present requiements on the attitude control subsystem do not allow any control torques to be applied during attitude determination. Attitude errors are not to be corrected until the error exceeds five degrees. Present estimates indicate that this may be once every five days.

The horizon sensor used on HDS measures one angle, the spin axis relationship to the local horizontal plane. Because of the inertial properties of a spinning vehicle, this angle varies as a sine function with respect to orbit position. Thus, the maximum error can only be detected twice per orbit. The output of the horizon sensor will be monitored continually whether the control is on-board or through ground commands. A decision will be made on the ground when attitude error is to be corrected.

Magnetic torquing will provide torques for correcting the attitude error. Certain field conditions must be met if the desired attitude correction is to be made. Figure 37 shows the magnetic field relationships to the angle as measured by the V-head sensor. This figure shows the local vertical

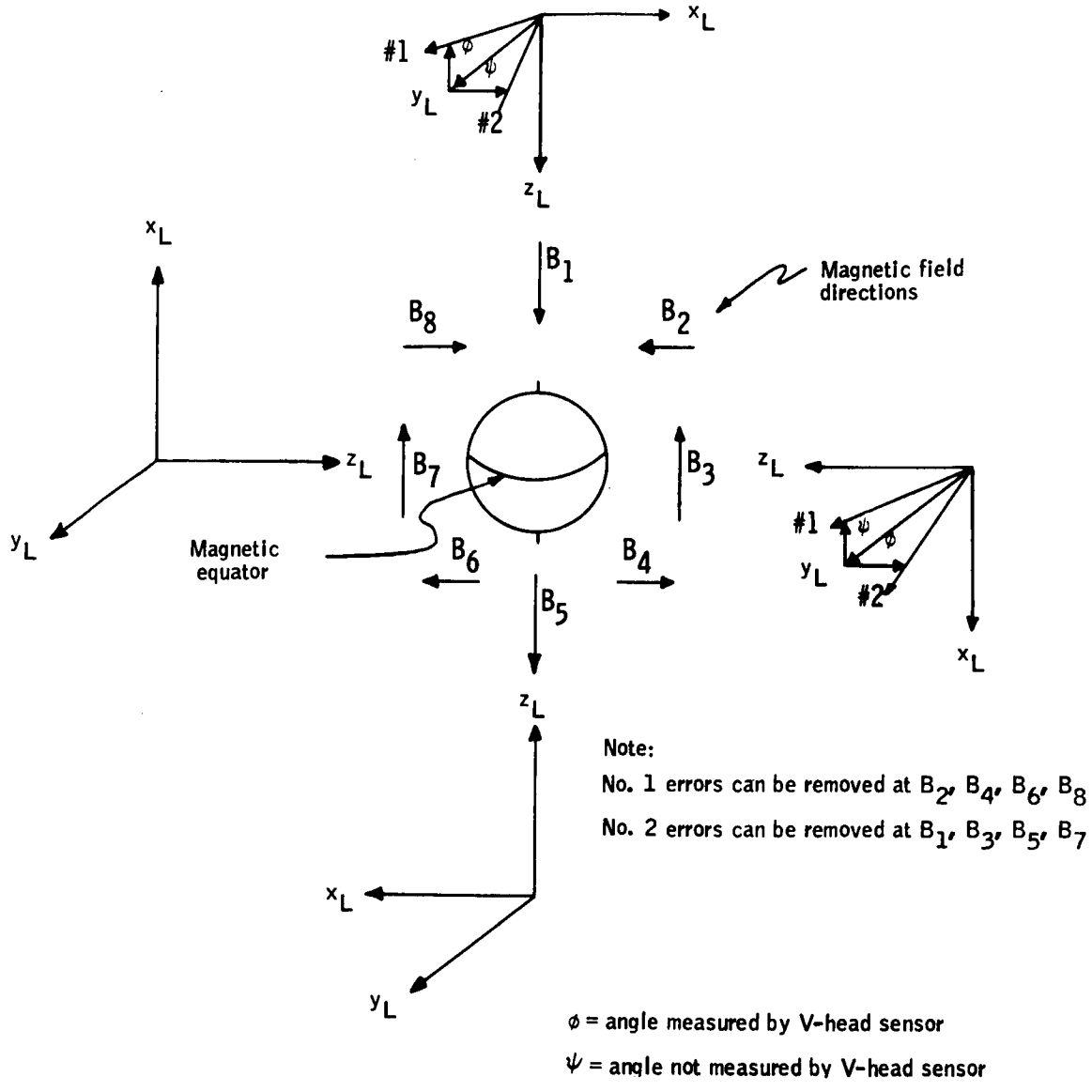

Figure 37. Magnetic Field and Local Vertical Relationships

coordinate system as it is rotated about the earth and the direction of the magnetic field at various points in the orbit. The vector representing field direction must be coincident with the vector representing the desired attitude correction in order to correct attitude. A ϕ error over the magnetic pole cannot be corrected over the poles or the magnetic equator; it must be corrected between these two points. A ϕ error over the magnetic equator can be corrected while over the equator or the pole; however, it can only be measured over the equator.

Thus, to provide the desired control requires knowledge of the error, where it occurred, and knowledge of the field directions throughout the orbit so the proper torquing period can be selected.

A complicated change takes place in the magnitude and direction of the earth's magnetic field not only within an orbit but from orbit to orbit. Knowledge of this field direction is required. For on-ground determination, the field can be computed by computer and interpreted on the ground. If control were to be accomplished on-board the spacecraft, this computation would have to be done by a computer on-board or have an ephemeris of the field stored on-board. An alternate method would be the use of magnetometers to measure components of the field in all three axes. The magnetometers would have to be located far enough from the torquer coils so that their outputs would not be significantly affected by the magnetic field of the coil.

Additional logic and/or computers would be required to mechanize the control law for the attitude correction. Since the V-head sensor does not provide continuous information of the error to be corrected, the error must also be stored in the computer.

Since it is anticipated that attitude error corrections will only occur once per five days, the much greater complexity of an on-board control system is not warranted.

CONCLUSIONS AND RECOMMENDATIONS

CONCLUSIONS

The Conceptual Mechanization Studies for a Horizon Definition Spacecraft Attitude Control Subsystem has ascertained the following:

- A magnetic, torqued ground-commanded attitude control subsystem is feasible for the HDS spacecraft and should be used.
- Vehicle is stable about the maximum moment of inertia.
- For the HDS spacecraft the longitudinal axis must have an inertia greater than the transverse axes, $\frac{I_s}{I_t} > 1$.

- Computation of the inertia indicates that an inertia ratio of 1.2 can be obtained. Analysis has shown that the vehicle is stable for $r = 1.2$.

- Tip-off rates require that a cone-angle damper be supplied to reduce eight degrees of half cone initially. The operational plan provides for two orbits of damping prior to performing mission.

- The symmetric body model is adequate for attitude control when the asymmetry is less than three percent.

- The attitude prediction model must include asymmetry.

- The complex motion due to asymmetry can be minimized by maintaining small asymmetry and cone angle.

- The major environmental torques for the HDS spacecraft are the residual magnetic-moment torque and the eddy-current torque.

- The solar pressure and aerodynamic torque are the next most significant.

- A spin rate of three rpm was selected because of the minimum composite effect of the residual magnetic moment and eddy-current torque on the pointing vector prediction. Additionally, the lower spin rate increases the energy received by the radiometer on each interception of the horizon.

- Spin rate need be updated only once every 125 orbits to keep spin rate within five percent of nominal.

- Attitude correction due to spin-axis precession needs updating once per 55 orbits if the residual moment is not compensated. With compensation for residual moment and orbit regression, the update period can possibly be extended to 300 orbits.

- Magnetic torques cause no significant increase in cone angle over a period of four orbits.

- Damping to a half-cone angle of 0.5 degree is feasible.

- V-head horizon sensor attitude measurement accuracy is ± 0.29 degree employing the 14- to 16-micron CO_2 energy band and a simple horizon locator (50 percent normalized radiance).

RECOMMENDATIONS

From the analyses performed the following recommendation are made:

- As the design becomes better defined, further analyses are required to determine the exact effect of the radiometer calibration mechanism on the vehicle's motion.
- Further analyses must be conducted to determine the effects of the meteoroid impacts.

APPENDIX A
MODEL OF ENVIRONMENTAL TORQUES

APPENDIX A
MODEL OF ENVIRONMENTAL TORQUES

SOLAR PRESSURE DISTURBANCE TORQUES

Interplanetary radiation originates primarily from our own solar system. Compared to solar radiation, galactic radiation contributes little to the total radiation pressure exerted on a unit area of a spacecraft.

Solar radiation is further divided into electromagnetic radiation and particle radiation. Electromagnetic radiation consists of quanta called photons which propagate in waveforms having wavelengths in the continuous spectrum. Photons have zero rest mass, no electrical charge, and no magnetic moment, but they do possess energy resulting in a force producing a pressure termed "light pressure". Particle radiation, however, consists of electrons, protons, neutrons, alpha and beta particle plasma, and many other subparticles. These particles, which have a rest mass, are expelled from the sun at velocities of from 400 to 1500 km per second. This particle radiation which sweeps throughout interplanetary space is termed "solar wind".

Electromagnetic Radiation

The intensity of electromagnetic radiation is inversely proportional to the square of the distance to the sun. About 99 percent of this solar energy is concentrated in the narrow range from 3000 to 4000 angstroms (ref. 10), with the remaining one percent distributed in the ultraviolet, infrared, and radio frequencies. The rate at which solar electromagnetic radiation is received outside the earth's atmosphere, on a unit surface normal to the incident radiation and at a distance of one astronomical unit from the sun, is called the solar constant. This quantity which produces "light pressure" is virtually unchanged with high solar activity. The solar constant has the value of 1396 watts/meter^2 and is uncertain to ±1 percent due to gradual long-term variations and instrument measurement error. Dividing the solar constant by the speed of light and converting the units produces the quantity of solar light pressure exerted on a unit area.

$$P = \frac{(1394\ \text{W})\left(\quad \text{hp} \quad\right)(550\ \text{ft-lb-sec}^{-1})\ (10^{-4}\ \text{m}^2)\ (2.54\ \text{cm})^2\ (144\ \text{in.}^2)}{\left(\quad \text{m}^2\ \right)(746\ \text{W})\left(\qquad \text{hp} \qquad\right)\left(\quad \text{cm}^2\ \right)\left(\quad \text{in.}^2\ \right)\ \left(\quad \text{ft}^2\ \right)}$$

$$0.83514 \times 10^{-8}\ \frac{\text{ft}}{\text{sec}}$$

$$P = 0.970814 \times 10^{-7}\ \text{lb/ft}^2$$

Partical Radiation

The solar atmosphere is composed primarily of ionized particles that flow continuously outward from the sun. This flow which represents an expansion of the solar corona is called the "solar wind". The corona is composed primarily of hydrogen; hence, the solar wind consists primarily of highly ionized hydrogen particles (electrons and protons). Since the mass of the proton is 1837 times the mass of the electron, the energy of the solar wind can be determined from the particle energy of the proton alone, which is about one keV during quiet sun periods.

The mass of a proton (ref. 11) is given as

$$M = 1.67 \times 10^{-24} \text{ g}$$

During quiet sun periods, the solar wind particles at one astronomical unit are traveling at a velocity of about 400 kilometers per second with a density of about 10 particles per cubic centimeter (ref. 10).

$$P = M N V^2 \cos \theta \qquad \text{(A1)}$$

where

- M = particle mass
- N = particle density
- V = particle velocity
- θ = particle incident angle

A surface exposed 90° to the solar wind will have a zero incident angle. In this case:

$$P = M N V^2$$

$$P = (1.67 \times 10^{-24} \text{ g}) \left(\frac{10}{\text{cm}^3}\right)\left(4 \times 10^7 \frac{\text{cm}}{\text{sec}}\right)^2$$

$$P = 267.2 \times 10^{-10} \frac{\text{g}}{\text{cm-sec}^2}$$

Converting the units:

$$P = \left(267.2 \times 10^{-10} \frac{\text{g}}{\text{cm-sec}^2}\right)\left(\frac{\text{dynes}}{\frac{\text{g-cm}}{\text{sec}^2}}\right)\left(\frac{1 \times 10^{-5} \text{ newton}}{\text{dyne}}\right)\left(\frac{\text{lb}_f}{4.448222 \text{ newton}}\right)\left(\frac{929.03 \text{ cm}}{\text{ft}^2}\right)$$

$$P = 5.581 \times 10^{-11} \frac{\text{lb}}{\text{ft}^2}$$

which is the quiet sun-particle pressure.

During active sun periods, however, the solar pressure due to particle radiation is greatly magnified. Solar flares cause a rapid expansion of the corona, producing an increase in the velocity and density of the solar plasma.

Solar flares vary in magnitude and brightness and are classified according to their area (percent of solar disk involved). Observations have shown that the frequency and duration of solar flares vary as a function of their class (ref. 12). Small flares (class 1) occur every few hours and have durations of about 10 to 40 minutes.

Conversely, the large flares (class 3 and class 3+) occur more rarely but have longer durations. As many as six or seven class 3+ flares with mean durations of about three hours may be expected in one year during the active portion of the eleven-year solar cycle.

As a result of a class 3+ flare, the solar plasma velocity may increase to about 1500 kilometers per second with particle density increasing to as high as 100 particles per cubic centimeter (ref.'s 10 and 13). During this brief period, the solar particle radiation pressure increases as follows:

$$P = M N V^2$$

$$P = 1.67 \times 10^{-24}\ g \left(\frac{100}{cm^3}\right)\left(15 \times 10^7\ \frac{cm}{sec}\right)^2$$

$$P = 37575.0 \times 10^{-10}\ \frac{g}{cm\text{-}sec^2}$$

Converting the units:

$$P = 7.848 \times 10^{-9}\ \frac{lb_f}{ft^2}$$

which is the particle radiation pressure during a class 3+ flare.

Solar Pressure Coefficient

Based upon the foregoing analysis, the particle radiation pressure, even during a large flare, is more than an order of magnitude less than the electromagnetic radiation pressure. Therefore, particle radiation pressure may be neglected.

In developing the solar pressure disturbance torque model, a constant pressure of $1 \times 10^{-7}\ lb_f/ft^2$ may be used for a surface normal to the sun-line with no variation due to solar activity.

The vehicle model considered in this study consists of a right hexagonal cylinder as the basic spacecraft with six rectangular solar panels attached to the spacecraft to form a "hat" configuration. This configuration is illustrated in Figure A1.

The spacecraft body area is determined by the projection of the hexagonal surfaces and reduced by the solar panel shadowing. Figure A2 shows a 45° sun-line projection and the shadowing that results for one rotational orientation.

The solar pressure can be represented in an inertial frame by three direction cosines (i_I, j_I, k_I). Let S_o represent the magnitude of the pressure - lb/ft^2. Then, by successive transformation to a set of coordinates in the vehicle body, $\vec{S}$ the solar pressure magnitude and direction can be represented in body axes. The surfaces of the vehicle which will be exposed to the sun are identified and represented by a direction and a magnitude. Also, a moment arm is identified with each surface. The magnitude of the force on each identified surface is obtained by $\vec{S}\cdot\vec{A}_i$ where $\vec{S}$ is the solar pressure in body coordinate and $\vec{A}_i$ is the surface in body coordinate. The direction of the force in body coordinates is parallel to the direction of the solar pressure vector.

Let the direction of the solar pressure be represented by a unit vector in inertial space (i_I, j_I, k_I). The components in body coordinates are:

$$\begin{bmatrix} i_E \\ j_E \\ k_E \end{bmatrix} = CE \cdot \begin{bmatrix} i_I \\ j_I \\ k_I \end{bmatrix} \qquad \text{(A2)}$$

The C and E transformations are given as follows:

$$C(\epsilon_1, \epsilon_2, \epsilon_3) = \begin{bmatrix} (\cos\epsilon_3\cos\epsilon_1 - \sin\epsilon_1\sin\epsilon_2\sin\epsilon_3) & (\sin\epsilon_1\cos\epsilon_3 + \cos\epsilon_1\sin\epsilon_2\sin\epsilon_3) & (-\sin\epsilon_3\cos\epsilon_2) \\ (-\sin\epsilon_1\cos\epsilon_2) & (\cos\epsilon_1\cos\epsilon_2) & \sin\epsilon_2 \\ (\sin\epsilon_3\cos\epsilon_1 + \sin\epsilon_1\sin\epsilon_2\cos\epsilon_3) & (\sin\epsilon_3\sin\epsilon_1 - \cos\epsilon_1\sin\epsilon_2\cos\epsilon_3) & (\cos\epsilon_2\cos\epsilon_3) \end{bmatrix} \qquad \text{(A3)}$$

and

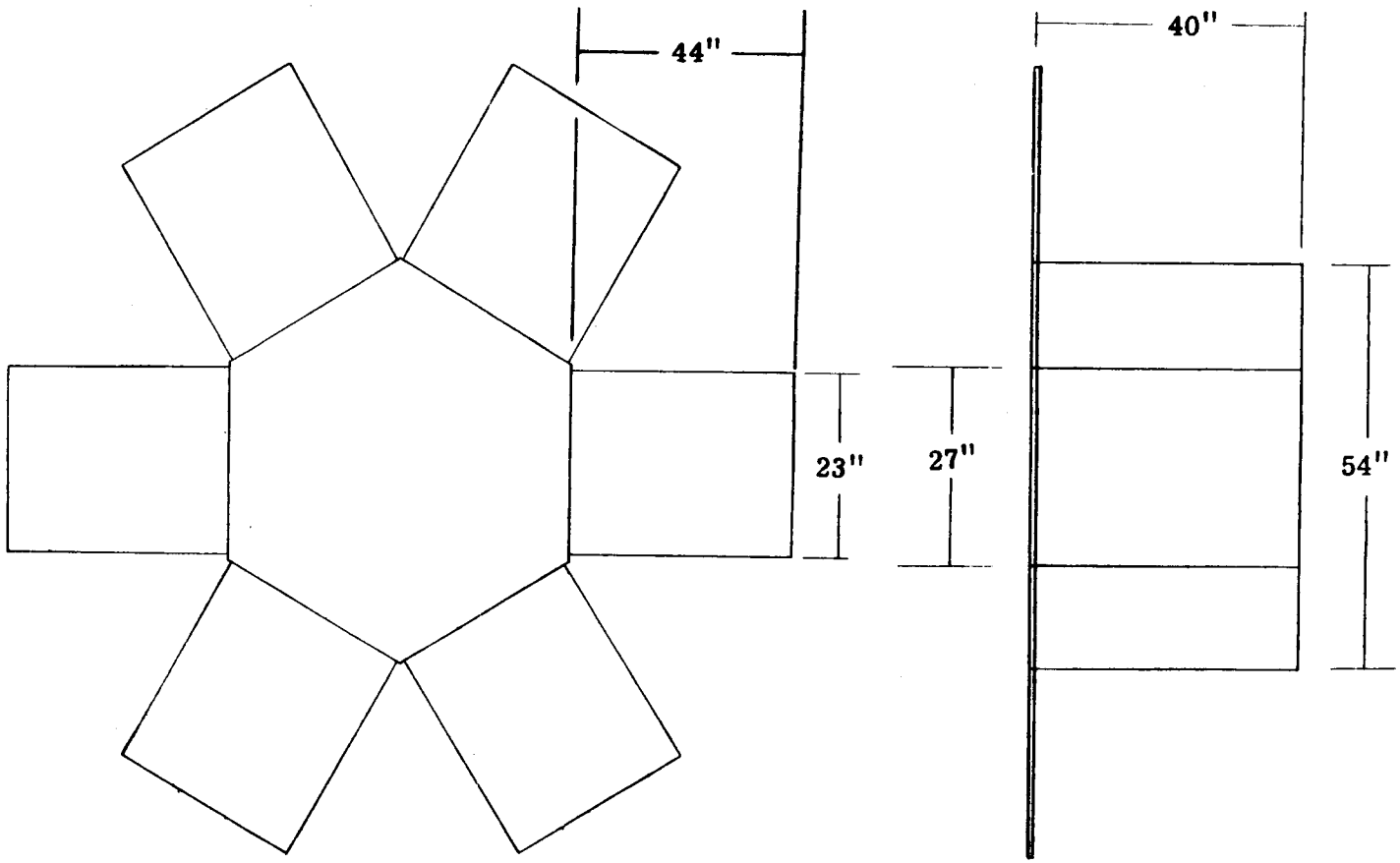

Figure A1. Vehicle "Hat" Configuration

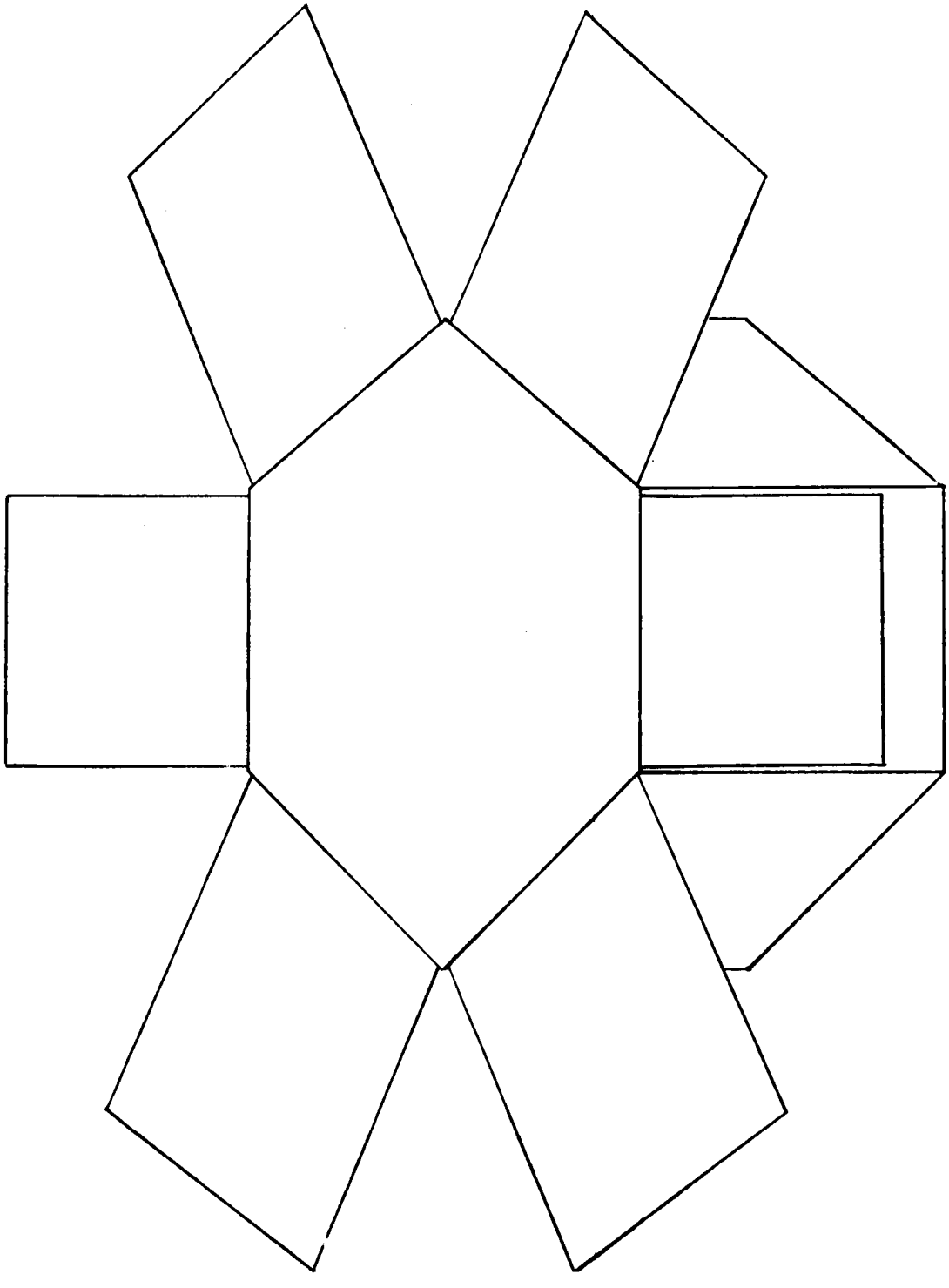

Figure A2. Vehicle Projection at 45° Sun-line

$$E(\psi, \phi, \theta) = \begin{bmatrix} (\cos\theta\cos\psi - \sin\psi\sin\phi\sin\theta) & (\sin\psi\cos\theta + \cos\psi\sin\phi\sin\theta) & (-\sin\theta\cos\phi) \\ (-\sin\psi\cos\phi) & (\cos\psi\cos\phi) & \sin\phi \\ (\sin\theta\cos\psi + \sin\psi\sin\phi\cos\theta) & (\sin\theta\sin\psi - \cos\psi\sin\phi\cos\theta) & (\cos\phi\cos\theta) \end{bmatrix} \quad \text{(A4)}$$

Working with i_E, j_E, k_E, the solar pressure torque is found to be

$$\tau_E \approx \begin{bmatrix} S_o\, j_E\, k_E\, (\ell_y A_y - \ell_x A_x) \\ 0 \\ -S_o\, i_E\, j_E\, (\ell_y A_y - \ell_x A_x) \end{bmatrix} \quad \text{(A5)}$$

where

$$A_y = 55.5 \text{ ft}^2$$

$$A_x = 3.12 \text{ ft}^2$$

$$\ell_x = 2.25 \text{ ft}$$

$$\ell_y = 1.57 \text{ ft}$$

and

$S_o = 1 \times 10^{-7}$ lb/ft^2, assuming a completely absorbing surface.

Then

$$\tau_x = 0.8 \times 10^{-5}\, j_E\, k_E$$

$$\tau_y = 0$$

$$\tau_z = -0.8 \times 10^{-5} i_E\, j_E$$

The solar torque was also determined for solar aspect angles of 30 to 65 degrees. The results are shown in Figure A3. The maximum value occurs at 45 degrees. This is the value which has been used in the computer program.

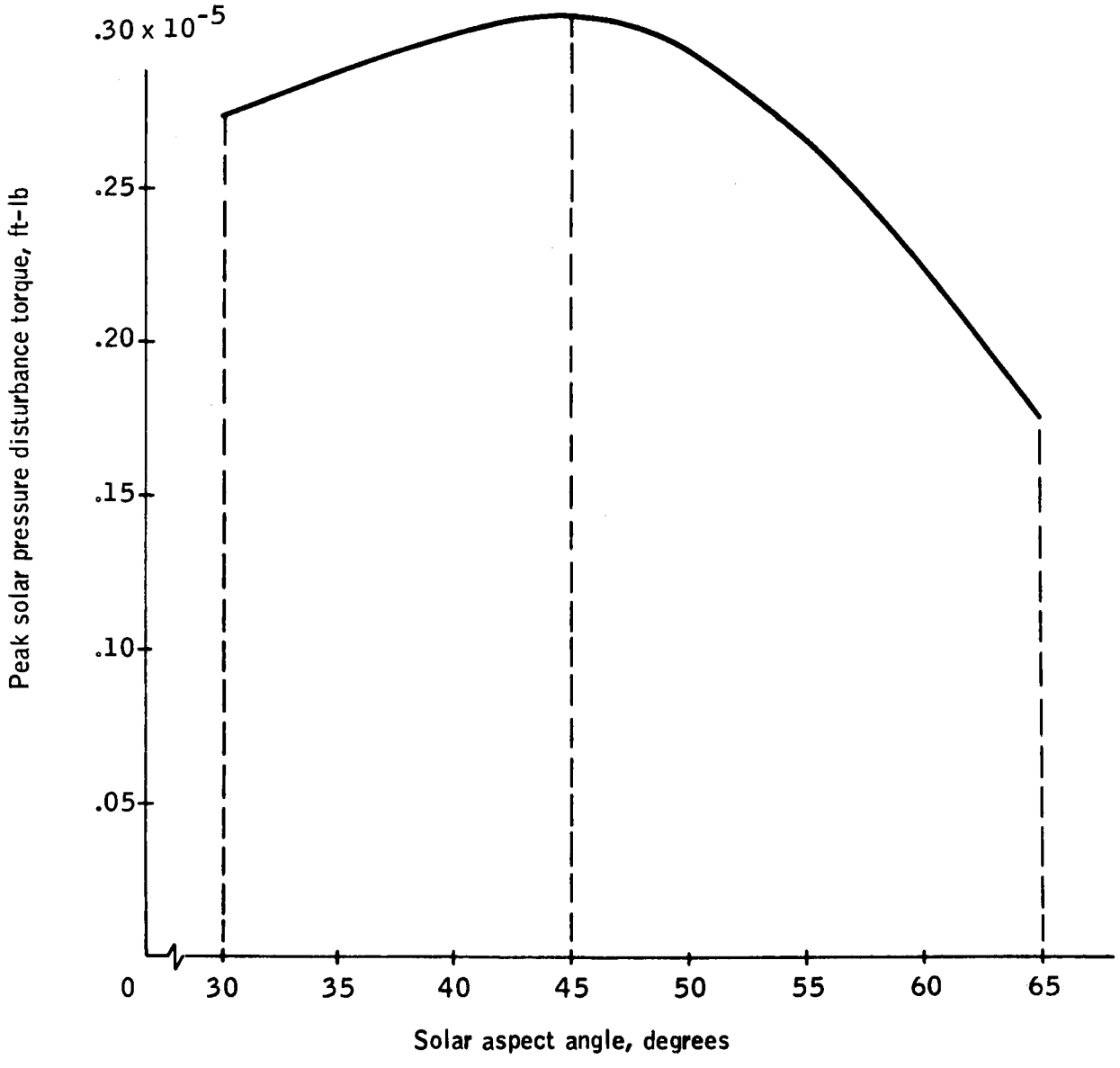

Figure A3. Solar Disturbance Torque as a Function of Solar Aspect Angle

AERODYNAMIC DISTURBANCE TORQUE

The magnitude of the aerodynamic torque on the HDS vehicle depends upon orbit altitude, vehicle orientation, and surface reflection coefficients. The vehicle "hat" configuration, consisting of a right hexagonal cylinder with six rectangular solar panels is shown in Figure A1. Since the vehicle spin axis is nominally normal to the orbit plane, the direction of the relative wind will be nominally perpendicular to the body $\dot{y}$ axis.

Assuming free molecular flow, the drag coefficient C_D, can be set equal to 2.0 and the normal and tangential stresses on the various vehicle flat surfaces are given as follows:

Pressure normal to a surface:

$$P_N = C_D (2-\sigma) q \sin^2 \beta \tag{A6}$$

Pressure tangential to a surface:

$$P_T = C_D \sigma q \sin \beta \cos \beta \tag{A7}$$

where

C_D = aerodynamic drag coefficient

σ = surface reflection coefficient

q = dynamic pressure

β = yaw angle of attack

In this study, a drag coefficient of 2.0 and a dynamic pressure value of 2×10^{-7} will be used. The nature of the surface material to transfer momentum from a molecule of atmosphere to the spacecraft strongly influences the value of σ. In these preliminary studies, a value of 0.8 will be used for σ. Parametric curves are generated in which the angle of attack β is varied. Using these values, the pressure equations reduce to

$$P_N = 4.8 \times 10^{-7} \sin^2 \beta \tag{A6a}$$

and

$$P_T = 3.2 \times 10^{-7} \sin \beta \cos \beta \tag{A7a}$$

The torque about the vehicle center of gravity is obtained by multiplying these pressure values by the area and moment arm of each surface. Also, the angle of attack β is the yaw angle error between the vehicle y axis and the normal to the orbit plane in the local geocentric coordinate system.

At a zero angle of attack, which is the control null condition, there is no aerodynamic disturbing torque due to vehicle symmetry. This assumes that the solar panels are very thin structures and, hence, present a negligible area to the relative wind. However, as the angle of attack increases, an aerodynamic torque on the vehicle is experienced.

If it is assumed that the center of gravity of the vehicle is coincident with the geometric center, the normal force component on each exposed surface passes through the vehicle center of gravity. In this case there is a zero moment arm and no torque results. However, the tangential component on each surface produces a force which does not pass through the center of gravity and hence, a component of torque results.

For positive values of β (see Figure A4), the tangential torque equation is developed with $F_{Y_E} > 0$ and conversely for negative values of β as shown in Figure A5.

Aerodynamic torque is derived in the same manner as solar pressure. The aerodynamic pressure is represented in experiment axes by three transformations from local vertical. The surfaces of the spacecraft presented to the aerodynamic pressure are dependent upon whether the aerodynamic pressure is positive or negative along the body y axis (see Figures A4 and A5).

Therefore, two equations are required to represent the aerodynamic torque.

The form of the equations are shown in (A8) and (A9).

If $F_{\bar{y}_E} \leq 0$

$$\tau_E = \begin{bmatrix} F_o\left[\left(\sum_{n=1}^{m} \ell'_{yn} A'_{yn}\right) j_E k_E - \left(\sum_{n=1}^{m} \ell'_{zn} A'_{yn}\right) j_E j_E\right] \\ F_o\left[\left(\sum_{n=1}^{m} \ell'_{zn} A'_{yn}\right) j_E j_E - \left(\sum_{n=1}^{m} \ell'_{xn} A'_{yn}\right) k_E j_E - \ell'_{x1} A'_{x1} i_E k_E\right] \\ F_o\left[\left(\sum_{n=1}^{m} \ell'_{xn} A'_{yn}\right) j_E j_E - \left(\sum_{n=1}^{m} \ell'_{yn} A'_{yn} + \ell'_{x1} A'_{x1}\right) i_E j_E\right] \end{bmatrix} \quad \text{(A8)}$$

where F_o is the aerodynamic pressure, lb/ft^2, and ℓ_{xn}, ℓ_{yn}, and ℓ_{zn} are the component moment arms of each surface A_{yn} and A_{xn}. The coefficients for the above equations were calculated, and the equations are summarized:

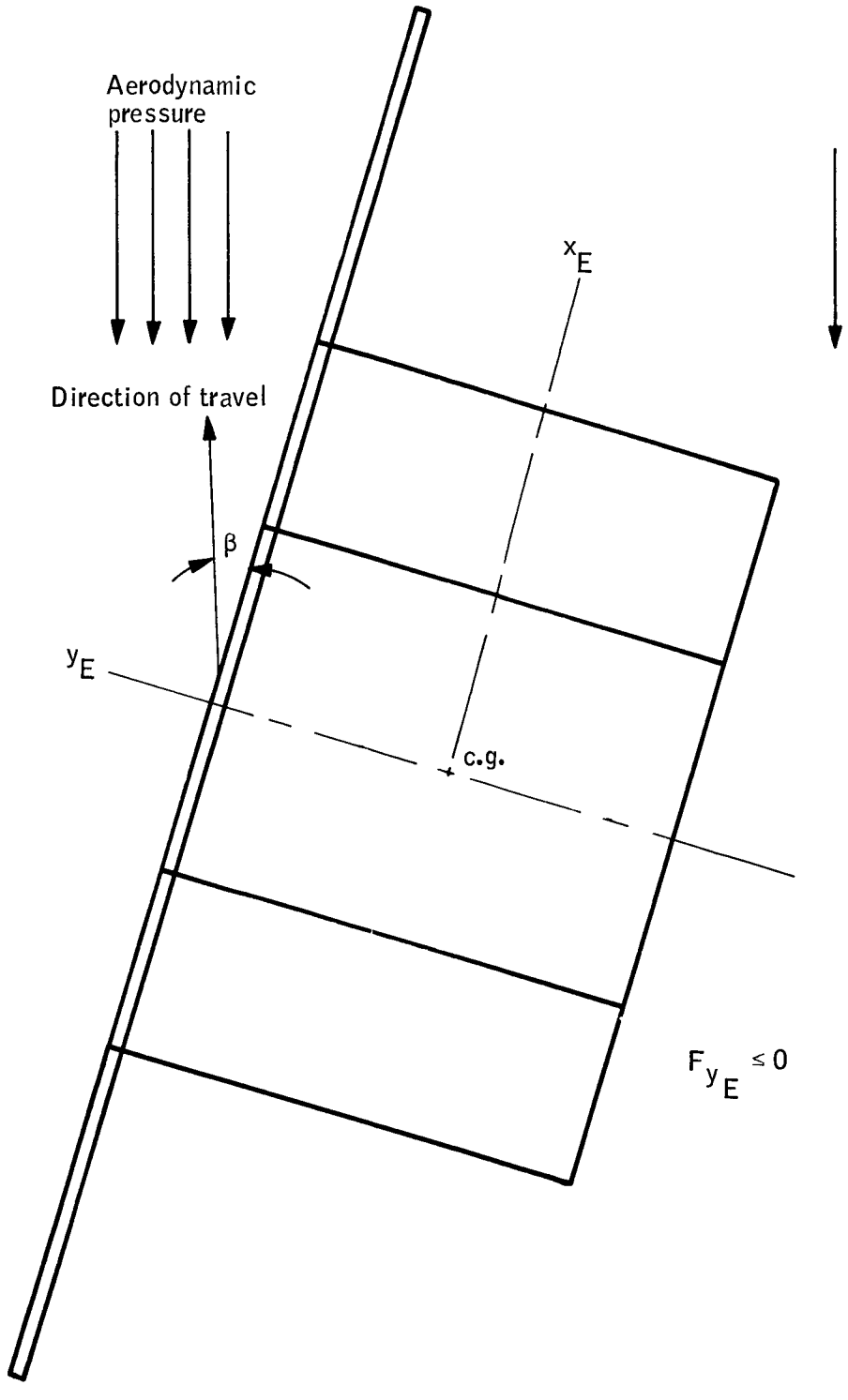

Figure A4. Aerodynamic Projections for Positive B

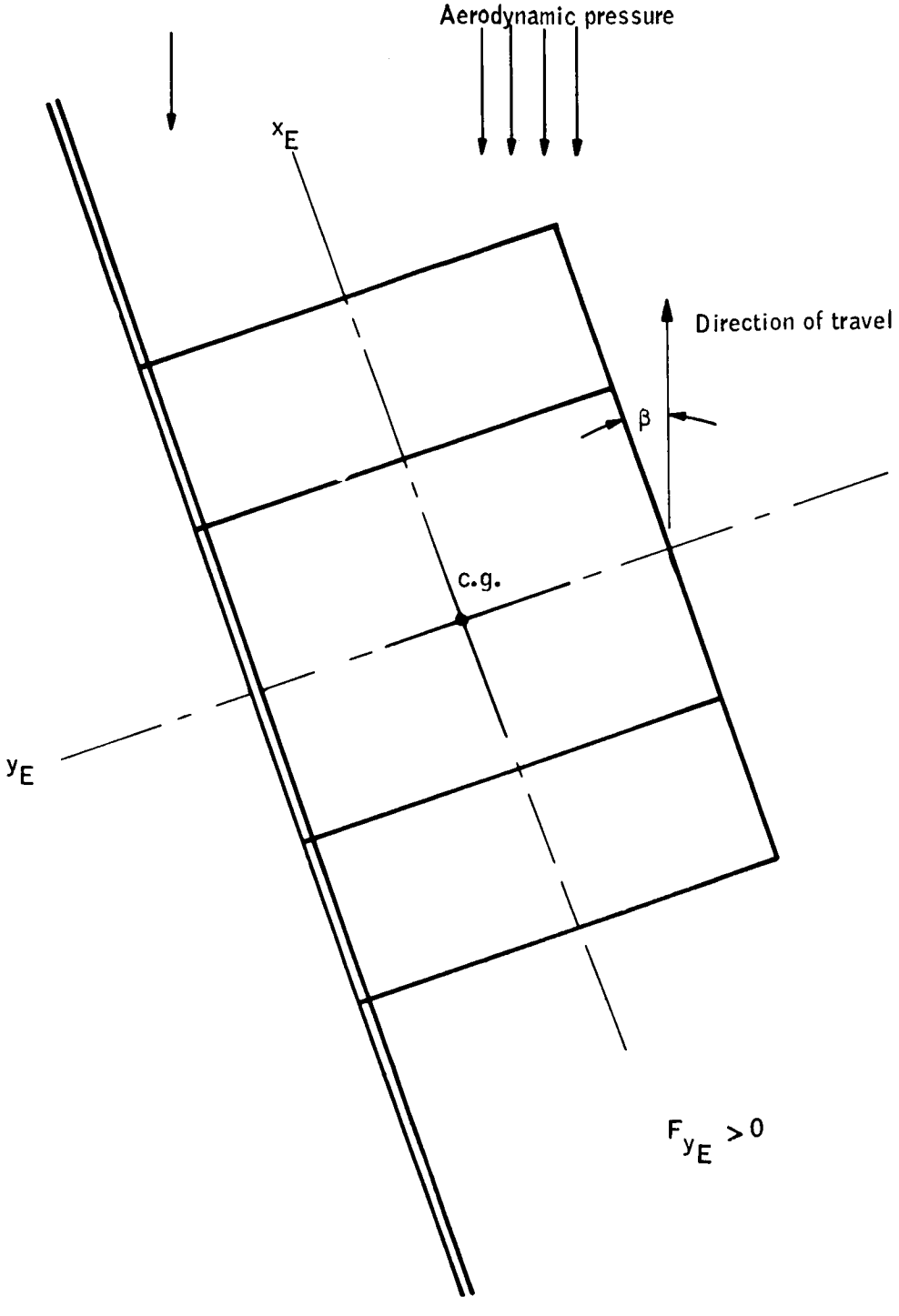

Figure A5. Aerodynamic Projections for Negative β

$$\left.\begin{aligned} \tau_x &= 2.8064 \times 10^{-5}\ j_E\, k_E \text{ ft-lb} \\ \tau_y &= 0 \\ \tau_z &= -8.4224 \times 10^{-5}\ i_E\, j_E \text{ ft-lb} \end{aligned}\right] \qquad \text{(A8a)}$$

If $F_{y_E} > 0$

$$\tau_E = \begin{bmatrix} F_o\left[\left(\sum_{n=1}^{m} \ell_{yn} A_{yn}\right) j_E k_E - \left(\sum_{n=1}^{m} \ell_{zn} A_{yn}\right) j_E j_E\right] \\ F_o\left[\left(\sum_{n=1}^{m} \ell_{zn} A_{yn}\right) j_E j_E - \left(\sum_{n=1}^{m} \ell_{xn} A_{yn}\right) k_E j_E - \ell_{x1} A_{x1}\, i_E k_E\right] \\ F_o\left[\left(\sum_{n=1}^{m} \ell_{xn} A_{yn}\right) j_E j_E - \left(\sum_{n=1}^{m} \ell_{yn} A_{yn} + \ell_{x1} A_{x1}\right) i_E j_E\right] \end{bmatrix} \qquad \text{(A9)}$$

Calculating the coefficients, the torques are

$$\left.\begin{aligned} \tau_x &= 1.0061 \times 10^{-5}\ j_E\, k_E \\ \tau_y &= -8.102 \times 10^{-6}\ j_E\, k_E \\ \tau_z &= 8.102 \times 10^{-6}\ j_E\, j_E - 1.9389 \times 10^{-5}\ i_E\, j_E \end{aligned}\right] \qquad \text{(A9a)}$$

The transformations are

$$\begin{bmatrix} i_E \\ j_E \\ k_E \end{bmatrix} = \text{CEL} \begin{bmatrix} 0 \\ -1 \\ 0 \end{bmatrix} = \text{CE} \begin{bmatrix} i_I \\ j_I \\ k_I \end{bmatrix} \qquad \text{(A9b)}$$

where

$$L = \begin{bmatrix} \cos\Omega & -\sin\Omega & 0 \\ \sin\Omega & \cos\Omega & 0 \\ 0 & 0 & 1 \end{bmatrix} \cdot \begin{bmatrix} 1 & 0 & 0 \\ 0 & \cos i & -\sin i \\ 0 & \sin i & \cos i \end{bmatrix} \cdot \begin{bmatrix} \cos\omega_\nu (t-t_o) & -\sin\omega_\nu (t-t_o) & 0 \\ -\sin\omega_\nu (t-t_o) & \cos\omega_\nu (t-t_o) & 0 \\ 0 & 0 & 1 \end{bmatrix}$$

$$\begin{bmatrix} i_I \\ j_I \\ k_I \end{bmatrix} = \begin{bmatrix} \cos\Omega \sin\omega_\nu (t-t_o) + \sin\Omega \cos i \cos\omega_\nu (t-t_o) \\ \sin\Omega \sin\omega_\nu (t-t_o) - \cos\Omega \cos i \cos\omega_\nu (t-t_o) \\ -\sin i \cos\omega_\nu (t-t_o) \end{bmatrix}$$

and

E = Euler transformation from inertial to body principal

C = Euler angle transformation matrix from body principal axes to body experiment axes

t_o = initial time

Ω = longitude of the ascending node

i = orbit inclination

ω_ν = orbit rate

To express the torque in body principal axes, the torques are transformed from experimental axes to the body principal axes by the inverse C transformation

$$\tau_B = C^{-1} \tau_E \tag{A10}$$

GRAVITY GRADIENT TORQUE

A gravity-gradient torque on the vehicle is due to the variation of earth's gravity field with altitude. This torque is a function of mass distribution, inertia ratios, and orientation relative to the gravity gradient. If the mass of the vehicle is symmetrically distributed about the vehicle center of gravity such that the inertias are identical or if the orientation of the principal axes is coincident with the local vertical coordinate system, no torque will result. However, as the HDS vehicle with an inertia ratio of greater than one assumes an attitude error in roll or yaw, a proportionate gravity-gradient torque will result. This torque is given by the expression

$$T_g = \frac{3G}{2R^3} (I_s - I_t) \sin 2\lambda \tag{A11}$$

where

G = gravitational constant, $1.408159 \times 10^{-6} ft^3/sec^2$

R = distance from center of earth to spacecraft, feet

I_s = moment of inertia about principal spin axis, slugs-ft^2

I_t = moment of inertia about principal lateral axis, slugs-ft^2

λ = angle between principal axes and local vertical coordinates

At the altitude of 270 nautical miles, the orbit radius is given by

$$R = (270)(6080) + 20\,909\,200$$

$$R = 22\,550\,800 \text{ feet}$$

The torque about the x_N axis is given by

$$T_{x_N} = \frac{3G}{R^3}(I_y - I_z) \sin\lambda \cos\lambda \qquad \text{(A11a)}$$

To relate the angle λ to the Euler angles ϕ and ψ, the following substitution is made

$$\sin\lambda = \sin\phi \cos\psi$$

$$\cos\lambda = \cos\phi$$

With this substitution, the torque about the x_L axis in terms of ϕ and ψ is given as

$$T_{x_N} = \frac{3G}{R^3}(I_y - I_x) \sin\phi \cos\psi \cos\phi \qquad \text{(A11b)}$$

The transformation from torque about the x_N axis to torque about the x_B and z_B axes is made through a transformation matrix internally programmed in the computer simulation.

METEOROID DISTURBANCE TORQUE

This section provides a description of the meteoroid environment encountered by the earth and its satellites and a definition of the meteoroid torque equations to be used in the HDS disturbance torque model.

This analysis is based upon a review of the current literature concerning satellite measurement of the meteoroid environment and a study of the hypervelocity impact phenomenon.

Initially, it is important to distinguish the word meteoroid from meteor or meteorite. Meteoroids are restricted to particles or debris travelling in space. Meteors designate the luminous phenomena associated with meteoroids as they enter the earth's atmosphere. A meteorite denotes a meteoroid which has been found on the earth's surface. The scientific investigation of

meteoroids is confined to masses ranging from perhaps 10^{-13} gram to about 100 grams. In size, they vary down to perhaps 1 or 2 μ in diameter. When the dimensions of meteoroids reach this limiting order, the large increase in the ratio of particle area to its mass results in the dominance of solar light pressure effect over solar gravitational force. These tiny particles are driven away from the sun by the radiation pressure, and little or no data is available concerning them.

Origin and Composition of Meteoroids

Meteoroids are generally classified into two groups which are defined by their origin; asteroidal or cometary. A third possible existing group, constituting a very small percent of the meteoroid distribution, is that of interstellar debris.

The asteroidal particles represent less than 10 percent of the total influx of particles entering the earth's atmosphere. They originate in the asteroidal belt which astronomers believe to have resulted from the fragmentation of a planet into smaller bodies, the asteroids. Iron, nickel, and various stony materials in varying amounts make up the composition of these bodies. The particle densities of of the order of 3.5 g/cm^3.

The cometary particles represent some 90 percent or greater of the total influx of particles. Their porous nature, low density (0.03 to 0.05 g/cm^3), and frangible characteristics, favor the production of a flaring meteor. (See ref. 14.)

Meteoroid Streams

Nearly 70 percent of all incoming meteors are generally classified as belonging to streams in some conic path about the sun. These streams are either narrow with closely packed particles, or very broad in extent with widely separated particles. Of the total incoming flux, about 30 percent is associated with particular streams, e.g., the Leonids; the remainder is referred to as sporadic. Present-day classification describes all meteoroids as belonging to streams; however, the streams are classed as periodic or sporadic (see ref. 15).

Tables and graphs describing meteoroid flux per square unit per unit time represent statistical averages over long periods. The meteoroid flux rate is never constant - even after correction for the observed effects of large-particle showers. The variation in flux rate is one or two orders of magnitude with periods of low or high flux measurements of a few days duration. Certain of these variations are due to known meteor showers and cause annual variations. Random variations also exist with periods of a few days, and can be dealt with only on a statistical basis. Hence, shortlived satellites or rockets may give meteoroid flux measurements very different from the average. Therefore, meteoroid interception by impact sensors is dependent upon both the probability of intercepting a meteoroid stream of known average density and the probability of encountering a given flux intensity during the sampling period.

Meteor data is made up of two components, sporadic meteors and shower meteors belonging to the well-defined, short-period comets and meteor streams. The shower meteors are distinguished by their common radiants and make up about 20 to 30 percent of the meteors sighted. The peak activity during these showers may be four to five times the sporadic meteor rate and much greater on extremely rare occasions. For example, a rate increase of 5000 was reported on 9 to 10 October 1946 when the Giacobinid-Zinner comet orbit was crossed by earth. One of the most spectacular visual displays was that of the Leonids shower in 1833 in which a rate increase estimated to be 20 000 times the normal rate was observed.

Meteoroid Velocity

Meteoroids encountered by the earth will have velocities relative to the earth, ranging from 11 km/sec to 72 km/sec. This is based on the fact that for a particle following a parabolic path about the sun the maximum velocity it could have at the distance of earth from the sun is approximately 42 kilometers per second. If such a particle meets earth head on, as it orbits the sun at a velocity of approximately 30 kilometers per second, a combined velocity (neglecting earth's gravitational attraction) of approximately 72 kilometers per second is obtained. To achieve higher velocities, the particles would have to be following hyperbolic paths and thus be of interstellar origin. The lower limit occurs when the particles obtain their velocity relative to earth by earth gravitational attraction alone. For space vehicles encountering these particles the range of relative velocities could be somewhat greater. This is due to the velocity of the space vehicle.

Brighter meteors have higher velocities and fainter meteors are slower. In reference 16, a total of 2529 photographs of meteors were evaluated to determine a mean meteoroid velocity of 28 km per second. It is pointed out, however, that many meteoroids are much slower and that they enter the earth's atmosphere unobserved. Hence the mean meteoroid velocity should be reduced to about 22 km per second.

A second argument shown in reference 16 indicates that the determination of the meteor ionizing efficiency is proportional to its velocity to the fourth power. This would result in a mean meteoroid velocity calculation of greater than 30 km per second.

Since the mean velocity is not well defined, a conservative value of 30 km per second is generally accepted by most authors.

Meteoroid Flux Density

The meteoroid flux density could have a day-to-day variation of several orders of magnitude due to encountering the orbits of known meteoroid streams. There may be as many meteoroids striking a spacecraft in one day due to a meteoroid stream as there are in a whole year due to sporadic meteoroids. Also, the meteoroids in a particular stream are all traveling in the same orbit with the same relative velocity. For example, the Geminid stream has a mean velocity of 36.2 km per second and the Orionid stream has a mean

velocity of 67.7 km per second (ref. 12). Sporadic meteoroids, however, are omni-directional, vary in velocity from 11 to 72 km per second, and have a very low flux density.

Numerous attempts have been made to determine an average value of the meteoroid flux environment in the vicinity of earth. Due to assumptions and differing methods, these calculations have resulted in flux density values which are several orders of magnitude apart. Reference 17 cites several flux equations which result in widely varying densities. Two values are given (3.4×10^{-8} g/m^2 - sec, and 1.96×10^{-10} g/m^2 - sec) using two different approximations to the density curve shown in Figure A6. Both calculations, however, are biased toward the smaller, more dense particles and are highly susceptible to the assumed particle size cut-off point. It is assumed that particles smaller than a certain magnitude are all swept away by solar radiation pressure. Additionally, two other quantities are given (3.62×10^{-11} g/m^2 - sec) and (3.0×10^{-11} g/m^2 - sec) which are biased toward the larger particles and are somewhat insensitive to the smaller particles. In this case, the assumed cut-off point on the large particle end of the scale strongly influences the calculation. Since the larger particles occur more rarely, a cut-off point of one impact per square meter per year could be made, which would result in reducing the flux calculation by more than an order of magnitude (2.5×10^{-12} g/m^2 - sec).

Since wide disagreement exists in the literature concerning the development of an averaged flux density equation, another approach is to determine the momentum of each meteoroid of each size and examine its probability of occurrence. The control system, then, would be sized to balance the disturbance induced by each meteoroid impact separately. Meteors may be classed accordingly to their visual magnitude. Magnitudes fainter than +5 which cannot be observed visually, are detected by radar observations of ion trails. The data shown in Figure A6 then corresponds to the mass and particle frequency versus visual magnitude shown in Table A1. Using this data, the momentum of each meteoroid of each size together with its frequency of occurrence is used to determine the total control impulse required to balance the disturbance. All of these calculations assume that all meteoroids impinge on the surface and there is a pure momentum transfer to the impacted surface. Modification to this momentum transfer assumption is discussed in the next section of this report.

In Table A1, column 1 shows the visual meter magnitude as a function of meteoroid mass (column 2) assuming an average relative velocity of 30 km/sec. Column 3 shows the accumulated flux density of meteoroid mass m and larger, which corresponds to the curves shown in Figure A6 (ref. 18). The meteoroid flux density within each visual magnitude is then shown in column 4. Using an estimated vehicle surface area of eight square meters and a one-year mission time, the probability of encountering a meteoroid of mass m is shown in column 5. The momentum of a meteoroid of each size, shown in columns 6 and 7, is multiplied by the probability of occurrence to determine

TABLE A1. - METEOROID MOMENTUM DATA

Meteor visual magnitude	Mass, m, grams	Flux density, N, lb/meter^2-sec accumulative	Flux density in each magnitude, N_M	Impacts in one year in each mag, N_M	Momentum of each meteoroid size, MV, $\frac{g\text{-}cm}{sec}$	MV, lb_f-sec	MV N_M, lb_f-sec
5	0.250	1.82×10^{-11}	1.82×10^{-11}	4.65×10^{-3}	7.50×10^{5}	1.69	7.87×10^{-3}
6	9.95×10^{-2}	5.30×10^{-11}	3.48×10^{-11}	8.90×10^{-3}	2.98×10^{5}	6.70×10^{-1}	5.97×10^{-3}
7	3.96×10^{-2}	1.34×10^{-10}	8.10×10^{-11}	2.08×10^{-2}	1.19×10^{5}	2.67×10^{-1}	5.55×10^{-3}
8	1.58×10^{-2}	3.35×10^{-10}	2.01×10^{-10}	5.15×10^{-2}	4.74×10^{4}	1.07×10^{-1}	5.50×10^{-3}
9	6.28×10^{-3}	8.41×10^{-10}	5.06×10^{-10}	1.30×10^{-1}	1.88×10^{4}	4.23×10^{-2}	5.49×10^{-3}
10	2.50×10^{-3}	2.12×10^{-9}	1.28×10^{-9}	3.28×10^{-1}	7.50×10^{3}	1.69×10^{-2}	5.54×10^{-3}
11	9.95×10^{-4}	5.30×10^{-9}	3.18×10^{-9}	8.14×10^{-9}	2.98×10^{3}	6.70×10^{-3}	5.46×10^{-3}
12	3.96×10^{-4}	1.34×10^{-8}	8.10×10^{-9}	2.08	1.19×10^{3}	2.67×10^{-3}	5.55×10^{-3}
13	1.58×10^{-4}	3.35×10^{-8}	2.01×10^{-8}	5.15	4.74×10^{2}	1.07×10^{-3}	5.52×10^{-3}
14	6.28×10^{-5}	8.41×10^{-7}	5.06×10^{-8}	1.30×10^{1}	1.88×10^{2}	4.23×10^{2}	5.49×10^{-3}
15	2.50×10^{-5}	2.12×10^{-7}	1.28×10^{-7}	3.28×10^{1}	7.50×10^{1}	1.69×10^{-4}	5.54×10^{-3}
16	9.95×10^{-6}	5.30×10^{-7}	3.18×10^{-7}	8.14×10^{1}	2.98×10^{1}	6.70×10^{-5}	5.46×10^{-3}
17	3.96×10^{-6}	1.34×10^{-6}	8.10×10^{-7}	2.08×10^{2}	1.19×10^{1}	2.67×10^{-5}	5.55×10^{-3}
18	1.58×10^{-6}	3.35×10^{-6}	2.01×10^{-6}	5.15×10^{2}	4.74	1.07×10^{-5}	5.52×10^{-3}
19	6.28×10^{-7}	8.41×10^{-6}	5.06×10^{-6}	1.30×10^{3}	1.88	4.23×10^{-6}	5.49×10^{-3}
20	2.50×10^{-7}	2.12×10^{-5}	1.28×10^{-5}	3.28×10^{3}	7.50×10^{-1}	1.69×10^{-6}	5.54×10^{-3}
21	9.95×10^{-8}	5.30×10^{-5}	3.18×10^{-5}	8.14×10^{3}	2.98×10^{-1}	6.70×10^{-7}	5.46×10^{-3}
22	3.96×10^{-8}	1.34×10^{-4}	8.10×10^{-5}	2.08×10^{4}	1.19×10^{-1}	2.67×10^{-7}	5.55×10^{-3}
23	1.58×10^{-8}	3.35×10^{-4}	2.01×10^{-4}	5.15×10^{4}	4.74×10^{-2}	1.07×10^{-7}	5.52×10^{-3}
24	6.28×10^{-9}	8.41×10^{-4}	5.06×10^{-4}	1.30×10^{5}	1.88×10^{-2}	4.23×10^{-8}	5.49×10^{-3}
25	2.50×10^{-9}	2.12×10^{-3}	1.28×10^{-3}	3.28×10^{5}	7.50×10^{-3}	1.69×10^{-8}	5.54×10^{-3}
26	9.25×10^{-10}	5.30×10^{-3}	3.18×10^{-3}	8.14×10^{5}	2.98×10^{-3}	6.70×10^{-9}	5.46×10^{-3}
27	3.96×10^{-10}	1.34×10^{-2}	8.10×10^{-3}	2.08×10^{6}	1.19×10^{-3}	2.67×10^{-9}	5.55×10^{-3}
28	1.58×10^{-10}	3.35×10^{-2}	2.01×10^{-2}	5.15×10^{6}	4.74×10^{-4}	1.07×10^{-9}	5.52×10^{-3}
29	6.28×10^{-11}	8.41×10^{-2}	5.06×10^{-2}	1.30×10^{7}	1.88×10^{-4}	4.23×10^{-10}	5.49×10^{-3}
30	2.50×10^{-11}	2.12×10^{-1}	1.28×10^{-1}	3.28×10^{7}	7.50×10^{-5}	1.69×10^{-10}	5.54×10^{-3}
31	9.95×10^{-12}	5.30×10^{-1}	3.18×10^{-1}	8.14×10^{7}	2.98×10^{-5}	6.70×10^{-11}	5.46×10^{-3}

the expected impulse exerted against the vehicle (column 8). The sum of column 8 results in a total of 0.146 lb-sec. Assuming that a meteoroid may strike anywhere on the vehicle and estimating an average distance of impact from the center of gravity of 2.5 feet with a control moment arm of 2.5 feet, 0.146 lb-sec of control impulse is required to balance the meteoroid disturbance torque. Since the control system will be required to compensate for the individual impacts of the larger more sparse meteoroids, the impulse required to balance a magnitude 5 meteoroid impacting at 2.5 feet from the center of gravity and traveling at 72 km per second could be as high as 3.3 lb-sec. However, the probability of encountering a meteoroid of magnitude

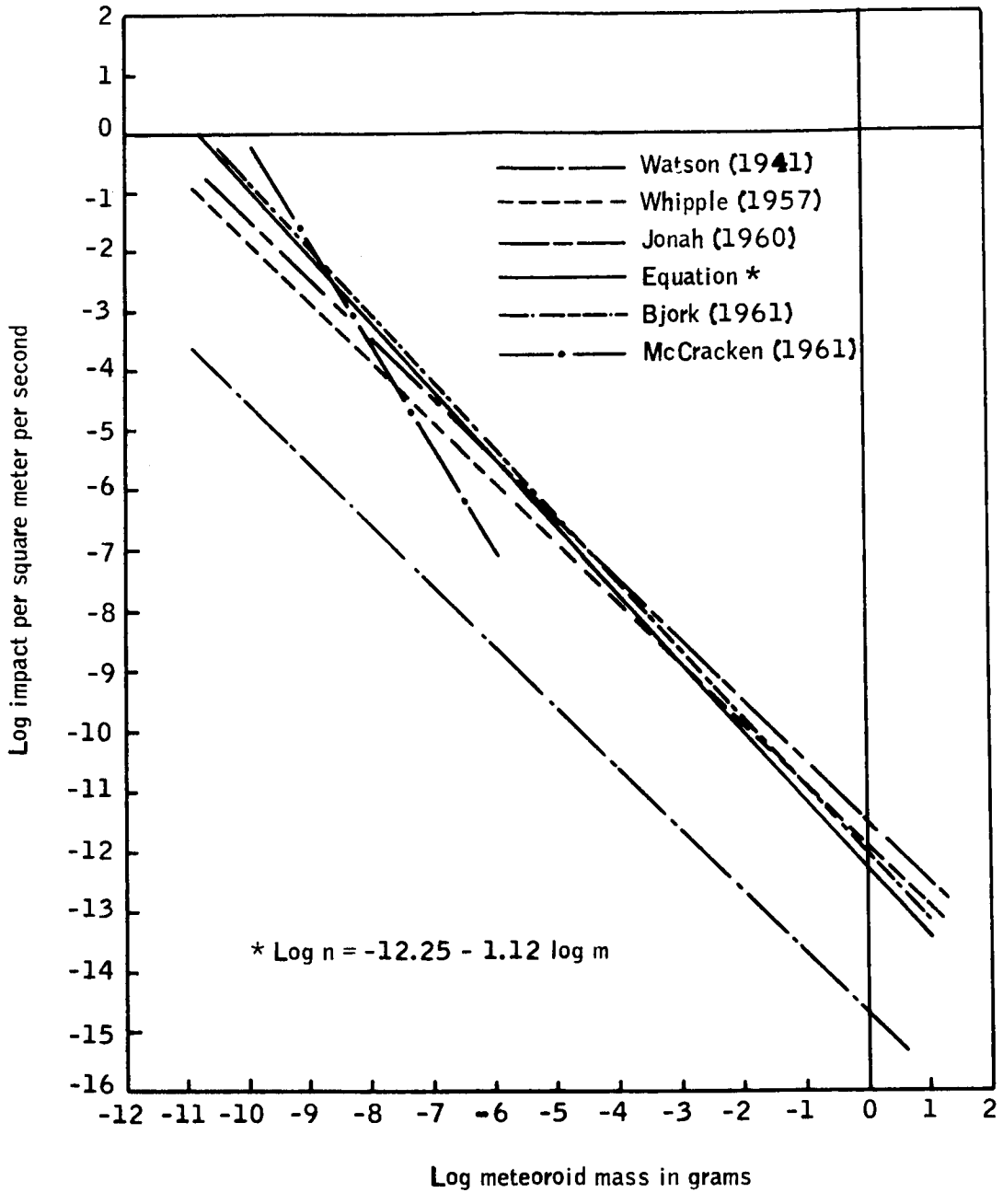

Figure A6. Meteroid Extrapolations

5 traveling at 72 km per second is less than once in 200 years. Further, an impact of this nature would penetrate several inches of material, causing most of the meteoroid to continue through the spacecraft resulting in lower momentum exchange and possible damage to the spacecraft.

For comparison, 0.146 lb-sec of total impulse converts to 4.61×10^{-10} gm/m^2 - sec average flux density as follows:

$$\left(\frac{\text{sec}}{30 \times 10^5 \text{ cm}}\right)\left(\frac{0.146 \text{ lb-ft-sec}}{63 \times 10^6 \text{ sec}}\right)\left(\frac{1}{8 \text{ ft}^2}\right)\left(\frac{4.448 \text{ newtons}}{\text{lb}_f}\right)\left(\frac{1 \times 10^5 \text{ dynes}}{\text{newtons}}\right)\left(\frac{\text{ft}^2}{0.0929 \text{ m}^2}\right)\left(\frac{\frac{\text{g-cm}}{\text{sec}^2}}{\text{dyne}}\right)$$

This compares favorably to the mean of the previously stated average flux density calculations. Since this results in a pressure force of 5.89×10^{-10} lb/ft^2 it may be concluded that meteoroid impact provides a disturbance torque which is several orders of magnitude below solar radiation pressure (1×10^{-7} lb/ft^2). It is restated, however, that this assumes a one to one momentum exchange from the meteoroid to the spacecraft.

Momentum Amplification

Several theoretical calculations have been proposed concerning a momentum amplification due to hypervelocity meteoroid impact. Since a meteoroid can displace or expel more than its own material mass from a surface, several authors (ref. 17) have advanced the theory of momentum amplification ranging from a factor of 2 to a factor as high as 36. A factor of 2 is conceivable for the smaller particles which may strike a surface and "bounce back" at nearly the same velocity. Larger or faster meteoroids, however, will cause craters resulting in expelling material (ejecta) from the surface. This phenomenon gives rise to the momentum amplification theory. Still other particles will completely penetrate the surface and continue through the spacecraft carrying some material with them; this could result in a slightly less than one momentum exchange factor.

The material erosion on satellites necessary to substantiate a high momentum amplification factor has not been observed. Therefore, it is assumed that through the spectrum of meteoroids, there could be momentum amplification factors ranging from slightly less than 1 to possibly greater than 2 or 3. Using an average momentum amplification factor of 2, the impulse becomes 0.392 lb-sec.

Torque Equations

To evaluate the effects of meteoroids impacts on the vehicle, it is assumed that the vehicle will respond to each individual impact and that there is no cancelling of momentum due to omni-directional impact. Each impact,

therefore, will induce an impulsive step input into the vehicle body rates. A magnitude 9 meteoroid traveling at 72 km/sec will induce an impulse of 8.5×10^{-2} lb-sec to the vehicle. The probability of encountering smaller meteoroids increases, but the individual impact effect decreases. Therefore, for this analysis, 8.5×10^{-2} lb-sec will be considered maximum. The step into each vehicle body rate is given as

$$\left.\begin{aligned} \Delta\omega_y &= \frac{0.085\ell_1}{I_y} \\ \Delta\omega_x &= \frac{0.085\ell_2}{I_x} \\ \Delta\omega_z &= \frac{0.085\ell_3}{I_z} \end{aligned}\right\} \quad \text{(A12)}$$

where

ℓ_1, ℓ_2, ℓ_3 are the impact moment arms (currently 2.25 feet), and

I_x, I_y, I_z are the vehicle moments of inertia

It is anticipated that computer simulation will indicate that these disturbances are negligible, and, if so, the cross product terms will not have to be included.

DISTURBING TORQUES DUE TO ROTATING INTERNAL EQUIPMENT

Rotating equipment within the HDS spacecraft will induce opposing rotational torques. Since the solar panels are to be fixed rather than rotating, no rotational disturbance torque will result from these sources. Also, if there are no tape recorders used in this vehicle there are no recorder start-up torques.

The radiometer calibration system contains three moving components generating angular impulses during each calibration period (rotation period). Although each motion reverses itself during the period, cancelling can be assumed only about the vehicle spin axis. Rates imposed about the transverse axis will produce coning or wobble motion which should not be expected to cancel. Component forward and reverse motions have been calculated to produce from 0.0018 to 0.063 in.-lb-sec. However, the orientation of this motion relative to the spacecraft body axes is not entirely defined. If aligned with the vehicle spin axis, spin rate increase and decrease increments as large as 16 arc sec/sec can be encountered twice per rotation. At a spin rate of three rpm, a calibration actuation about a transverse axis will produce a half-cone angle of about 100 arc sec. Clearly, this could result in vehicle wobble angles of several degrees in one orbit which would have to be damped out. This implies that radiometer actuation torque balancing may be a requirement.

VEHICLE OUTGASSING DISTURBANCE TORQUES

Outgassing from the vehicle produces an unpredictable disturbance torque about some axis of rotation. Sources of outgassing torques to be considered for the HDS vehicle are

- Trapped air in crevices and joints
- Reaction jet valve leakage
- Cooling system outgassing

Trapped air pockets in crevices and joints will produce an exponentially decaying torque. While the magnitude of this torque cannot be easily determined, its decay is rapid and it may be considered negligible in this analysis.

The cooling system is the only source of vehicle outgassing. Although current plans are to provide porting along the spin axis, which would theoretically produce no disturbing torque, port alignment errors may result. The outgassing port misalignment may be similar to typical reaction jet misalignment characteristics. In this case, a displacement d from the c.g. and an angular misalignment E may be statistically considered. Since the errors are considered statistical, they may occur in either axis. Therefore, the given torque error equation may be used in either the x or the z axis.

The torque due to a displacement from the c.g. is given as

$$\text{Torque} = Fd \tag{A13}$$

where

F = outgassing force, lbs

d = displacement error, feet

The torque due to an angular misalignment is given as

$$\text{Torque} = FL_1 \sin E \tag{A14}$$

where

L_1 = distance from c.g. to port, feet

E = angular misalignment error

The values to be used in this preliminary analysis are

$F = 2.75 \times 10^{-8}$ lb

$d = 0.05$ feet, 3σ

$L_1 = 2.25$ feet (radius of cylinder)

$E = 0.25$ degrees, 3σ

The rss of the two torque values results in a 3σ probable disturbance torque during the entire one-year mission of

$$\text{Torque} = \left[(0.138 \times 10^{-8})^2 + (0.0247 \times 10^{-8})^2\right]^{1/2}$$

$$\text{Torque} = 0.14 \times 10^{-8} \text{ ft-lbs}$$

For analysis purposes it is estimated that 70 pounds of neon could be required to provide detector cooling. This results in an expulsion flow rate of approximately 2×10^{-6} lb-sec. The expulsion exit velocity is calculated to be about 3 inches/sec, resulting in a calculated value for outgassing thrust of

$$F = \frac{(\text{flow rate})\,(\text{exit velocity})}{g} \tag{A15}$$

$$F = \frac{2 \times 10^{-6} \text{ lb/sec } (3 \text{ inches/sec})}{(12 \text{ inches/foot})\,(32.2 \text{ ft/sec}^2)}$$

$$F = 2.75 \times 10^{-8} \text{ lb}$$

where

g = gravity acceleration

Over the one-year period, this amounts to incorporating only 0.044 ft-lb-sec momentum. Therefore, this disturbing force may be neglected in all axes.

MAGNETIC INTERACTION TORQUE

A disturbance torque will exist due to the interaction of the current flow in the vehicle electrical circuits and the earth's magnetic field. While the design of the vehicle wiring and conducting elements can reduce the effective disturbance, a residual magnetic moment will remain. Further, it can be expected that this residual moment will vary in magnitude and direction as a function of control mode and power usage.

The earth's magnetic field at an altitude of 500 km varies from 0.20 gauss at the South American anomaly to as high as 0.48 and 0.54 gauss at the North and South Poles, respectively. The field at this altitude is quite stable. The altitude is high enough to avoid minor surface anomalies but not so high as to be significantly affected by large solar flares. Poles of the magnetic field are oriented about 17 degrees from the earth's polar axis. The field intensity is shown in Figure A7.

The general torque equation due to the interaction of the spacecraft residual magnetic moment with the earth's magnetic field is

$$\vec{T} = \vec{M} \times \vec{B} \tag{A16}$$

In body axes, this reduces to

$$\left.\begin{aligned} T_{x_m} &= M_y B_z - B_y M_z \\ T_{y_m} &= M_z B_x - B_z M_x \\ T_{z_m} &= M_x B_y - B_x M_y \end{aligned}\right] \tag{A17}$$

where

M_x, M_y, M_z = body axis residual magnetic moments, ft-lb/gauss

B_x, B_y, B_z = body axis components of the earth's magnetic field, gauss

The residual magnetic moment is normally given in the units of amp-turns-meters^2, which can be transformed into ft-lb/gauss directly. The magnetic field is determined by the solution of the Jenson and Cain 100-term Polynomial, providing the three components (B_ϕ, B_ψ and B_r) in geocentric coordinates. A transformation from geocentric to body coordinates is then used to obtain the body components of the field.

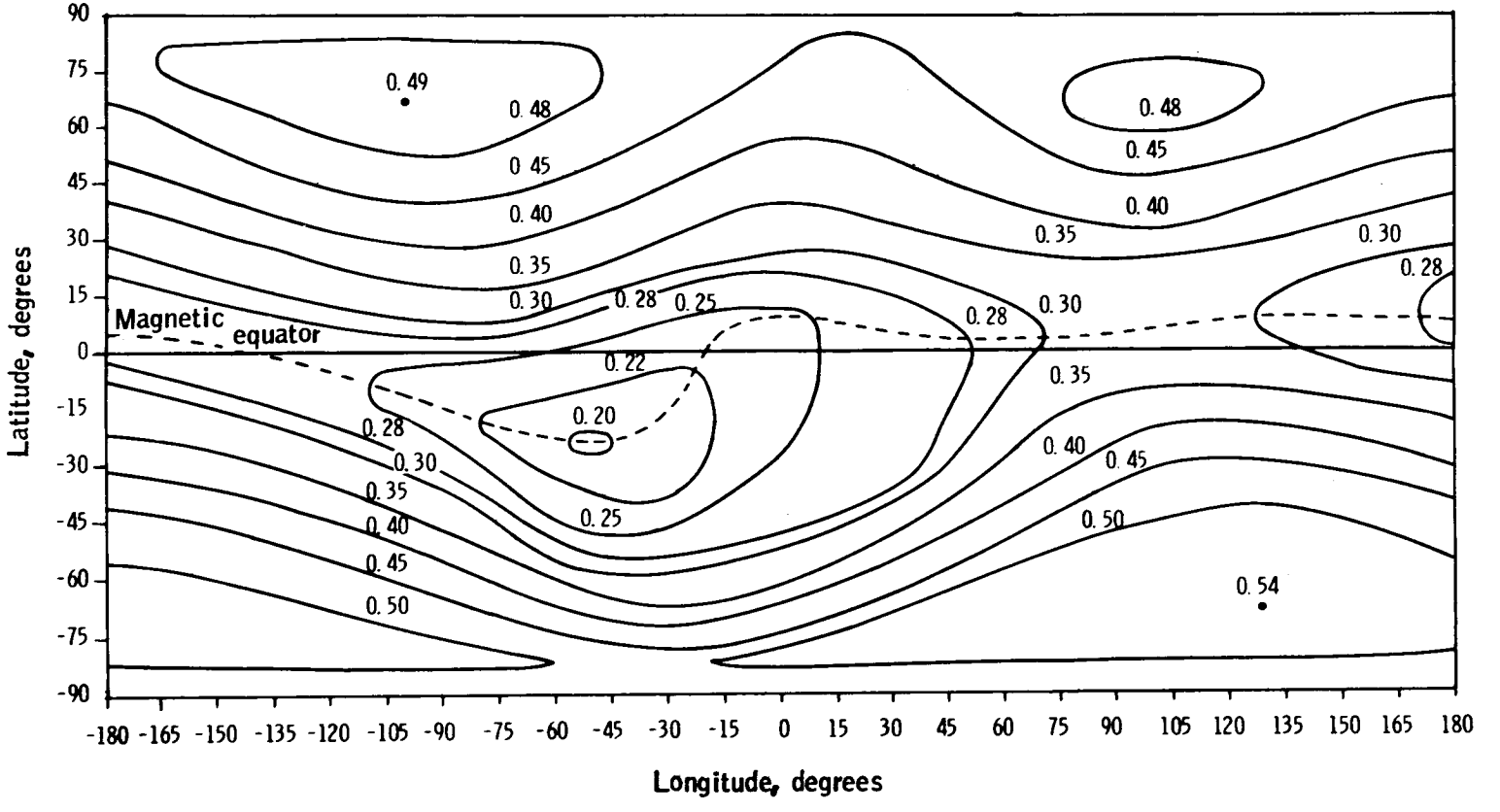

Figure A7. Magnetic Field Intensity - B, Gauss - at Altitude of 500 Kilometers

EDDY-CURRENT TORQUE

Eddy current disturbance torques result since the spacecraft is a rotating conductor in a magnetic field. This torque tends to retard the vehicle spin rate and produce a precession of the spin axis. The general eddy current torque expression is

$$\vec{T} = K(\vec{\omega} \times \vec{B}) \times \vec{B} \tag{A18}$$

Expanding the eddy current torque equation, the body axis expressions are obtained based on a conducting sphere derivation. This is considered an adequate representation for the purpose of this analysis. (See ref. 9 and 19).

$$\left.\begin{aligned} T_{x_E} &= -K\left[(B_y^2 + B_z^2)\,\omega_x - (B_x B_y \omega_y + B_x B_z \omega_z)\right] \\ T_{y_E} &= -K\left[(B_x^2 + B_z^2)\,\omega_y - (B_x B_y \omega_x + B_y B_z \omega_z)\right] \\ T_{z_E} &= -K\left[(B_x^2 + B_y^2)\,\omega_z - (B_x B_z \omega_x + B_y B_z \omega_y)\right] \end{aligned}\right\} \tag{A19}$$

The eddy current coefficient is a function of the conductivity of the spacecraft. At this point in the system definition the conductivity coefficient is a nebulous quantity. However, for purposes of this study, the observed spin rate decay of other satellites results in the calculation of a value $K = 2.86 \times 10^{-5}$ ft-lb-sec/gauss^2.

APPENDIX B

ERROR ANALYSIS OF A HORIZON SENSOR FOR A SPINNING BODY

APPENDIX B

ERROR ANALYSIS OF A HORIZON SENSOR FOR A SPINNING BODY[a]

SPECIAL DESIGN FEATURES

The proposed sensor is similar to an existing design used on the Tiros program but will be uniquely modified to incorporate the results of a recently completed company-sponsored development program for improving sensor accuracy.

The sensor operates as a horizon crossover indicator when installed in a spinning space vehicle and provides discrete output pulses at the leading and trailing edge horizons. When operating at synchronous altitude with a nominal spin rate of 38 rpm, the accuracy is significantly better than specification requirements.

The proposed sensor has several attractive design features which can be briefly described as follows:

Spectral Band

The spectral band of operation is the 14 to 16 μ, CO_2 band. It has been well established by a number of investigations that earth radiance in this region varies by a factor of no more than 2:1. Minimizing the range of radiance contrasts is a necessary step in achieving high orbital accuracy.

In addition it permits the use of a simple differentiating type amplifier to drive leading and trailing edge pulses of the earth. In other spectral bands, the pressure of cold clouds requires special logic or thresholding techniques to preclude the generation of erroneous horizon presence information.

Radiance Compensation

It is generally recognized that in high accuracy horizon sensors and horizon crossing indicators the selection of an appropriate system threshold level will have a considerable effect on the sensor's orbital accuracy. This influence is directly proportional to the difference in earth radiance manifest at the leading and trailing edges of the earth scan. For almost any sensor threshold value established, it can be shown that the points of intersection with an earth radiance waveform that is asymmetric (i.e., where there is a difference in

[a]This Appendix consists of excerpts from Barnes Engineering Proposal BEC P-1092.

radiance level between the two horizons) will not be centered with respect to the center point of the earth waveform. This uncertainity in the precise location of the center (actually a variable time delay) becomes one of the prime components of sensor error.

For the unique case where the threshold is located at 50 percent of the leading and trailing radiance levels, the center of the earth waveform, irrespective of its symmetry, remains at the midway point between the two threshold crossovers. This is apparent when one considers that the time to traverse each horizon is the same and that selection of a threshold value at the center of each ramp results in the selection of a pivotal point which will not vary in time occurrence with radiance variations at either edge. It is therefore most advantageous to utilize a system threshold of 50 percent and completely eliminate all radiance variation errors.

Although the 14 to 16 μ band is relatively isoradiant, it can still exhibit variations of approximately 2:1 which may result in significant sensor errors. To preclude this possibility, Barnes proposes to incorporate an exceedingly simple but effective electronic technique which will always locate the threshold at 50 percent of both the leading and trailing edges, regardless of earth radiance. This technique does not rely on averaging but functions in real time to instantaneously establish a correct and separate threshold for each horizon crossover.

The threshold circuit of the sensor operates in the following manner. The bolometer output signal is processed in an amplifier which passes only high frequency components of the signal. The output, comprising a train of positive and negative pulses corresponding to the leading and trailing portions of the earth signal, is entered into three parallel circuits. One of these circuits is a simple RC network that locates a zero voltage reference at the space level. The other two circuits are clamps which separate and clamp the peak leading edge (positive) excursion to ground and the peak trailing edge (negative) excursion to ground.

The leading edge crossing point is determined by summing the averaged pulses with the pulses clamped to zero at the positive peak. The resultant sum passes through zero at 50 percent of the maximum pulse height regardless of the pulse amplitude. The trailing edge crossing point is similarly determined by summing the averaged pulses with the pulses clamped to zero at the negative peak.

SYSTEM ACCURACY ANALYSIS

Signal Processing

As has been pointed out previously, the signal processing method employed in this instrument completely eliminates errors due to radiance variations. The remaining source of error is the system noise at the threshold. To compute this error it is necessary to discuss the waveform generated by the passage of the detector field of view across the horizon and to understand how this signal is modified for the radiance compensating circuitry.

The field of view is 1° x 1° and oriented so that its diagonal is in line with the scan path across the earth. In this configuration the radiance waveform generated at the bolometer as the field crosses the horizon is a ramp of 1.41° in duration. This radiance signal is then converted by the immersed bolometer to an electrical signal which is then filtered. The radiance signal is acted on by the following transfer function which include the effect of the bolometer time constant.

$$F(s) = \frac{s}{(\tau_{bol} s + 1)(\tau_1 s + 1)(\tau_2 s + 1)^2}$$

For the computations shown later

$\tau_{bolometer} = 1.0 \times 10^{-3}$ sec,

$\tau_1 = 5.0 \times 10^{-3}$ sec, and

$\tau_2 = 1.0 \times 10^{-3}$ sec.

The result of passing the radiance signal through this filtering is a partially differentiated waveform. Pulses generated by a leading edge radiance ramp of 1.4° are shown in Figure B1 for three spin rates, 28, 38 and 48 rpm. The level reached by each pulse is between 0.425 and 0.500 indicating that sufficient bandwidth has been retained to yield a pulse height relatively independent of spin rate.

The filtering has however resulted in an attenuation of the peak signal. This attenuation factor must be taken into account in the S/N calculation. The bandwidth has been designed to be narrow enough to permit the leading edge transient to completely die down before the trailing edge appears.

Bolometer noise in the system is filtered by the following transfer function:

$$F_N(S) = \frac{S}{(\tau_1 S + 1)(\tau_2 S + 1)^2}$$

since the bolometer time constant does not affect noise. The filtering seen by noise is shown in Figure B2. From the figure it can be seen that noise is also attenuated, though by a less significant factor. Noise out is attenuated by 2.1 dB or a factor of 0.785. Bandwidth between the 3 dB points is 118 Hz.

Signal-to-Noise Ratio

Signal. -- An earth of 200°K radiates 420 μ W/cm^2 in a one-micron interval centered at 15 μ. A conservative estimate of the radiance available after filtering and attenuation by the objective and immersion lenses is 100 μ W/cm^2. The aperture selected is 0.5 in. or 1.27 cm in radius, and the

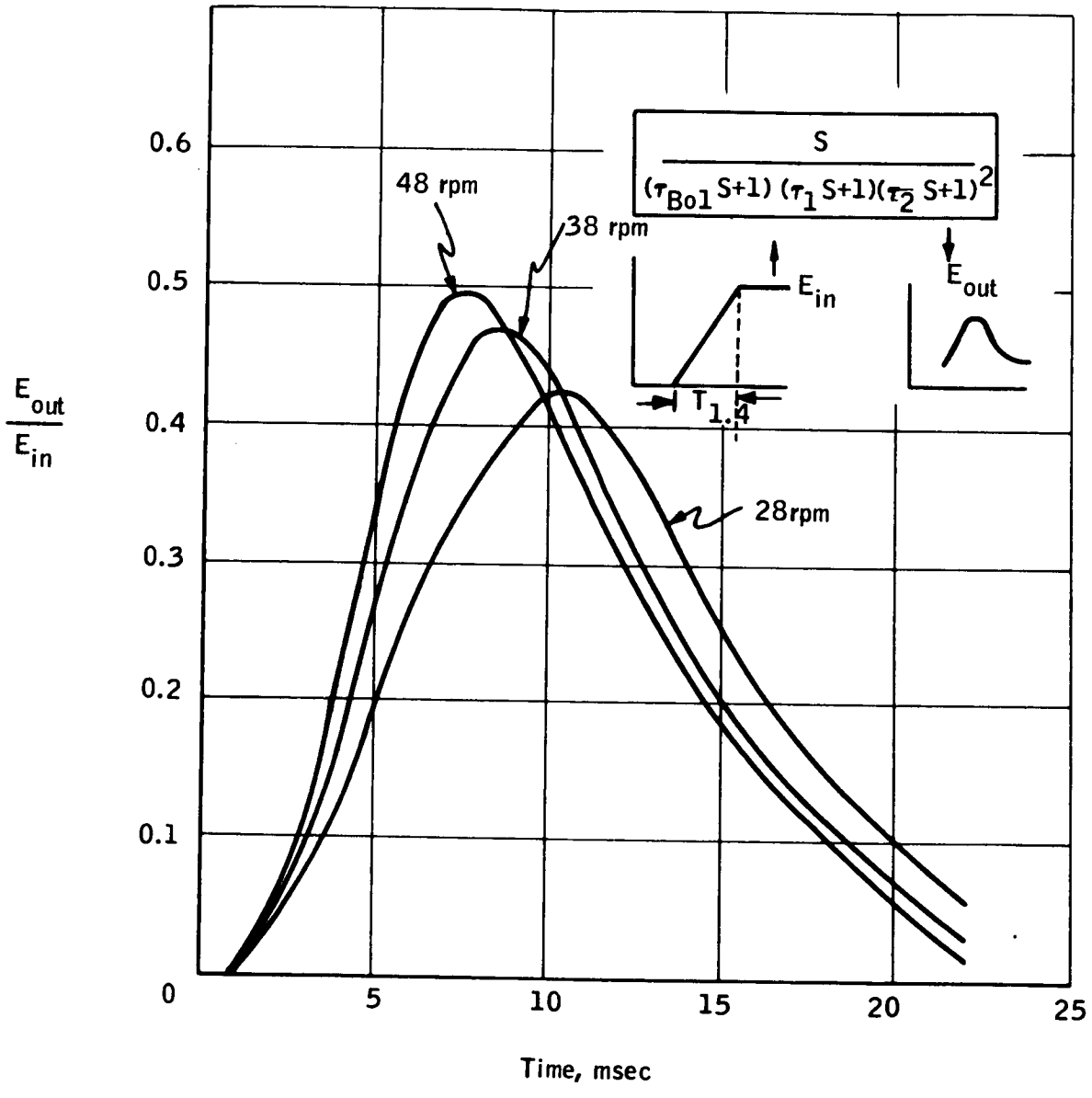

Figure B1. Filter Response for Ramp-Step Input

field of view is 0.01745 x 0.01745 steradians; thus, the radiant power available at the bolometer is

$$\frac{100\ \mu\ W/cm^2}{\pi} \times \pi\ (1.27\ cm)^2 \times (0.01745)^2 = 490 \times 10^{-10}\ W$$

As was previously mentioned, this will be further attenuated by the signal processing filtering. Filter factors as seen from Figure B1 pulse heights vary from 0.499 to 0.425. Assuming the worst case, 0.425, the signal from the bolometer has an equivalent radiant power of 490×10^{-10} W x 0.425 or 209×10^{-10} W.

Noise. -- The noise equivalent (NEP) of a Barnes Engineering Company bolometer with a compensator flake is given by

$$NEP = 6.3 \times 10^{-10} \sqrt{\frac{A\Delta F}{\tau}}$$

where A is in mm^2, ΔF in Hz, and τ in milliseconds. The resulting value is the equivalent noise rms radiant power. A constant current bias technique currently in use on conical scan horizon sensors eliminates the need for the compensating flake and thus eliminates its contribution to noise. Without the compensator flake,

$$Nep = \frac{6.3 \times 10^{-10}}{\sqrt{2}} \sqrt{\frac{A\Delta F}{\tau}} = 4.46 \times 10^{-10} \sqrt{\frac{A\Delta F}{\tau}}$$

With a germanium immersion lens the F number will be 0.21; a 2.54 cm diameter objective lens therefore yields a focal length of 5.33 mm and a detector size of

$$5.33 \times 0.01745 = 0.093\ mm$$

The detector time constant will be 1.0 msec.

$$NEP = \frac{4.46 \times 10^{-10} \times 0.093 \times \sqrt{\Delta F}}{1}$$

From Figure B2, ΔF = 118 Hz, so

$$NEP = 4.50 \times 10^{-10}\ W\ rms$$

Corresponding to the signal gain factor is a noise gain factor due to the filtering of 0.785.

$$NEP = 4.50 \times 10^{-10} \times 0.785 = 3.54 \times 10^{-10}\ W\ rms$$

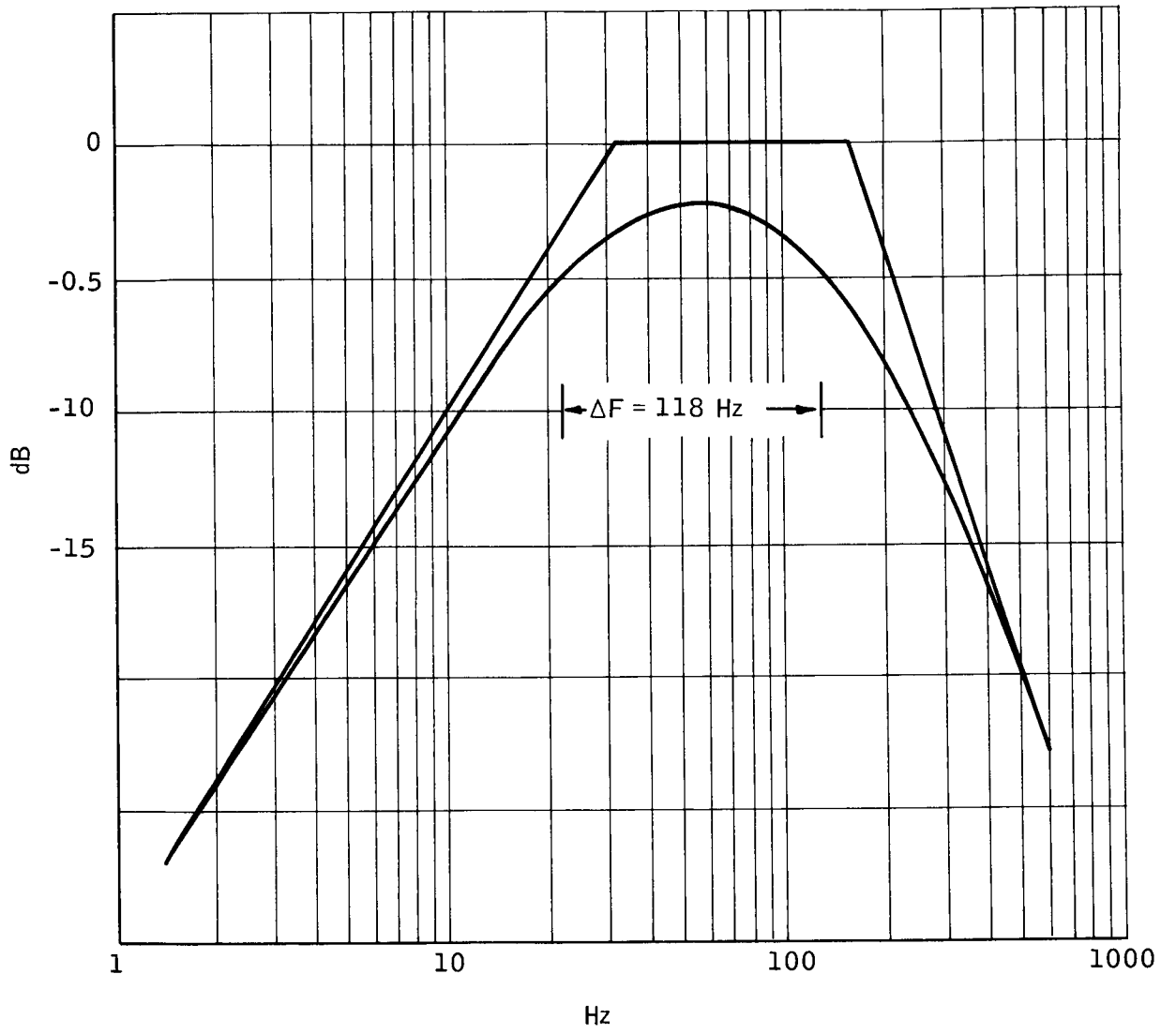

Figure B2. Filter Characteristic

In order to guarantee that noise spikes will never penetrate the threshold, multiply the NEP above by five, yielding 17.70×10^{-10} W for 5σ peaks.

At the 50 percent point for a 200°K earth, the equivalent radiant power will be

$$\frac{209 \times 10^{-10}}{2} = 105 \times 10^{-10} \text{ W}$$

Signal to noise at the threshold will therefore be

$$\frac{105 \times 10^{-10} \text{ W}}{17.7 \times 10^{-10} \text{ W}} = 5.9$$

Error at Threshold Due to Noise

Error will result from variation of the signal pulse leading edge caused by noise. In the previous section noise was computed to have an rms or 1σ value of 3.54×10^{-10} W. This noise will introduce an error at the threshold dependent upon the pulse slope of the threshold in the figure below.

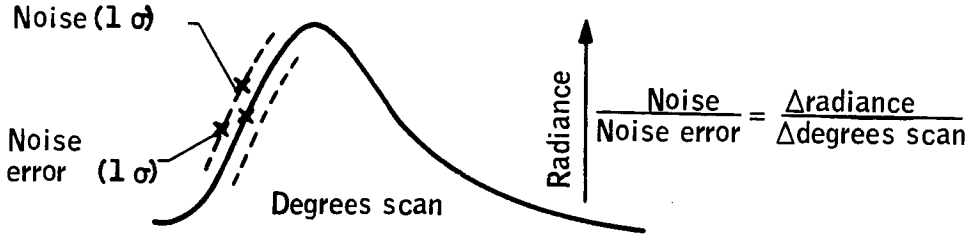

To compute noise error it is necessary to know the change in effective radiance per degree of scan. Filter parameters have been selected so that the slopes of each of the pulses of Figure B1 are proportional to the slopes of the respective ramps which generated them, so that $\frac{\Delta\text{radiance}}{\Delta\text{degrees}}$ is the same for each. Taking the 28 rpm pulse, the slope is

$$\frac{0.256 - 0.130}{2 \times 10^{-3} \text{ sec}} = 63 \text{ units sec}^{-1}$$

From the previous section, one unit or unit gain gives 490×10^{-10} W for 200°K earth. At 28 rpm, one second corresponds to $\frac{28 \times 360}{60}$ degrees = 168°.

The slope is therefore $\frac{63 \text{ units}}{\text{sec}} \times \frac{490 \times 10^{-10} \text{ W/unit}}{168°/\text{sec}} = 184 \times 10^{-10} \text{ W/deg}$

$$\frac{\text{Noise}}{\text{Noise error}} = 184 \times 10^{-10} \text{ W/degree}$$

$$\text{Noise error } (1\sigma) = \frac{3.54 \times 10^{-10} \text{ W}}{184 \times 10^{-10} \text{ W/degree}} = 0.019° \ (1\sigma)$$

The 3σ error due to noise at one edge is therefore about $0.06° \ (3\sigma)$. This error will be the same for other pulses generated at the nominal (38 rpm) and maximum (48 rpm) spin rates. A similar error will be generated at the trailing edge. An error of $0.06° \ (3\sigma)$ at the leading edge will cause an error of $0.03° \ (3\sigma)$ in the determination of the midpoint between the pulses. The same error will be present at the trailing edge, and the effects of the two will yield an error in the midpoint with a 3σ of $0.03\sqrt{2}$ or $0.042° \ (3\sigma)$.

The method of determination of the time of midpoint crossing implies the use of the next leading edge. Therefore, the uncertainity of this edge must be accounted for in the total accuracy computation.

Therefore, $(0.042)^2 + (0.06)^2 = 0.073° \ (3\sigma)$ is the total error in the determination of midpoint accuracy.

ERROR DUE TO VARIATION IN SYSTEM DELAY ΔT

The method of determination of the direction to the center of the earth employed with this system uses the time T_1 to compute the midpoint between the leading and trailing edge pulses and then subtracts a fixed delay ΔT to determine the time delay required after the next leading edge. If the required delay is T_3,

$$T_3 = k T_1 - \Delta T$$

where $k = 0.500$, and ΔT is a constant dependent on the filter parameters. An examination of the signal pulses (Figure B1) shows this delay to be about 1.80 milliseconds. According to theory, the delay is approximately

$$\Delta T = \sqrt{(\tau_{bol})^2 + 2\tau_2^2}$$

The value τ_2 is determined in two separate RC circuits and can therefore be controlled at a constant value independent of temperature, age, etc. Circuit designs presently in use at BEC will be employed to keep the effective bolometer time constant stable at 1.0 millisecond over the temperature range. Over a period of time the bolometer time constant can be expected to vary

no more than 10 percent (3σ). At 10 percent change in time constant (0.1 msec) is a change of $\frac{0.1}{\sqrt{3}}$ or 0.058 msec in ΔT. At the fastest spin rate the scan rate is 288°/sec giving 0.016° (3σ). This error would cause a shift in the indicated earth center of 0.016° (3σ) which is negligible.

ERROR IN DETERMINATION OF SPIN-AXIS ORIENTATION

Errors resulting from analysis on the ground for determination of spin-axis orientation will be negligible, since noise is the principal source of error and this will be averaged out over many scans. Other factors such as telemetry noise will predominate as error sources.

REFERENCES

1. Leimanis, Eugene: The General Problem of the Motion of Coupled Rigid Bodies about a Fixed Point. Springer-Verlay Inc., New York, 1965.

2. Russell, Ivan W.; Peterson, David C., Jansson, Richard M.; and Jensen, Clarence J.: Conceptual Mechanization Studies for a Horizon Definition Spacecraft Structures and Thermal Subsystem. NASA CR-66380, May, 1967.

3. Thomson, William T.; and Reiter, Gordon S.: Attitude Drift of Space Vehicles. Journal of Astronautical Sciences, Volume VII, No. 2, Summer 1960, pp. 29-34.

4. Vogelzang, William F.; Baltes, James J.; and Scharmack, David K.: Orbital Operations and Analysis for a 15-Micron Horizon Radiance Measurement Experiment. NASA CR-66376, May 1962.

5. Thomas, John R.: Derivation and Statistical Comparison of Various Analytical Techniques Which Define the Location of Reference Horizons in the Earth's Horizon Radiance Profile. NASA CR-726, October 1966, p. 51.

6. Hazeltine, W.R.: Nutation Damping Rates for a Spinning Satellite. Aerospace Engineering, volume 21,no. 3, March 1962, pp. 10-17.

7. Alper, J.R.: Analysis of Pendulum Damper for Satellite Wobble Damping. J. Spacecraft and Rockets, volume 2, no. 1, January-February 1965, pp. 50-54.

8. Mobley, F.F.; Teener, J.W.; Brown, R.D.; and Tossman, B.E.: Performance of the Spin Control System of the DME-A Satellite. AIAA/ JACC Guidance and Control Conference, August 1966, pp. 463-477.

9. Yu, E. Y.: Spin Decay, Spin-Precession Dampirg, and Spin-Axis Drift of the Telstar Satellite. Bell System Tech. J., volume 42, no. 5, 1963, pp. 2169-2193.

10. Fourth Weather Group, United States Air Force: The Radiation Environment. 4WGP-80-6-1, 1 June 1965.

11. Anon.: Handbook of Chemistry and Physics. Thirty-ninth ed., Chemical Rubber Publishing Co.

12. Kuiper, G. P., ed: The Solar System, Vol. I. The Sun. University of Chicago Press, 1953.

13. Anon.: The Physics of Solar Flares. NASA SP-50, 1963.

14. Davidson; and Winslow: Space Debris Hazard Evaluation. NASA TN D-1105, December 1961.

15. McCracker; and Alexander: Distribution of Small Interplanetary Dust Particles in the Vicinity of the Earth. NASA TN D-1349, July 1962.

16. Whipple, F. L.: Meteoroid and Dust. Symposium on Bio-Astronautics and the Exploration of Space, December 1965.

17. Finger, F.; and Woolf, H. M.: An Experiment Designed to Determine the Diurnal Temperature and Wind Variation and to Detect Possible Errors in Rocketsonde Temperature Measurements in the Upper Stratosphere. NASA TM X-1298, November 1966, p. 19.

18. Anon.: Preliminary Survey of Meteroid Effects on Space Vehicles. SID 62-658-2, North American Avaiation, 1962.

19. Smith, Louis G.: Effects of Magnetically Induced Eddy-Current Torques on Spin Motions of an Earth Satellite. NASA TN D-2198, April 1965.